Contents

Introduzione

E' esperienza comune osservare l'acqua di un fiume, un cascata, il fumo di un camino o il soffiare di un vento forte. E' esperienza altrettanto comune accorgersi che questi fenomeni possiedono alcune caratteristiche simili, quali una natura caotica, un comportamento estremamente irregolare e impredicibile; o ancora la presenza di strutture di diversa scala, vortici più piccoli e moti più estesi. In tutti questi casi, quello che stiamo osservando un flusso turbolento. Nelle applicazioni ingegneristiche, poi, i flussi turbolenti sono prevalenti. I processi che coinvolgono gas e liquidi in turbine, pompe, compressori sono turbolenti; i flussi di aria ed acqua che circondano aerei, automobili, sottomarini, sono turbolenti. Ancora, il mescolamento di sostanze chimiche in numerose reazioni avviene tramite meccanismi turbolenti, così come quello di aria e carburante nei motori. Solitamente, una reazione chimica desiderata si deve portare a termine il più in fretta possibile; altre volte, quando il processo di mescolamento dannoso, si vorrebbe cercare di rallentarne l'evoluzione. La presenza di turbolenza rende più efficaci il trasporto e il mescolamento dei fluidi, ed è dunque di fondamentale importanza conoscerne le caratteristiche, quando si voglia controllare l'evoluzione di un *turbulent mixing*.

Allo scopo di studiare i flussi turbolenti reali, un grosso sforzo viene fatto per comprendere a fondo le caratteristiche di quello che è il modello ideale più semplice, la turbolenza omogenea isotropa. Gli approcci a tale argomento sono sostanzialmente due. L'approccio teorico ha permesso, nel corso degli anni e grazie soprattutto al contributo del grande matematico russo Andrei Nikolevich Kolmogorov, di sviluppare una elegante teoria che descrive (statisticamente) le dinamiche, i contributi delle varie scale presenti, e permette di predire il comportamento spettrale di una turbolenza isotropa. L'approccio sperimentale, oltre a validare tale teoria nei suoi aspetti essenziali, ne ha evidenziato alcune mancanze ed inesattezze, contribuendo ad evidenziare aspetti che erano rimasti in secondo piano nel disegno di Kolmogorov, quali la pre-

senza e l'importanza di strutture coerenti articolate all'interno del flusso, che rendono fondamentale un'analisi *locale*, basata sullo studio delle dinamiche di tali strutture.

Lo scopo della tesi vuole essere il seguente. Da una parte, la definizione di una grandezza locale, di semplice misurazione, ma che permetta di dare indicazioni sull'evoluzione del flusso turbolento omogeneo isotropo a livello globale. Uno studio statistico delle proprietà di tale quantità viene effettuato, con l'obiettivo di capire quali siano le strutture che più concorrono a determinarne il comportamento e i valori. Dall'altra, si desidera effettuare alcune considerazioni a partire proprio da questa grandezza. Tale quantità viene definita come rapporto di grandezze fisicamente significative, quali lo stretching e la vorticità del campo di velocità; permette dunque di avere informazioni sull'interazione delle scale e delle strutture coerenti all'interno di un flusso turbolento.

Un secondo argomento è poi affrontato: il mescolamento di due flussi turbolenti (in assenza di sforzi di taglio medio). Scopo della trattazione è uno studio delle caratteristiche del mescolamento al variare del gradiente di energia tra le turbolenze. In particolare vengono presentati dati a conferma della presenza di intermittenza in un mescolamento turbolento, e della dipendenza di tale intermittenza dal gradiente di energia.

Lo schema della trattazione è il seguente. Nei primi tre capitoli vengono presentati gli strumenti necessari per affrontare lo studio della dinamica della turbolenza. In particolare, nel primo capitolo vengono richiamate le equazioni della fluidodinamica, gli strumenti statistici di base e vengono introdotte le prime considerazioni fisiche sull'interazione tra strutture di varie scale nella celebre *cascata di Richardson*. La teoria di Kolmogorov viene presentata nel secondo capitolo; se ne mostra la consistenza con il sistema di Navier-Stokes e si riportano alcuni risultati classici sul comportamento statistico del campo di velocità in un flusso turbolento. Vengono poi introdotti gli spettri di energia, diffusamente usati nel seguito. Nel terzo capitolo viene segnalato come la pratica sperimentale abbia riscontrato inesattezze nella teoria di Kolmogorov; i fenomeni che generano tali discrepanze vanno sotto il nome generico di *intermittenza*.

Il capitolo quattro introduce la qunatità oggetto di studio, la *funzione* f; tale grandezza viene definita come criterio per la localizzazione delle piccole scale in una simulazione numerica di tipo LES (*large eddy simulation*).

Lo studio sistematico della funzione e del legame fisico tra questa e le scale della turbolenza è oggetto del quinto capitolo. In esso vengono riportati i risultati ottenuti tramite un lavoro di filtraggio del flusso: modificando il campo di velocità in modi diversi è stato possibile analizzare il legame statistico tra la quantità f e le strutture della turbolenza, evidenziando così un più evidente significato fisico di f.

Infine, il capitolo sesto è dedicato al problema del *shearless mixing layer*, ovvero al mescolamento di due flussi turbolenti. Benchè i flussi siano isotropi, la differenza relativa di energia genera disomogeneità nel mescolamento. Lo studio de tale problema, soprattutto tramite simulazioni numeriche, argomento relativamente recente. In questo lavoro viene analizzata l'evoluzione del mixing layer, mettendo in risalto il ruolo dell'energia turbolenta (o meglio, del rapporto tra le energie dei due flussi) come parametro fondamentale che regola l'intermittenza del mescolamento.

Chapter 1

Equations of turbulence

1.1 The equations of fluid dynamics

We briefly review the equations governing the motion of Newtonian fluids. The basic idea is the *continuum hypothesis*, i.e. the assumption that a fluid, although having a discrete molecular nature, can be regarded as a continuum fluid. The continuum fluid properties are obtained by averaging the molecular properties of the fluid on volume which is small compared with the flow scale, but large enough so that the average is independent of the choice of the integration volume. Using this fundamental assumption, one can derive *balance equations* for physical quantities as density, momentum, kinetic or total energy, and so on. The first is the *continuity equation*, which expresses the mass-conservation principle:

$$\frac{\partial \rho}{\partial t} + \nabla \cdot (\rho \mathbf{U}) = 0 \tag{1.1}$$

where $\mathbf{U}(\mathbf{x}, t)$ is the velocity of the fluid particle in $\mathbf{x}$ at time t, and $\rho(\mathbf{x}, t)$ the density. The object of our discussion will be *constant density* fluids (in time and space)

$$\rho(\mathbf{x}, t) = \rho = const;$$

in this case the evolution equation has the simpler form

$$\nabla \cdot \mathbf{U} = 0 \tag{1.2}$$

thus stating that the field is *divergence-free* or *solenoidal*.

The momentum equation is based on Newton's second law; it relates the particle acceleration to the forces (body forces and surface forces) acting on

the fluid. In the case of Newtonian fluids, this equation takes the form of the well known *Navier-Stokes equation*

$$\rho(\frac{\partial U_i}{\partial t} + U_j \frac{\partial U_i}{\partial x_j}) = -\frac{\partial p}{\partial x_i} + \mu \frac{\partial^2 U_i}{\partial x_j x_j} \tag{1.3}$$

where $p(\mathbf{x}, t)$ is the *(modified) pressure* (a term which takes into account both the pressure and the gravitational potential), and the constant μ is the *viscosity* coefficient. Using the material derivative

$$\frac{D}{Dt} = \frac{\partial}{\partial t} + U_j \frac{\partial}{\partial x_j}$$

the equation is often written in the form

$$\frac{DU_i}{Dt} = -\frac{1}{\rho}\frac{\partial p}{\partial x_i} + \nu \frac{\partial^2 U_i}{\partial x_j x_j} \tag{1.4}$$

where $\nu = \mu/\rho$ is called *kinematic viscosity*. The flow of a constant-property Newtonian fluid is governed by equations (1.2) and (1.4). At a solid wall, the usual boundary conditions are the impermeability condition $\mathbf{n} \cdot \mathbf{U} = 0$ and the no-slip condition $\mathbf{U} - \mathbf{n}(\mathbf{n} \cdot \mathbf{U}) = 0$.

1.1.1 The vorticity equation

The concept and effects of vorticity play a central role in our discussion and in the study of turbulence in general. So we spend a few more words about its definition and properties.

The *vorticity* of a fluid motion is defined as

$$\boldsymbol{\omega} = curl(\mathbf{U})$$

so it is a vector field defined in each point, at each time. As we shall see in a moment, the vorticity corresponds to the rotation of the fluid. A flow with $\boldsymbol{\omega} = 0$ is called *irrotational flow*.

In order to understand the physical significance of vorticity, we compare two examples. The first one is the so-called *ideal vortex field*, i.e. every fluid particle is moving on a circular path above the z-axis, with a radial distribution of velocity. In cylindrical coordinate we have

$$U_\Phi = \frac{K}{r}, \quad U_r = U_z = 0$$

(K is a constant). Taking the curl of this field we obtain

$$\omega_r = \omega_z = 0$$

$$\omega_\Phi = \frac{1}{r}\frac{\partial}{\partial r}(rU_\Phi) = 0$$

for $r \neq 0$. It can be seen from Stokes theorem that the vorticity goes to infinity on the axis $r = 0$. Thus, this is a case of irrotational motion everywhere (except the axis).

The second example is the shear-flow

$$U = U(y), \quad V = W = 0$$

whose vorticity vector is

$$\omega_x = \omega_y = 0, \quad \omega_z = -\frac{\partial U}{\partial y}$$

so that, in general, there can be non-zero vorticity in each point.

Let's compare these examples. In the first case all the fluid particles (for $r \neq 0$) move around a circular path, but the vorticity is zero. In the second case, each particle moves in a straight line, but it has vorticity. This shows one important feature of the *rotation* described by the vorticity vector: it does not correspond to motion of particles on a close path, but to a *change of orientation* in space. Thus, in the second example a change in orientation is given by the presence of stress ($\frac{\partial U}{\partial y}$) which deforms the particle; while in the first case the particles are moving on a circular path, but conserve the same orientation in space, so that the vorticity is null.

The evolution equation for vorticity can be obtained by taking the curl of the Navier-Stokes equation. With the help of continuity equation, one finally obtains

$$\frac{D\boldsymbol{\omega}}{Dt} = \boldsymbol{\omega} \cdot \nabla \mathbf{U} + \nu \nabla^2 \boldsymbol{\omega} \tag{1.5}$$

which is referred to as the *vorticity equation*, and gives the rate of change of the vorticity of a fluid particle.

The first term on the right-hand side represents the action of the velocity variations on vorticity. For sake of simplicity, let's consider a fluid which is *inviscid*, i.e. the effects of viscosity can be neglected; hence the viscous term disappears in the vorticity equation. Consider a particle whose vorticity is in

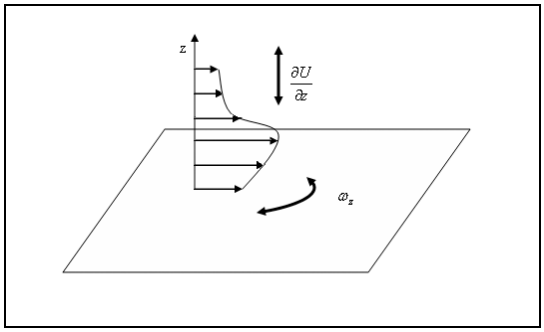

Figure 1.1: Sketch of the contributions to the stretching-twisting term

the z-direction (just by so choosing the axes); for that particle the vorticity vector is $(0, 0, \omega_z)$. Thus the vorticity equation becomes

$$\frac{D\boldsymbol{\omega}}{Dt} = \omega_z \frac{\partial \mathbf{U}}{\partial z}$$

Writing the three components separately one obtains

$$\frac{D\omega_x}{Dt} = \omega_z \frac{\partial U}{\partial z}$$
$$\frac{D\omega_y}{Dt} = \omega_z \frac{\partial V}{\partial z}$$
$$\frac{D\omega_z}{Dt} = \omega_z \frac{\partial W}{\partial z}$$

Let's consider now the first of these three equations. If $\frac{\partial U}{\partial z}$ is non-zero, it means that particles instantaneous separated in the z-direction are acquiring a separation in the x-direction too. And this generates vorticity in the x-direction. The second equation can be interpreted in the same way. This phenomenon is known under the name of *vortex twisting*.

The third equation says that the magnitude of z-component of vorticity is increased when $\frac{\partial W}{\partial z}$ is positive, i.e. when the fluid particle is elongating in the same direction of vorticity. Note that, when a particle is elongating in the z-direction, it must be contracting in the x and y-directions to conserve mass. And now we see that it rotates faster (as a solid body of decreasing moment of inertia). This is the phenomenon of *vortex stretching*.

The *stretching-twisting* term $\boldsymbol{\omega} \cdot \nabla \mathbf{U}$ is very important in turbulent processes, because deformation and the arising of small scales are dominated by vorticity. As we would like to show, this term can give important information about the features of a turbulent flow.

1.2 Statistical description of turbulence

So far, we have described the well known model of fluid-dynamics; it applies both to laminar and to turbulent flows. The case of laminar flows has been studied for one century, and Navier-Stokes equation can be used to predict values of the velocity field. Now we have a high degree of confidence that the predicted values will agree with measured ones. When we apply the same model to the study of turbulence, the aim of our theory must be different. This difference is due to the intrinsically *random nature* of turbulence.

Let us consider for example the measured values for a velocity field. We can consider for exemple data from a hot-wire probe placed in a wind tunnel, but they present features which can be extended to all turbulent velocity fields. First of all, we directly perceive the presence of structures with time-scale of very different orders, from one second to one-hundredth of a second, and maybe smaller. This makes the signal highly disorganized. Second, the signal is highly unpredictable in detail. If we consider the velocity field obtained from the same probe some time later, we see that it cannot be predicted from the behavior of the previous one. Despite this fact, it is possible to find some predictable feature.

In fact, what is reproducible in turbulence is the *statistical behavior*; this leads to the necessity of a statistical approach. The contrast between the random nature of turbulent flows and the deterministic nature of the equation described so far is only apparent; and lyes in the fact the the Navier-Stokes model can be seen as a *chaotical dynamical system*. This kind of approach is beyond the aim of our discussion; let us say that one of the most important aspects is the *extreme sensitivity to initial conditions*. Let's consider one experiment that can be repeated under the same specified set of conditions (for example the wind tunnel with the probe). The problem is that perturbations to these nominal conditions are always present: vibrations of the apparatus, small temperature differences, details of the surfaces... Thus, in practice, we can reduce but not eliminate perturbations. This is true in every kind of experimental consideration, and does not explain itself the random nature of turbulence. The fact is that, above all for high Reynolds numbers, the evolution equation of the flow is strongly sensitive to changes in initial conditions, boundary conditions and material properties. If we consider two initial conditions *practically indistinguishable* (let's say, for example, that the difference can be of the order of 10^{-8}) and we let the system evolve, the evolution will be the same at the beginning; but after a certain time (let's

say t_0) the two trajectories can separate and evolve in a completely different way. The consequence of this fact is that, if the initial state is known to within 10^{-8}, no useful prediction can be made beyond the time t_0. That's why unpredictability arises.

In this section we briefly introduce the notation used in the following chapters. The random vector velocity field $\mathbf{U}(\mathbf{x}, t)$ is completely described *at each point, at each time*, by the probability density function (in the following *pdf*) $f(\mathbf{V}; \mathbf{x}, t)$. The *mean* velocity field is by definition

$$\langle \mathbf{U}(\mathbf{x}, t) \rangle = \iiint_{-\infty}^{\infty} \mathbf{V} f(\mathbf{V}; \mathbf{x}, t) d\mathbf{V}$$

Through the mean we can define the *fluctuation* of $\mathbf{U}$

$$\mathbf{u} = \mathbf{U} - \langle \mathbf{U} \rangle$$

(from now on we skip the space and time dependence) and in general the *n-th central moment* is defined to be

$$\langle \mathbf{u}^n \rangle = \iiint_{-\infty}^{\infty} (\mathbf{V} - \langle \mathbf{U} \rangle)^n f(\mathbf{V}) d\mathbf{V}$$

We will indicate the *variance* of $\mathbf{U}$ with both $\langle \mathbf{u}^2 \rangle$ and $Var(\mathbf{U})$; the *standard deviation* will be denoted by σ, $\langle \mathbf{u}^2 \rangle^{1/2}$ or r.m.s. (root mean square). We will be also dealing with *standardized moments*. If σ is the standard deviation of $\mathbf{U}$, the standardized random variable from $\mathbf{U}$ is

$$\hat{\mathbf{U}} = \frac{\mathbf{U} - \langle \mathbf{U} \rangle}{\sigma}$$

the standardized pdf of $\mathbf{U}$ is

$$\hat{f}(\hat{\mathbf{V}}) = \sigma f(\langle \mathbf{U} \rangle + \sigma \hat{\mathbf{V}}))$$

and the *n-th standardized moments* are defined as

$$\frac{\langle \mathbf{u}^n \rangle}{\sigma^n} = \iiint_{-\infty}^{\infty} \hat{\mathbf{V}}^n \hat{f}(\hat{\mathbf{V}}) d\hat{\mathbf{V}}$$

We will consider mostly the third standardized moment, the *skewness*, and the forth standardized moment, the *kurtosis*.

For a complete characterization, we should know the *N-time, N-time* joint pdf

$$f_N(\mathbf{V}^{(1)}, \mathbf{x}^{(1)}, t^{(1)}, \mathbf{V}^{(2)}, \mathbf{x}^{(2)}, t^{(2)}, ..., \mathbf{V}^{(N)}, \mathbf{x}^{(N)}, t^{(N)})$$

for all space-time points. This is obviously impossible; in practice, a random velocity field cannot be fully characterized. The simplest statistic that contains some spatial information about the structure of the field is the *one-time, two-point autocovariance*

$$R_{ij}(\mathbf{r}, \mathbf{x}, t) = \langle u_i(\mathbf{x}, t) u_j(\mathbf{x} + \mathbf{r}, t) \rangle$$

This is often referred to as the *two-point correlation*, and is examined in more detail in section 2.3.

A random field is said to be *statistically stationary* if the statistics are invariant under a shift in time. It means that, given a time shift T, the N-point joint pdf f_N must remain unchanged when we replace $(\mathbf{x}^{(n)}, t^{(n)})$ with $(\mathbf{x}^{(n)}, t^{(n)} + T)$ for all N points.

A random field is *statistically homogeneous* if all the statistics are invariant under a shift in space. The definition of *homogeneous turbulence* requires that only the *fluctuation* field $\mathbf{u}$ is statistically homogeneous. If the statistics of the field are independent of one (or two) spatial directions, $\mathbf{U}$ is said to be *statistically two-dimensional* (or *one-dimensional*). This will be the case in most our simulations.

A random field is *statistically isotropic* if it is statistically homogeneous and also invariant under rotations and reflections of the coordinate system. The (approximately) isotropic condition is one of the most studied case, as much of the theory centers on isotropic turbulence.

1.3 Route to turbulence

"No short but complete definition of turbulence seems to be possible. One has rather to describe the features that are implied by the use of the name. One can formulate a brief summary, rather then a formal definition, that attempts to incapsulate the description. Perhaps the best is that turbulence is *a state of continuous instability*". According to this consideration by Tritton, the aim of these initial paragraphs is to give a description of the general features of a turbulent flow. In this purpose, both theoretical and experimental aspects play a fundamental role. Furthermore, the physical experiment by

which the turbulence is generated has a little importance, in a sense which will be made more clear later: this allows us to refer to different types of turbulent flows, generalizing the conclusions to all kinds of turbulent flows.

The first relevant feature is the *lost of symmetries*. Let's consider the well known example of a stationary flow of uniform velocity $(V, 0, 0)$ incident from the left to an (infinite) circular cylinder, parallel to the z-axis. According to the *similarity principle* (see chapter 2), the system can be completely described with just one parameter, the *Reynolds number*

$$Re = \frac{LV}{\nu} \tag{1.6}$$

where L is the characteristic scale (in our example, the diameter of the cylinder), and ν is the kinematic viscosity. Visualizations of the flow at low Reynolds numbers $Re \approx 10^{-1}$ show that it presents some kind of *symmetries*:

- left-right symmetry;
- up-down symmetry;
- time-invariance;
- space-invariance in direction z.

Now let the Reynolds number grow up. The first symmetry which is broken is the left-right one; this happens at $Re \approx 1$. Actually, we must remark that the right-left symmetry is *non consistent* with the Navier-Stokes equation. This is due to the presence of the nonlinear term. But it is consistent with the Stokes equation, which is the momentum equation without the nonlinear term. Actually, this symmetry is not exact, and it is present only if the Reynolds number is very low, so that the contribution of the nonlinear term is weak.

At $Re \approx 5$ the right-left symmetry is even stronger, and the flow begins to *separate*: circulating eddies form behind the cylinder. The flow is still stationary.

At $Re \approx 40$ there happens the first real breaking of symmetry: the flow becomes *time-periodic*. Figures show the presence of the well-known periodic *Karman street* of alternating vortices, driven downward by the flow. Through this bifurcation point, the time-invariance becomes a *discrete* time invariance. Also the up-down symmetry goes under a slight change, for it is no more

exact, but each vortex up is the exact mirror of a vortex down after half a period.

The last symmetry to be broken is the z-direction invariance. The critical value for this to happen is not exactly known, but simulations seem to show that it is somewhere between 40 and 70. The flow, which was essentially two-dimensional, becomes truly *three-dimensional*, with the generation of a velocity component in the third direction. Three-dimensionality, and the mathematical terms generating it, is a very important feature of a turbulent flow, and we will come back to this topic in the following chapters.

Finally, there is also a Reynolds number threshold beyond which the flow breaks also the discrete time-dependence, and become *chaotic*. This values is approximately around 200-300. Visualizations of marked fluid particles show the erratic, random paths.

Thus, increasing the Reynolds number, all the symmetries are spontaneously broken, and the flow becomes chaotic. We say that a flow is *turbulent* when successive instabilities have reduced the level of predictability so much that a statistical description is necessary. Thus, in a turbulent flow, random features are dominant; nevertheless the flow involves organized structures. As we have seen in the previous chapter, at very high Reynolds numbers the symmetries are restored in a statistical sense: this state is referred to as *fully developed turbulence*.

A statistical mechanics similar to kinetic theory of gases requires too many, and not always valid, assumption; thus, much of knowledge and theory about the behavior of turbulence comes from experiments. Nevertheless, one can obtain evolution equations for some statistical quantity from the Navier-Stokes equation, which remains the model of reference. Both aspects play a central role in the study of turbulence, and we try to discuss both of them in the following chapters.

1.4 Reynolds equations

When treating the problem of turbulent flows, it is necessary to develop and deal with statistical tools like means, correlation functions, etc. Equations of evolution for such quantities must be derived from the Navier-Stokes model. The most basic of these equations was obtained by Reynolds in 1894, and describes the evolution of the mean field $\langle \mathbf{U}(\mathbf{x}, t) \rangle$.

We call *Reynolds decomposition* the splitting of the velocity field in two parts: the mean flux $\langle \mathbf{U}(\mathbf{x},t)\rangle$, and the *fluctuation* $\mathbf{u}(\mathbf{x},t)$, such that

$$\mathbf{U}(\mathbf{x},t) = \langle \mathbf{U}(\mathbf{x},t)\rangle + \mathbf{u}(\mathbf{x},t), \tag{1.7}$$

. The continuity equation (1.2) $\nabla \cdot \mathbf{U} = \nabla \cdot (\langle \mathbf{U}\rangle + \mathbf{u}) = 0$ must be satisfied by the mean term, as the differentiation and the mean operators commute:

$$\nabla \cdot \langle \mathbf{U}\rangle = \langle \nabla \cdot \mathbf{U}\rangle = 0; \tag{1.8}$$

and by subtraction we see that the same relation holds for the fluctuation term

$$\nabla \cdot \mathbf{u} = 0 \tag{1.9}$$

When we want to take the mean of the momentum equation (1.4) we must pay attention to the nonlinear term. Actually, by taking the mean of the substantial derivative

$$\langle \frac{DU_j}{Dt}\rangle = \frac{\partial \langle U_j\rangle}{\partial t} + \frac{\partial \langle U_i U_j\rangle}{\partial x_i}$$

we have to deal with the nonlinear term $\langle U_i U_j\rangle$. It can be decomposed into

$$\begin{aligned}\langle U_i U_j\rangle &= \langle (\langle U_i\rangle + u_i)(\langle U_j\rangle + u_j)\rangle \\ &= \langle U_i\rangle\langle U_j\rangle + \langle u_i u_j\rangle\end{aligned}$$

(as obviously fluctuations have zero mean). Thus the previous equation is rewritten as

$$\langle \frac{DU_j}{Dt}\rangle = \frac{\partial \langle U_j\rangle}{\partial t} + \langle U_i\rangle \frac{\partial \langle U_j\rangle}{\partial x_i} + \frac{\partial}{\partial x_i}\langle u_i u_j\rangle.$$

By defining the *mean substantial derivative*

$$\frac{\bar{D}}{\bar{D}t} = \frac{\partial}{\partial t} + \langle \mathbf{U}\rangle \cdot \nabla$$

the result can be re-expressed in the form

$$\langle \frac{DU_j}{Dt}\rangle = \frac{\bar{D}}{\bar{D}t}\langle U_j\rangle + \frac{\partial}{\partial x_i}\langle u_i u_j\rangle$$

Finally, we can take the mean of the momentum equation and express it as

$$\frac{\bar{D}}{\bar{D}t}\langle U_j\rangle = \nu \nabla^2 \langle U_j\rangle - \frac{1}{\rho}\frac{\partial \langle p\rangle}{\partial x_j} - \frac{\partial}{\partial x_i}\langle u_i u_j\rangle \tag{1.10}$$

which is known as the *Reynolds equation*. This equation is different from the laminar flow equation by the last term, $\langle u_i u_j \rangle$. This term is referred to as *Reynolds stresses*; it is due to nonlinearity, and represents, as we shell see, the action (the stress) produced by the velocity fluctuations on the mean flow. As this term is usually large compared with the viscous term, the mean velocity distribution is very different from the corresponding laminar flow.

1.4.1 Reynolds stresses

As we have pointed out, the very different behavior of the velocity field $\mathbf{U}$ and the mean velocity field $\langle \mathbf{U} \rangle$ is due to the presence of the term $\langle u_i u_j \rangle$ in the evolution equation of the latter. The meaning of the terms is made clearer if we rewrite this equation as

$$\frac{\bar{D}}{\bar{D}t}\langle U_j \rangle = \frac{\partial}{\partial x_i}[\mu(\frac{\partial \langle U_i \rangle}{\partial x_j} + \frac{\partial \langle U_j \rangle}{\partial x_i}) - \langle p \rangle \delta_{ij} - \rho \langle u_i u_j \rangle]$$

that is, in the form of a general momentum conservation equation. The right hand side terms represent the stresses. The first one is the viscous stress, due to momentum transfer at molecular level. The second one is the isotropic stress, generated by the mean pressure field. The third one is the stress arising by the fluctuation velocity field. Although the stress term is $-\rho \langle u_i u_j \rangle$, it is usual to refer to $\langle u_i u_j \rangle$ as the *Reynolds stress*.

The Reynolds stress is a second-order symmetric tensor. The diagonal components are called normal stresses, while the off-diagonal terms are shear stresses. Using this tensor we define the *turbulent kinetic energy*:

$$\mathsf{k} = \frac{1}{2}\langle u_i u_i \rangle \tag{1.11}$$

so it is half the trace of the tensor; it represents the mean kinetic energy (per unit mass) of the fluctuating field.

As usual, the tensor can be decomposed in one isotropic and one deviatoric part. The isotropic component is

$$\frac{2}{3}\mathsf{k}\delta_{ij}$$

so that the anisotropic part is

$$a_{ij} = \langle u_i u_j \rangle - \frac{2}{3}\mathsf{k}\delta_{ij}$$

This deviatoric part has the only effective contribution to the momentum transport; so, if we look at the pressure stress term, the isotropic part can be absorbed in a modified mean pressure term and we can write

$$\frac{\partial\langle p\rangle}{\partial x_j} + \rho\frac{\partial}{\partial x_i}\langle u_i u_j\rangle = \rho\frac{\partial a_{ij}}{\partial x_i} + \frac{\partial}{\partial x_j}(\langle p\rangle + \frac{2}{3}\rho\mathsf{k})$$

It should be noted that the presence of the Reynolds stress term causes a closure problem for the model described so far, as we have four equations for more than four unknowns. So we need another system of equations for this term. The simplest way is to model the tensor a_{ij}, proceeding in a way analogous to the stress-rate of strain relationship for a Newtonian fluid. That is, we suppose that a_{ij} is proportional to the mean rate of strain tensor:

$$a_{ij} = \langle u_i u_j\rangle - \frac{2}{3}\mathsf{k}\delta_{ij} = \rho\nu_T(\frac{\partial\langle U_i\rangle}{\partial x_j} + \frac{\partial\langle U_j\rangle}{\partial x_i})$$

This assumption is called *turbulent-viscosity assumption*, and the coefficient ν_T is referred to as *turbulent viscosity* or *eddy viscosity*. If this coefficient can be specified, the closure problem is solved; furthermore the conservation equation can be expressed in the new form

$$\frac{\bar{D}}{\bar{D}t}\langle U_j\rangle = \frac{\partial}{\partial x_i}[\nu_{eff}(\frac{\partial\langle U_i\rangle}{\partial x_j} + \frac{\partial\langle U_j\rangle}{\partial x_i})] - \frac{1}{\rho}\frac{\partial}{\partial x_j}(\langle p\rangle - \frac{2}{3}\rho\mathsf{k}) \tag{1.12}$$

where $\nu_{eff}(\mathbf{x},t) = \nu + \nu_T(\mathbf{x},t)$ is called the *effective viscosity*. Note that this equation is formally the same of Navier-Stokes equation, with ν_{eff} instead of ν, the mean flux $\langle\mathbf{U}\rangle$ instead of the velocity $\mathbf{U}$, and with the use of the modified pressure term $\langle p\rangle - \frac{2}{3}\rho\mathsf{k}$.

1.5 Energy cascade and vortex stretching

The turbulent flow is divided into interacting motion structures, called eddies of different sizes. An eddy is different from a Fourier component (see section 2.4). A single Fourier component extends over the whole flow; an eddy is localized, its extent is indicated by its length scale. However, small eddies contribute to large wave-number components of the spectrum; the spectrum is often interpreted as the energy associated to eddies of various sizes. Note that value of spectrum at wave-number k is influenced by all eddies smaller than $1/k$.

A basic fact in the study of a turbulent flow is the generation of smaller and smaller structures. This phenomenon needs an explanation from the energetic point of view; the answer is found in the *Richardson energy cascade* model, described in the following.

According to this model, the energy fed into the turbulence goes primarily to the larger eddies. Then, smaller eddies are generated from these ones, and then still smaller ones. During this process the viscosity is supposed to be *negligible*; so the energy is almost *completely transferred* from larger to smaller structures. This cascade goes on until the the scale is small enough for the viscosity to be important: then dissipation occurs, and the energy is transformed into heat.

The higher is the Reynolds number, the longer is the cascade; that is, the largest is the difference between the large eddies, where the external forced energy is absorbed, and the smallest eddies, where this energy is dissipated. A central point is that the dissipation is determined by rate of energy supply to the cascade, and it is independent of the dynamics of the small eddies, in which the energy is in fact dissipated. The rate of dissipation ε is thus *independent of the viscosity magnitude* ν.

The main mechanism governing this energy transfer is the strong presence of *vortex stretching* (see section 1.1). Actually, consider two fluid particles initially close together. For the random nature of turbulence, it is more likely that they are much further apart any time after; the turbulence carries them over different paths. When this happens to particles in the same vortex line, it generates the so-called vortex stretching. As a consequence, it increases the magnitude of vorticity; but because of continuity it also reduces the cross-section of the vortex tube. Thus the motion at smaller scales is increased, with a consequent transfer of energy to smaller structures.

Chapter 2

Turbulence mathematical model: Kolmogorov's K41 theory

2.1 The Kolmogorov hypothesis

At this point, the next step would be the description of a mathematical model, starting from the Navier-Stokes equations, which could lead to the experimental results described before. Unfortunately, such a complete deductive theory is still missing. Still, what is possible is to formulate some hypothesis which are compatible with experiments, and which make possible some further prediction. This corp of propositions was elaborated first by Kolmogorov in 1941, and consequently is usually referred to as *K41 theory*. Here they are presented from a modern point of view, following the aim of Frish [7] our starting point are considerations on symmetries.

As we have seen, the Navier-Stokes equations possesses a list of symmetries: time-invariance, space-translation, rotations, etc. Are they preserved by turbulence? It is easily seen that they are soon broken, as the Reynolds number increases. For example, let's consider a steady flow with time-independent boundary conditions and driving force. As the Reynolds number grows up, the flow is shown to become time-periodic (an Andronov-Hopf bifurcation occurs); if Re is increased further, the flow becomes chaotic. It happens that the continuous time invariance is restored in a discrete form, when the flow is periodic, and in a statistical sense when it becomes chaotic.

In other words, the statistical properties are found to be stationary, i.e. time-invariant.

If we try to generalize these considerations to the other type of symmetries, we meet more difficulties. Let's think for example to a cylinder-generated turbulence. The physical domain does not allow spatial symmetries: for instance, velocity fluctuations must vanish at rigid boundaries, so fluctuations next to the cylinder must be different from fluctuations far from it. A sort of symmetry is conceivable for a grid-generated turbulence, but only in the grid direction, and for multiples of the mesh. Thus, in general it is true that the mechanism which generates turbulence is *not consistent* with the listed symmetries. On the other hand, we have seen in previous chapters that many turbulent flows are characterized by a sort of *homogeneity* and *isotropy*. Interpretation of these conflicting aspects needs the help of some hypothesis. Let's consider the *velocity differences*

$$\delta v_{\mathbf{r}}(l) = [\mathbf{U}(\mathbf{x}+\mathbf{r}) - \mathbf{U}(\mathbf{x}))] \cdot \mathbf{r}. \tag{2.1}$$

The Kolmogorov assumptions on the velocity differences, presented in the following, represent the core of the K41 theory about turbulence.

Hypothesis 1 (Local Isotropy) *In the limit of infinite Reynolds number, all possible symmetries, although broken by the mechanism producing turbulence, are restored in a statistical sense, at small scales and far from rigid boundaries.*

The *small scales* are the scales *small enough* compared to the integral scale (i.e. the diameter of the cylinder or the length of the mesh). Thus, under the Hypothesis 1, there exists a range of scales $L \ll L_0$ in which velocity increments are statistically invariant under translation $\mathbf{r}_0$ (*homogeneity*)

$$\delta v_{\mathbf{r}+\mathbf{r}_0}(l) = \delta_{\mathbf{r}} v(l) \text{ in law},$$

under rotation R (*isotropy*)

$$R(\delta_{\mathbf{r}} v(R(l))) = \delta_{\mathbf{r}} v(l) \text{ in law},$$

and under *parity*

$$-\delta_{\mathbf{r}} v(-l) = \delta_{\mathbf{r}} v(l) \text{ in law}.$$

Kolmogorov argued that all the information about the geometry of the flow, carried by the large scales, is *lost* down the energy cascade. This fact

has the consequence that the statistics of the small-scale motions are in this sense *universal*, i.e. they are the same, no matter how the turbulence is generated. But on which parameter do they depend? If we have a look at the energy cascade (see section 1.5), we find out that the main parameters that control such a mechanism are basically two: the rate at which the energy is transferred from larger to smaller scales at the top, and the kinematic viscosity at the bottom. Another important principle is that energy is just transferred down the cascade, and dissipated just at the end. As a consequence, we can assume that the rate at which the smaller scales receive energy from the bigger ones is comparable to the dissipation rate ε. Now we can understand the sense of the following statement:

Hypothesis 2 (First similarity assumption) *At very high, but finite, Reynolds number, all the small scale statistical properties are uniquely and universally determined by the mean dissipation rate ε and the viscosity ν.*

Given the two parameters ε and ν, simple dimensional consideration lead us to see that there is only one possibility to obtain length, velocity and time scales. Actually, on dimensional ground and within multiplicative constants, they must be written as

$$\eta \sim (\nu^3/\varepsilon)^{\frac{1}{4}}$$
$$\delta u_\eta \sim (\nu\varepsilon)^{\frac{1}{4}}$$
$$\tau_\eta \sim (\nu/\varepsilon)^{\frac{1}{2}}$$

η is called *Kolmogorov scale*. Let's show how the *universality* stated in the hypothesis comes out. We consider the non-dimensional coordinate at a point $(\mathbf{x}_0, t)$

$$\mathbf{y} = \frac{\mathbf{x} - \mathbf{x}_0}{\eta}$$

and the relative normalized velocity-difference field

$$\mathbf{w}(\mathbf{y}) = \frac{\mathbf{U}(\mathbf{x}, t_0) - \mathbf{U}(\mathbf{x}_0, t_0,)}{\delta u_\eta}.$$

Actually, no non-dimensional parameter can be defined using ε and ν; thus, the universal form of the statistics of $\mathbf{w}(\mathbf{y})$ cannot depend on these two parameters. As a consequence of the Kolmogorov first hypothesis, given different high-Reynolds-number turbulent flows, the velocity fields $\mathbf{w}(\mathbf{x})$ are *statistically similar* at the small scales, i.e the statistics are *identical* when the field is normalized using the Kolmogorov scales.

As immediate consequence of these definitions, the resulting Reynolds number is

$$Re_\eta = \frac{\eta u_\eta}{\nu}, = 1.$$

It is clearly seen that an uncertainty about the definition of *small* scales is left. This hypothesis con be regarded as just saying that *there exists a range os scales, much smaller than* L such that the statistics depends only on η and ν. Experiments and flow visualizations show that the ratio η/L increases as the Reynolds number grows up; so the higher is the Reynolds number, the longer is the energy cascade. This means that, at sufficiently high Re, one can find a range of scales l very small compared to L, but still very large compared to the dissipative scale η:

$$\eta \ll l \ll L$$

. The second similarity hypothesis, supported by experimental evidences, states that the motion of such scales is little affected by viscosity; so that

Hypothesis 3 (Second similarity assumption) *In the limit of infinite Reynolds number, all the statistical properties of the scales* $\eta \ll l \ll L$ *are uniquely and universally determined by the mean dissipation rate* ε*, independent of* ν*.*

It is evident that length-scales, velocity-scales and time-scales cannot be defined on the base of ε alone. In this case, given any scale $\eta \ll l \ll L$, velocity- and time-scales will depend on l as well:

$$\delta u(l) \sim (\varepsilon l)^{1/3}$$
$$\tau(l) \sim (\frac{l^2}{\varepsilon})^{1/3}.$$

As a consequence, these scales decrease as l decreases.

So, the picture we have described so far is this: the set of scales generated in a turbulent flow at high Reynolds number can be divided into three ranges, with different behaviors. The first range contains the largest scales $l \sim L$; we shall see that this range contains the bulk of the energy of turbulence, so that it is called the **energy-containing range**. The second range contains the

bottom of the cascade, the smallest scales $l \sim \eta$. This range is dominated by viscosity and diffusion, and is called **Kolmogorov** or **dissipation range**. In between, the behavior of the velocity field is independent both of the larger scales and boundary conditions, and of the smaller scales and the viscosity. This is called **inertial range**.

Before going on, one important remark must be done. We presented the Kolmogorov hypothesis in a form which is quite usual, see [14]). However one must keep in mind that the original formulation was given by Kolmogorov in terms of *joint probability distribution function* of the *velocity difference field*. Consider a domain in a turbulent flow and n points inside this domain, say $\mathbf{x}_0, \mathbf{x}_1, \mathbf{x}_2, \ldots, \mathbf{x}_n$. One can define

$$\mathbf{y} = \mathbf{x} - \mathbf{x}_0$$

$$\mathbf{v}(\mathbf{y}) = \mathbf{U}(\mathbf{x}, t) - \mathbf{U}(\mathbf{x}_0, t)$$

and consider the the N-joint pdf f_N (and all the statistics) of $\mathbf{v}$ in the points $\mathbf{y}_0, \mathbf{y}_1, \mathbf{y}_2, \ldots, \mathbf{y}_n$. We point out that the Kolmogorov statements refer to f_N and to the relative statistics; thus, the K41 theory must be applied *only* to the statistics of the velocity differences.

2.2 Consequences of the similarity hypothesis

2.2.1 Phenomenological point of view

An important branch in turbulence theory is the so called *phenomenology of turbulence*. Phenomenology is a kind of useful shortcut: in this contest reasonings are made, above all on dimensional ground, in order to recover theoretical results in a simpler way. We notice that we silently introduced this point of view in our presentation of the Kolmogorov hypothesis. Now we make it more clear and precise, we look back to some physical concepts in this new light, and we obtain further predictions.

When we are dealing with phenomenology, the basic tools are the orders of magnitude of physical quantities. So we need to define:

- the length-scale under consideration l. The integral scale is now l_0, while the Kolmogorov scale is as usual η;

- v_l the velocity-scale (the scale of the r.m.s. velocity) associated to l;

We will write $v_0 \sim v_{l_0}$ for the r.m.s. velocity fluctuations. Furthermore we can define

$$t_l \sim \frac{l}{v_l}$$

the so-called *eddy-turnover time* associated to scale l. It represents the typical time for a structure of size l to undergo a significant distortion due to the relative motion of its components. Thus, it is also the typical time for the transfer of energy from scales $\sim l$ to smaller scales. The energy flux Π_l can be estimated as the ratio between the kinetic energy (per unit mass) associated with eddy motion on scale $\sim l$, and the typical time of this transfer. We obtain

$$\Pi_l \sim \frac{v_l^2}{t_l} \sim \frac{v_l^3}{l}$$

Now recall the energy cascade picture introduced by Richardson. In this model, the inertial range is characterized by the absence of direct energy input and direct energy dissipation; the energy is totally *transferred* from larger to smaller scales. When the scale is small enough (i.e. Kolmogorov scale) the energy is finally dissipated in heat. This means that, in the whole inertial range, the energy flux must be independent of l, and equal to the mean energy dissipation rate:

$$\Pi_l \sim \frac{v_l^3}{l} \sim \varepsilon$$

This relation can be expressed in the form

$$v_l \sim \varepsilon^{1/3} l^{1/3}$$

which shows the consistency between the Richardson cascade and the third Kolmogorov hypothesis.

Near the top of the inertial range, where $l \sim l_0$, this equation leads to the following estimate for the dissipation

$$\varepsilon \sim \frac{v_0^3}{l_0}$$

a very important relation, often used in empirical modelling.

Other considerations can be made about the distortion of eddies, controlled by the shear. One important assumption in the energy cascade idea

is the *localness* of scale interactions. In this frame, localness does not mean position in the physical space, bur refers to the fact that the dynamics of an eddy of length-scale l are induced by eddied of slightly larger dimension; and affects the behavior of slightly smaller eddies. Dealing with orders of magnitude, it means that the typical shear (and the predominant distortion) associated with scales $\sim l$ comes from the scales $l' \sim l$; recalling the relation $v_l \sim \varepsilon^{1/3} l^{1/3}$ we see that

$$s_l \sim \frac{v_l}{l} \sim \varepsilon^{1/3} l^{-2/3}$$

So, in the inertial range, the bigger is the scale, the smaller is the shear; the weaker shear is on the top of the inertial range, where $l \sim l_0$, while the larger is near its bottom, where $l \sim \eta$.

2.2.2 The structure function

In present section, our aim is to show how the listed hypothesis of K41 theory are used to predict the behavior of statistical quantities. As a typical example, let's show what can be inferred about the structure function.

The covariance of the velocity differences between two points $\mathbf{x}$ and $\mathbf{x}+\mathbf{r}$:

$$D_{ij}(\mathbf{x}, \mathbf{r}, t) = \langle [\mathbf{U}_i(\mathbf{x}+\mathbf{r}, t) - \mathbf{U}_i(\mathbf{x}, t)][\mathbf{U}_j(\mathbf{x}+\mathbf{r}, t) - \mathbf{U}_j(\mathbf{x}, t)] \rangle \qquad (2.2)$$

is usually referred as the *second-order velocity structure function*. We would like to make some prediction about the statistics of $D_{ij}(\mathbf{x}, \mathbf{r})$ (we skip the dependence on time, as it has no influence in the present discussion); but before we have to show that this quantity can be written as a function of $\mathbf{y}$ and $\mathbf{v}(\mathbf{y})$ written above. It is easy, as we can write

$$\begin{array}{ll} \mathbf{y}_1 = \mathbf{x} - \mathbf{x}_0 & \mathbf{y}_2 = (\mathbf{x}+\mathbf{r}) - \mathbf{x}_0 \\ \mathbf{v}(\mathbf{y}_1) = \mathbf{U}(\mathbf{x}) - \mathbf{U}(\mathbf{x}_0) & \mathbf{v}(\mathbf{y}_2) = \mathbf{U}(\mathbf{x}+\mathbf{r}) - \mathbf{U}(\mathbf{x}_0) \end{array}$$

thus the structure function can be rewritten as

$$D_{ij}(\mathbf{y}_1 + \mathbf{x}_0, \mathbf{y}_2 - \mathbf{y}_1) = \langle [\mathbf{U}_i(\mathbf{x}+\mathbf{r}) - \mathbf{U}_i(\mathbf{x})][\mathbf{U}_j(\mathbf{x}+\mathbf{r}) - \mathbf{U}_j(\mathbf{x})] \rangle$$

If we assume that all other conditions are satisfied (e.g. high Reynolds number), from the hypothesis of local isotropy it follows that D_{ij} is independent of $\mathbf{x}$; it is also evident by definition that D_{ij} depends on $\mathbf{y}_2 - \mathbf{y}_1$ and not on $\mathbf{y}_1, \mathbf{y}_2$ separately. So $D_{ij}(\mathbf{r}, t)$ is an isotropic function of $\mathbf{r}$.

As D_{ij} is a second order tensor, it follows that, to within scalar multiples, it must be written as

$$D_{ij}(\mathbf{r},t) = D_{NN}(\mathbf{r},t)\delta_{ij} + [D_{LL}(\mathbf{r},t) - D_{NN}(\mathbf{r},t)]\frac{r_i r_j}{r^2} \tag{2.3}$$

where D_{LL} and D_{NN} are called respectively the longitudinal and the transverse structure function.

In homogeneous isotropic turbulence in which the mean flow is supposed to be null, the continuity equation leads to the relation

$$\frac{\partial}{\partial r_i} D_{ij}(\mathbf{r},t) = 0 \tag{2.4}$$

This is easily seen by noting first of alla that $D_{i,j}$ can be written in function of the two-point correlations

$$R_{ij}(\mathbf{x},\mathbf{r},t) = \langle u_i(\mathbf{x}+\mathbf{r},t)u_j(\mathbf{x},t)\rangle$$

(which are studied in more detail in the next section). Actually, $\langle \mathbf{U}\rangle = 0$ implies

$$D_{ij}(\mathbf{r}) = \langle [u_i(\mathbf{r}) - u_i(0)][u_j(\mathbf{r}) - u_j(0]\rangle =$$
$$\langle u_i(\mathbf{r})u_j(\mathbf{r}) - u_i(0)u_j(\mathbf{r}) + u_i(0)u_j(0) - u_i(\mathbf{r})u_j(0)\rangle =$$
$$2R_{ij}(0) - R_{ij}(\mathbf{r}) - R_{ji}(\mathbf{r}) = 2R_{ij}(0) - R_{ij}(\mathbf{r}) - R_{ij}(-\mathbf{r})$$

and it is easy to see that, by imposing the continuity equation $\frac{\partial u_j}{\partial x_j} = 0$ one obtains

$$\frac{\partial R_{ij}}{\partial r_i} = \frac{\partial D_{ij}}{\partial r_i} = 0$$

Combining equations (2.3) and (2.4) one can determine D_{NN} in function of D_{LL}:

$$D_{NN}(r,t) = D_{LL}(r,t) + \frac{r}{2}\frac{\partial D_{LL}}{\partial r}(r,t) \tag{2.5}$$

Thus, in homogeneous isotropic turbulence, D_{ij} depends on the only scalar quantity $D_{LL}(r,t)$.

Let's now apply the similarity hypothesis. There exists a range, the Kolmogorov range, in which D_{ij} is completely determined by ε and ν. For dimensional reasons it is convenient to consider also the scale-length r; the quantity $(\varepsilon r)^{2/3}$ can be used to make $D_{i,j}$ non-dimensional. Therefore, within scalar multiples we can write

$$D_{LL}(r,t) = (\varepsilon r)^{2/3}\hat{D}_{LL}(r/\eta) \tag{2.6}$$

In the inertial range, the D_{ij} should be independent of ν. In this case there is no non-dimensional relation which can be formed by r, ν only. So D_{LL} can be written using a constant C

$$D_{LL}(r,t) = (\varepsilon r)^{2/3} \cdot C$$

where this constant must be universal. As a straight consequence

$$D_{NN} = \frac{4}{3} D_{LL} = \frac{4}{3} C (\varepsilon r)^{2/3}$$

$$D_{ij}(\mathbf{r},t) = C(\varepsilon r)^{2/3}(\frac{4}{3}\delta_{ij} - \frac{1}{3}\frac{r_i r_j}{r^2})$$

Thus, in the inertial and Kolmogorov range, the second order structure function can be determined *a priori* using r, ε, and ν in the dissipative range.

This prediction has been tested in experimental way; this allows also to find the value for the universal constant C.

2.3 Deductions from Navier-Stokes equations

We have shown how the system of Kolmogorov hypothesis can be successfully used to make important statistical prediction. However we have already pointed out that these hypothesis have no direct connection to the Navier-Stokes equations. Thus, another way to get information about the energy cascade is to deduce results directly from the Navier-Stokes model. Earliest attempts in this direction were made by Taylor (1935) and Karman and Howarth (1938). Both are based on the *two-point correlation functions*

$$R_{ij}(\mathbf{x},\mathbf{r},t) = \langle u_i(\mathbf{x}+\mathbf{r},t) u_j(\mathbf{x},t) \rangle \tag{2.7}$$

Once we apply the homogeneity hypothesis, R_{ij} can be considered independent from $\mathbf{x}$. As we have found for D_{ij} in the previous section, one consequence of the homogeneity is that R_{ij} can be expressed using two scalar functions $f(r,t)$, $g(r,t)$:

$$R_{ij}(\mathbf{r},t) = u'^2(g(r,t)\delta_{ij} + [f(r,t) - g(r,t)]\frac{r_i r_j}{r^2}$$

where u' is related to R_{ij} by the correlation in the origin

$$R_{ij}(0,t) = \langle u_i u_j \rangle = u'^2 \delta_{ij}$$

and it is used to obtain non.dimensional f, g, called *longitudinal* and *transversal correlation functions*. Again in parallel with properties of D_{ij}, the continuity equations implies $\frac{\partial R_{ij}}{\partial r_j} = 0$. The combination of this equation with the expression for R_{ij} leads to

$$g(r,t) = f(r,t) + \frac{1}{2} r \frac{\partial}{\partial r} f(r,t) \tag{2.8}$$

Thus, in isotropic homogeneous turbulence, the two-point correlation R_{ij} is completely determined by the longitudinal correlation function $f(r,t)$.

2.3.1 Karman-Howarth equation

The Karman-Howarth equation is an evolution equation for $f(r,t)$. As we are concerned about its consequences, we just sketch the steps of its derivations. More details can be found in [9].

We can write the time-derivative of $R_{ij}(\mathbf{r},t)$ as

$$\frac{\partial}{\partial t} R_{ij}(\mathbf{r},t) = \langle \frac{\partial}{\partial t} u_i(\mathbf{x}+\mathbf{r},t) u_j(\mathbf{x},t) \rangle + \langle u_i(\mathbf{x}+\mathbf{r},t) \frac{\partial}{\partial t} u_j(\mathbf{x},t) \rangle \tag{2.9}$$

So we can use the Navier-Stokes equation

$$\frac{\partial u_j}{\partial t} = -\frac{\partial (u_i u_j)}{\partial x_i} - \frac{1}{\rho} \frac{\partial p}{\partial x_j} + \nu \frac{\partial^2 u_j}{\partial x_i \partial x_i} \tag{2.10}$$

to eliminate the time derivatives in equation 2.9. Thus three terms arise, convection, pressure-gradient and viscous term. The most important point is that the convective term involves *two-point triple velocity correlations*

$$S_{ijk}(\mathbf{r},t) = \langle u_i(\mathbf{x},t) u_j(\mathbf{x},t) u_k(\mathbf{x}+\mathbf{r},t) \rangle.$$

In the same way as for R_{ij}, in isotropic turbulence S_{ijk} is uniquely determined by the longitudinal correlation defined as

$$k(r,t) = S_{111}(\mathbf{e}_1 r, t)/u'^3 = \langle u_1(\mathbf{x},t)^2 u_1(\mathbf{x}+\mathbf{e}_1 r, t) \rangle / u'^3 \tag{2.11}$$

As final result, using series expansion of $k(r,t)$, one obtains an exact equation for the evolution of $f(r,t)$

$$\frac{\partial}{\partial t}(u'^2 f) - \frac{u'^3}{r^4} \frac{\partial}{\partial r}(r^4 k) = \frac{2\nu u'^2}{r^4} \frac{\partial}{\partial r}(r^4 \frac{\partial f}{\partial r})$$

which we refer to as the *Karman-Howart equation.*

The fact that we would like to underline here is that equation by itself is not closed. Actually, while one tries to find the evolution equation for the 2nd moment $f(r,t)$, one other quantity is involved: the third moment $k(r,t)$. One idea would be to find another evolution equation, for $k(r,t)$; but it is shown that the fourth moment would be involved. And so on. This term $k(r,t)$ comes from the inertial term in Navier-Stokes. Consequently, in Karman-Howart model, it is the one responsible for the energy transfer form larger to smaller scales, in the Richardson cascade. It is also remarkable that, if the probability distribution of $\mathbf{v}$ is a Gaussian, the third moment would be zero, as all odd moments. In this case, the closure problem would not exist. Hence, the energy cascade process depends on *non-Gaussian aspects* of the velocity field.

2.3.2 The Kolmogorov $\frac{4}{5}$ law

The same result is often presented in a different way. Actually, if we integrate the Karman-Howart equation we obtain the so called *Kolmogorov equation*:

$$\frac{3}{r^4}\int_0^r s^4 \frac{\partial}{\partial t} D_{LL}(s,t)\, ds \;=\; 6\nu \frac{\partial D_{LL}}{\partial r} - D_{LLL} - \frac{4}{5}\varepsilon r \tag{2.12}$$

which is here expressed in terms of the structure function D_{LLL}

$$D_{LLL}(r,t) = \langle [u_1(\mathbf{x}+\mathbf{e}_1 r, t) - u_1(\mathbf{x},t)]^3 \rangle \tag{2.13}$$

Here we just note a further consideration: Kolmogorov also argued that the unsteady term is zero in locally isotropic turbulence. Thus, in the inertial range where the viscosity is negligible, we obtain the *Kolmogorov $\frac{4}{5}$ law*:

$$D_{LLL} = -\frac{4}{5}\varepsilon r \tag{2.14}$$

Furthermore, Kolmogorov also argued that the skewness of the structure function

$$S' = \frac{D_{LLL}(r,t)}{D_{LL}(r,t)^{3/2}}$$

is constant. This allows to write D_{LL} as a function of ε and r:

$$D_{LL}(r,t) = (\frac{-4}{5S'})^{2/3} (\varepsilon r)^{2/3}$$

It is found that the result is the same as the prediction from the similarity hypothesis, see equation 2.6. It is therefore a proof of the consistency between the Kolmogorov hypothesis and Navier-Stokes equation.

2.4 Fourier domain

A further insight in turbulent behavior is gained by the use of Fourier modes. In this section we first introduce the notation that will be used in the following, and then we present the equations of fluid-dynamics in the spectral domain.

Let's consider a cube in the physical space, where the side L is large compared to the the integral scale. Suppose that the turbulent velocity field such that:

- the mean velocity is zero;
- the velocity field is spatially periodic of period L:

$$\mathbf{u}(\mathbf{x} + L\mathbf{N}, t) = \mathbf{u}(\mathbf{x}, t)$$

  for all vectors $\mathbf{N}$, for all t.

This allows us to describe the field in terms of Fourier series. The lowest wave-number is $k_0 = \frac{2\pi}{L}$. In the direction x_j, the n_j*-th Fourier mode* is written as

$$e^{ik_0 n_j x_j}$$

. The *wave-number vector* $\mathbf{k} = k_0\mathbf{n} = k_0(\mathbf{e}_1 n_1 + \mathbf{e}_2 n_2 + \mathbf{e}_3 n_3)$ allows a more compact form for the three-dimensional Fourier modes:

$$e^{i\mathbf{k}\cdot\mathbf{x}} = e^{ik_0 n_1 x_1} e^{ik_0 n_2 x_2} e^{ik_0 n_3 x_3}$$

The modes form an orthonormal system. For a generic periodic function $g(\mathbf{x})$ we write its *Fourier series*

$$g(\mathbf{x}) = \sum_{\mathbf{k}} e^{i\mathbf{k}\cdot\mathbf{x}} \hat{g}(\mathbf{k}) \tag{2.15}$$

where $\hat{g}(\mathbf{k})$ is the Fourier coefficient at wave-number $\mathbf{k}$. The Fourier coefficient of $g(\mathbf{x})$ can be determined from the projection

$$\hat{g}(\mathbf{k}) = \langle g(\mathbf{x}) e^{-i\mathbf{k}\cdot\mathbf{x}} \rangle_L$$

where the notation $\langle\cdot\rangle_L$ stands for the integration on the cube of size L. Given a function $g(\mathbf{x})$, the operator which determines the coefficient of the Fourier mode relative to wave-number is indicated as

$$\mathbf{F}\{g\}(\mathbf{k}) = \langle g(\mathbf{x}) e^{-i\mathbf{k}\cdot\mathbf{x}} \rangle_L = \frac{1}{L^3} \iiint_0^L g(\mathbf{x}) e^{-i\mathbf{k}\cdot\mathbf{x}} \, dx_1 \, dx_2 \, dx_3 \tag{2.16}$$

In the particular case of our velocity vector field we write the Fourier series

$$\mathbf{u}(\mathbf{x},t) = \sum_{\mathbf{k}} e^{i\mathbf{k}\cdot\mathbf{x}}\hat{\mathbf{u}}(\mathbf{k},t) \tag{2.17}$$

where the velocity coefficients are

$$\hat{u}_j(\mathbf{k},t) = \mathbf{F}\{u_j(\mathbf{x},t)\}(\mathbf{k}). \tag{2.18}$$

Note that, as the Fourier modes are deterministic and time-independent, all the time dependent and random nature of the turbulent flow is carried out by the Fourier coefficients.

Using the rules of derivatives and transforms, one can write the continuity and the Navier-Stokes equations in the Fourier domain. As the divergence of the vector $\mathbf{u}$ becomes

$$\mathbf{F}\{\frac{\partial u_j}{\partial x_j}\} = i\mathbf{k}\cdot\hat{\mathbf{u}},$$

the continuity equation assumes the form:

$$\mathbf{k}\cdot\hat{\mathbf{u}} = 0. \tag{2.19}$$

This equation just states that the vector $\hat{\mathbf{u}}$ is normal to the vector $\mathbf{k}$.

Now let's consider the Navier-Stokes equation

$$\frac{\partial u_j}{\partial t} + \frac{\partial (u_j u_k)}{\partial x_k} = \nu\frac{\partial^2 u_j}{\partial x_k \partial x_k} - \frac{1}{\rho}\frac{\partial p}{\partial x_j}$$

and apply the operator $\mathbf{F}\{\}(\mathbf{k})$ term by term. For the time derivative we obtain

$$\mathbf{F}\{\frac{\partial u_j}{\partial t}\} = \frac{\partial \hat{u}_j}{\partial t}$$

while the viscous term becomes

$$\mathbf{F}\{\nu\frac{\partial^2 u_j}{\partial x_k \partial x_k}\} = -\nu k^2 \hat{u}_j;$$

the pressure gradient term can be written as

$$\mathbf{F}\{\frac{1}{\rho}\frac{\partial p}{\partial x_j}\} = -ik_j\hat{p}.$$

If we now call the Fourier coefficient of the convection term

$$\mathbf{F}\{\frac{\partial(u_j u_k)}{\partial x_k}\}(\mathbf{k},t) = \hat{G}_j(\mathbf{k},t)$$

and combine all these results, we obtain the Fourier form of the Navier-Stokes equation:

$$\frac{\partial \hat{u}_j}{\partial t} + \nu k^2 \hat{u}_j = -ik_j\hat{p} - \hat{G}_j \tag{2.20}$$

When this equation is multiplied by k_j, continuity equation (2.19) says that the left-hand side vanishes, leaving

$$k^2\hat{p} = ik_j\hat{G}_j \tag{2.21}$$

which is the Poisson equation, obtained from Navier-Stokes model, in wave-number space. The equation can be solved in order to obtain the pressure term:

$$-ik_j\hat{p} = \frac{k_j k_k}{k^2}\hat{G}_k. \tag{2.22}$$

What does the right-hand side term represent? Let's consider a generic vector $\hat{\mathbf{G}}$, and examine its orientation relative to the wave-number vector $\mathbf{k}$. Obviously, $\hat{\mathbf{G}}$ can be decomposed into a component $\hat{\mathbf{G}}^{\parallel}$ parallel to $\mathbf{k}$, and a component $\hat{\mathbf{G}}^{\perp}$ normal to $\mathbf{k}$. Being $\mathbf{e} = \mathbf{k}/k$ the unit vector in the direction of $\mathbf{k}$, one has

$$\hat{\mathbf{G}}^{\parallel} = \mathbf{e}(\mathbf{e}\cdot\hat{\mathbf{G}}) = \mathbf{k}(\mathbf{k}\cdot\hat{\mathbf{G}})/k^2 = \frac{k_j k_k}{k^2}\hat{G}_k$$

So, coming back to equation (2.22), the pressure term exactly balances $-\hat{\mathbf{G}}^{\parallel}$, the component of $-\hat{\mathbf{G}}$ in the direction of $\mathbf{k}$. This also implies that what remains in the right-hand side of equation (2.20) is $\hat{\mathbf{G}}^{\perp} = (\delta_{ij} - \frac{k_j k_k}{k^2})\hat{G}_k$:

$$\frac{\partial \hat{u}_j}{\partial t} + \nu k^2 \hat{u}_j = -\hat{\mathbf{G}}^{\perp}. \tag{2.23}$$

We usually denote the projection operator as $P_{ij} = (\delta_{ij} - \frac{k_j k_k}{k^2})$. Finally, we can express $\hat{G}_j(\mathbf{k},t)$ in terms of $\hat{\mathbf{u}}_{\mathbf{k}}$; simple calculations lead to

$$\begin{aligned}\hat{G}_j(\mathbf{k},t) &= \mathbf{F}\{\frac{\partial}{\partial x_k}(u_j u_k)\}(\mathbf{k}) = ik_k\mathbf{F}\{u_j u_k\}(\mathbf{k}) \\ &= ik_k\sum_{\mathbf{k}'}\hat{u}_j(\mathbf{k}')\hat{u}_k(\mathbf{k}-\mathbf{k}')\end{aligned}$$

which can be substituted in (2.20) giving the final form of the evolution equation for $\hat{\mathbf{u}}(\mathbf{k}, t)$:

$$(\frac{\partial}{\partial t} + \nu k^2)\hat{u}_j(\mathbf{k}, t) = -ik_l P_{jk}(\mathbf{k}) \sum_{\mathbf{k}'} \hat{u}_k(\mathbf{k}')\hat{u}_l(\mathbf{k} - \mathbf{k}', t)$$

2.5 Velocity spectra

We have already defined a central quantity in the study of turbulence, the two-point velocity correlation

$$R_{ij}(\mathbf{r}, t) = \langle u_i(\mathbf{x} + \mathbf{r}, t)u_j(\mathbf{x}, t)\rangle$$

which is shown to be independent on $\mathbf{x}$ in the case of homogeneous turbulence. Furthermore, we assumed to consider only velocity fields with zero mean $\langle \mathbf{U}(\mathbf{x}, t)\rangle = 0$; thus R_{ij} plays a central role, being the next simplest statistic to consider. Its importance is made clear in the following.

2.5.1 Velocity spectrum tensor

Let's consider the covariance of two Fourier coefficients

$$\langle \hat{u}_i(\mathbf{k}', t)\hat{u}_j(\mathbf{k}, t)\rangle$$

It can be shown that this quantity is zero, i.e. the coefficients are uncorrelated, unless the two vectors $\mathbf{k}$ and $\mathbf{k}'$ have the property $\mathbf{k}+\mathbf{k}' = 0$. Therefore, the significative quantities are

$$\hat{R}_{ij}(\mathbf{k}, t) = \langle \hat{u}_i(-\mathbf{k}, t)\hat{u}_j(\mathbf{k}, t)\rangle \tag{2.24}$$

It can also be shown that these $\hat{R}_{ij}(\mathbf{k}, t)$ are the Fourier coefficients of the two-point velocity correlation:

$$\hat{R}_{ij}(\mathbf{k}, t) = \mathbf{F}\{R_{ij}(\mathbf{x}, t)\}(\mathbf{k}) \tag{2.25}$$

The *velocity spectrum tensor* is defined by

$$\Phi_{ij}(\mathbf{k}, t) = \sum_{\bar{\mathbf{k}}} \delta(\mathbf{k} - \bar{\mathbf{k}})\hat{R}_{ij}(\bar{\mathbf{k}}, t) \tag{2.26}$$

(note that the notation has changed: the integer wave-number vector is now $\bar{\mathbf{k}}$, while $\mathbf{k}$ is a continuous wave-number variable). Evidently, the two-point correlation and the velocity spectrum tensor form a Fourier pair:

$$\Phi_{ij}(\mathbf{k}) = \frac{1}{(2\pi)^3} \iiint_{-\infty}^{\infty} R_{ij}(\mathbf{r}) e^{-i\mathbf{k}\cdot\mathbf{r}}\, d\mathbf{r} \tag{2.27}$$

$$R_{ij}(\mathbf{r}) = \iiint_{-\infty}^{\infty} \Phi_{ij}(\mathbf{k}) e^{i\mathbf{k}\cdot\mathbf{r}}\, d\mathbf{k} \tag{2.28}$$

The velocity spectrum tensor represents the Reynolds-stress density in wave-number space: actually, $\Phi_{ij}(\mathbf{k})$ represents the contribution from the Fourier mode $e^{i\mathbf{k}\cdot\mathbf{x}}$ to the Reynolds stress $\langle u_i u_j \rangle$. The subscripts ij give the directions of the velocity in physical space. The wave-number direction $\mathbf{k}/|\mathbf{k}|$ give the direction, in physical space, of the Fourier mode; the wave-number magnitude $|\mathbf{k}|$ is associated to the length-scale of the mode $l = \frac{2\pi}{|\mathbf{k}|}$.

By noting that it is possible to write

$$\langle \frac{\partial u_i}{\partial x_k} \frac{\partial u_j}{\partial x_l} \rangle = \iiint_{-\infty}^{\infty} k_k k_l \Phi_{ij}(\mathbf{k}) e^{i\mathbf{k}\cdot\mathbf{r}}\, d\mathbf{k}$$

also the dissipation rate can be expressed using the velocity-spectrum tensor: we have

$$\varepsilon = \iiint_{-\infty}^{\infty} \nu k^2 \Phi_{ij}(\mathbf{k}) e^{i\mathbf{k}\cdot\mathbf{r}}\, d\mathbf{k} \tag{2.29}$$

2.5.2 Energy spectrum function

Instead of using the second-order tensor Φ_{ij}, a simpler, though less complete instrument is the *energy spectrum function E(k)*. This is defined starting from Φ_{ij} and removing all directional information. The information about the velocity field directions is lost by considering half the trace $\frac{1}{2}\Phi_{ii}$. The information about the direction of the Fourier modes is deleted by integrating over shells $S(k)$ of wave-number with the same magnitude $|\mathbf{k}| = k$. The resulting definition is

$$E(k) \;=\; \oint \frac{1}{2}\Phi_{ii}(\mathbf{k})\, dS(k) \;=\; \iiint_{-\infty}^{\infty} \frac{1}{2}\Phi_{ii}(\mathbf{k}) \delta(|\mathbf{k}| - k)\, d\mathbf{k} \tag{2.30}$$

Note that integration of $E(k)$ over all k is the same of integration of $\frac{1}{2}\Phi_{ii}$ over all $\mathbf{k}$. Thus we can obtain the turbulent kinetic energy as

$$\mathsf{k} = \int_0^\infty E(k)\, dk \tag{2.31}$$

and the dissipation as

$$\varepsilon = \int_0^\infty 2\nu k^2 E(k)\, dk \tag{2.32}$$

As we said before, in general there is a loss of information passing from Φ_{ij} to $E(k)$. But it can be shown that, if the turbulence is *isotropic*, Φ_{ij} is completely determined by $E(k)$. Actually, for the isotropy hypothesis, all the directional information is carried by $\mathbf{k}$; as a consequence we can write the generic second order tensor formed from $\mathbf{k}$ as

$$\Phi_{ij}(\mathbf{k}) = A(k)\delta_{ij} + B(k)k_i k_j$$

where $A(k)$ and $B(k)$ are scalar functions. Simple integrations over the generic shell of radius k lead to

$$E(k) = 6\pi k^2 A(k) + 2\pi k^4 B(k);$$

while the use of the continuity equation (2.19) leads to $\mathbf{k}\cdot\Phi = 0$ and therefore to write

$$B(k) = -A(k)/k^2.$$

From these equations one obtains that, in isotropic turbulence, the velocity spectrum tensor can be written as

$$\Phi_{ij}(\mathbf{k}) = \frac{E(k)}{4\pi k^2}(\delta_{ij} - k_i k_j) \tag{2.33}$$

stating its dependence on the energy spectrum.

2.5.3 One-dimensional spectra

As we have described, the nature of turbulence is intrinsically three-dimensional. It follows that all spectra and functions we need to describe this phenomenon must carry three-dimensional information. Although, if the turbulence is isotropic, one can define a one-dimensional spectrum and than show its relationship with $\Phi_{ij}(\mathbf{k})$ and $E(k)$ (see [14], [9]) .

The *one-dimensional spectra* $E_{ij}(k_1)$ (in the direction k_1) is defined as twice the one-dimensional Fourier transform of $R_{ij}(\mathbf{e}_1 r_1)$:

$$E_{ij}(k_1) = \frac{1}{\pi}\int_{-\infty}^{\infty} R_{ij}(\mathbf{e}_1 r_1) e^{-ik_1 r_1}\, dr_1 \tag{2.34}$$

If we consider for example the element $R_{22}(\mathbf{e}_1 r_1)$, which is a real and even function of r_1, also the the 1D spectrum is real and even; thus we can write

$$E_{22}(k_1) = \frac{2}{\pi}\int_{0}^{\infty} R_{22}(\mathbf{e}_1 r_1) cos(k_1 r_1)\, dr_1$$

with the inverse formula

$$R_{22}(\mathbf{e}_1 r_1) = \int_{0}^{\infty} E_{22}(k_1) cos(k_1 r_1)\, dk_1$$

It follows that, setting $r_1 = 0$ we obtain

$$R_{22}(0) = \int_{0}^{\infty} E_{22}(k_1)\, dk_1 = \langle u_2^2 \rangle$$

(so that's why a factor 2 was added in the definition).

The relation with the velocity spectrum tensor is given by

$$E_{22}(k) = 2\iint_{-\infty}^{\infty} \Phi_{22}(\mathbf{k})\, dk_2 dk_3 \tag{2.35}$$

Note that the wave-number vectors which contribute to the integral are all wave-number vectors in the plane $\mathbf{k}\cdot\mathbf{e}_1 = k_1$, so they can have a magnitude $|\mathbf{k}|$ even larger than k_1.

Finally, let's show that, in isotropic turbulence, one can describe the one-dimensional spectrum in terms of $E(k)$. Actually, if we write the equation for $E_{11}(k_1)$ and we write Φ as a function of $E(k)$ using equation (2.33), we obtain

$$E_{11}(k_1) = \iint_{-\infty}^{\infty} \frac{E(k)}{2\pi k^2}(1 - \frac{k_1^2}{k^2})\, dk_2 dk_3$$

This is the integration over the plane $k_1 = cost$, of a function which is radially symmetric about the k_1 axis. Introducing the radial coordinate $k_r^2 = k_2^2 + k_3^3 = k^2 - k_1^2$, and noting that $k_r\, dk_r = k\, dk$ the equation can be rewritten as

$$E_{11}(k_1) = \int_{k_1}^{\infty} \frac{E(k)}{k}(1 - \frac{k_1^2}{k^2})\, dk \tag{2.36}$$

It is not hard to show that $E_{11}(k_1)$ is a monotonically decreasing function of k_1; the maximum value is reached at $k_1 = 0$, irrespective of the shape of $E(k)$. Finally, this formula can be inverted, in order to obtain $E(k)$ in dependence of the 1D spectrum:

$$E(k) = \frac{1}{2}k^3\frac{d}{dk}(\frac{1}{k}\frac{dE_{11}(k)}{dk}) \tag{2.37}$$

We underline once again that this relation is valid only in the case of isotropic turbulence. In this case, it is a very useful tool, because it allows to measure the 1D correlation only, and than to desume the energy spectrum properties. We will often use this relationship in our experimental considerations in the next chapters.

2.5.4 The $-\frac{5}{3}$ law

In this section we introduce the famous -$\frac{5}{3}$ *Kolmogorov law*, which will be a central point in our discussion, and a constant reference for comparison of experimental results. This law essentially states that, at sufficiently high Reynolds numbers, the high wave-number portion of the velocity spectra assumes a form that is universal, i.e. does not depend of the flow under consideration. This low is deduced by applying the Kolmogorov hypothesis to the second-order statistics, as we made in previous sections, and than considering Fourier transforms; here we follow a simpler thus less rigorous way: we apply the K41 hypothesis directly to the spectra (as in [14]).

The first similarity hypothesis tells us that, at high Reynolds number, the statistics pertaining to the universal range must depend uniquely only on ε and ν. As a consequence, in this range (say $k > k_{EI}$) the shape of the function $E(k)$ must be universal, and determined by k, ε, and ν. Thus, we can think to use ε and ν to make $E(k)$ non-dimensional: we obtain

$$E(k) = (\varepsilon\nu^5)^{1/4}\varphi(k\eta) \tag{2.38}$$

where $\varphi(k\eta)$ is a universal non-dimensional function, called the *Kolmogorov spectrum function*. One other option is to use ε and k to make the energy spectrum non-dimensional; in this case we obtain

$$E(k) = \varepsilon^{2/3}k^{-5/3}\Psi(k\eta) \tag{2.39}$$

where $\Psi(k\eta)$ is the *compensated Kolmogorov spectrum function*. These equations hold in the universal equilibrium range, that is $k > k_{EI}$ which corresponds to $k\eta > \frac{2\pi\eta}{l_{EI}}$. The relationship between these two functions follows immediately from the definitions: actually

$$\Psi(k\eta) = \varepsilon^{2/3} k^{-5/3} \varphi(k\eta).$$

If we focus our attention on the inertial subrange, i.e. $k_{EI} < k < k_{DI}$, we can apply the second similarity hypothesis. It states that the statistics pertaining to this range have a universal form determined by ν, independent of ε. The consequence is that the energy spectrum function assumes thus the form

$$E(k) = \varepsilon^{2/3} k^{-5/3} \cdot C \tag{2.40}$$

where C is a universal constant. It is a particular case of eq. (2.39), with $\Psi = C$. This is the well-known $\frac{5}{3}$ *Kolmogorov spectrum*, which predicts a *power-law* energy spectrum function. This assertion has been tested for a long time; experimental data essentially agree with itand support the value $C = 1.5$ for the universal constant.

It is also easily checked out that the power-low form of the 3D spectrum is consistent with a power-low 1D spectrum $E_{11}(k_1)$. If we assume that, for some range of wave-numbers, the 1D spectrum has the form

$$E_{11}(k_1) = C_1 A k_1^{-p} \tag{2.41}$$

where C is a constant and A is a normalization factor, the resulting form of $E(k)$ is obtained from equation (2.37)

$$E(k) = CAk^{-p} \tag{2.42}$$

where $C = \frac{1}{2}(1+p)C_1$. This completely matches with the Kolmogorov power-low spectrum, where $p = \frac{5}{3}$; and leads to $C = \frac{18}{55}C \sim 0.49$.

Chapter 3

Intermittency

3.1 Definition of intermittency

The velocity field $\mathbf{U}(\mathbf{x}, t)$ in a turbulent flow is a random process. In laboratory experiments one can measure realizations of this process in order to get statistical information. For example, one can place a probe in a wind tunnel to measure the velocity field in a fixed point $\mathbf{x}_0$ and consider the process $\mathbf{U}_{\mathbf{x}_0}(t)$. Surprisingly, the qualitative behavior of $\mathbf{U}_{\mathbf{x}_0}(t)$ could *depend on the point* $\mathbf{x}_0$. We have said that, in homogeneous turbulence, the behavior of the random velocity field is *quasi-gaussian*, i.e. the low moments are close to Gaussian moments. It was observed that there are areas where the signal $\mathbf{U}_{\mathbf{x}_0}(t)$ is almost null, except for the presence of high, isolated *peaks*, showing a non-Gaussian behavior. Such a signal is said to be *intermittent*. Historically, the concept of intermittency has been introduced to indicate such an unexpected time evolution of the velocity field. Thus we say that a random signal $v(t)$ is said to be *intermittent* if it *displays activity during only a fraction of time, which decreases with the scale under consideration.*

In order to give a quantitative measure of this fact, some criteria has been introduced. For homogeneous isotropic turbulence, a formal criterion is given by Frisch [7], and it is obtained by observing the influence of a filtering operation on the kurtosis of such field. Let's consider the high-pass filtered signal $v_\Omega^>(t)$ where the filter-frequency is Ω; we can vary such a threshold and measure the kurtosis in these different cases. The signal $v(t)$ is intermittent if the kurtosis of this filtered signals *grows without bounds when* $\Omega \to \infty$.

Formally

$$K(\Omega) = \frac{\langle (v_\Omega^>(t))^4 \rangle}{\langle (v_\Omega^>(t))^2 \rangle^2} \to +\infty \ , \qquad \Omega \to +\infty \tag{3.1}$$

This is justified by the fact that the inverse of kurtosis is a measure of the fraction of time during which the high-pass filtered signal is active. Actually, consider a signal $v(t)$, and a second signal $v_\gamma(t)$ obtained from the first one by setting it to 0 for a fraction of time $1-\gamma$. Thus, if v is active for a time T, v_γ is active for a time γT. It can be shown that, if the moments exist, they are related by $\langle v_\gamma^2 \rangle = \gamma \langle v^2 \rangle$ and $\langle v_\gamma^4 \rangle = \gamma \langle v^4 \rangle$. If we now compute the kurtosis, we obtain

$$K_\gamma = \frac{\langle v_\gamma^4 \rangle}{\langle v_\gamma^2 \rangle^2} = \frac{1}{\gamma} \frac{\langle v^4 \rangle}{\langle v^2 \rangle^2}$$

which is a quantity that increases if γ decreases. As measure of intermittency we can thus consider the kurtosis, or other ratios of moments. Ratios of odd moments should be avoided as they can be zero for symmetry reasons.

A basic assumption of Kolmogorov theory is *self-similarity* of the velocity field in the inertial range. A self-similar signal is *not* intermittent. Actually, consider a signal $v(t)$ with self-similar increments, where the scaling exponent is h. We high-pass filter a self-similar signal with frequency Ω, and then with frequency $\lambda\Omega$; it can be shown that

$$v_{\lambda\Omega}^> = \lambda^{-h} v_\Omega^> \text{ in law}$$

Thus, when we calculate the kurtosis, the numerator anch the denominator are multiplied by the same factor λ^{-4h}, so this contribution disappear in the ratio $K(\Omega)$, leaving the kurtosis unchanged.

Note also that, if we modify a gaussian field with a linear operator, such as a high-pass filter, the distribution of the new field is again gaussian, thus it has kurtosis equal to 3 (independent of Ω).

Thus the K41 theory assume a *non intermittent* random velocity field. Is this assumption totally correct? The experimental results agree in the fact that intermittent features can appear when a signal is high-pass filtered, and the filter frequency is let growing. This intermittency becomes conspicuous *only when the scale associated to* Ω *are comparable or smaller to Kolmogorov dissipation scale*. Thus *intermittency is a characteristic of dissipation range*, not contradicting self-similarity of the inertial range, as in K41 theory. Thus,

the dissipation range intermittency is now a matter of fact. The existence of intermittency in the inertial range is a subtler question. Above all, it would invalidate the Kolmogorov theory.

3.2 Inertial range intermittency

In the K41 approach to turbulence, a central assumption is the existence of a range, the inertial range, in which the dissipation rate of energy ε becomes asymptotically independent of the viscosity ν. This assumption needs to be carefully considered, because the energy dissipation is an intrinsically viscous process. The classical answer is that the energy cascades from larger to smaller eddies, with negligible loss. When it reaches eddies small enough, the viscosity becomes effective, and the energy is dissipated in heat. The smaller is the viscosity, the longer is the cascade, but the dissipation threshold is always reached; the dissipation rate is controlled by the the energy quantity fed into the system.

As a consequence, the rate of energy transfer from one eddy to another of smaller size, should be the same for all scales, until the Kolmogorov dissipative scale η. Quantitatively, on dimensional ground the dissipation rate of one eddy of size l and velocity u_l should be

$$\varepsilon \sim u_l^3/l; \tag{3.2}$$

this implies

$$u_l \sim (\varepsilon l)^{1/3} \tag{3.3}$$

We have seen in previous section that this model leads to the $k^{-5/3}$ energy spectrum, and to the estimate of the dissipative scale as $\eta = (\nu/\varepsilon)^{1/4}$.

During the 50's evidence started to accumulate that significant deviations from the Kolmogorov scaling (3.3) are present. At any given instant, differences from both (3.2) and (3.3) equation can be expected, and they cannot be derived from the cascade hypothesis. These phenomena of local variability of the dissipation go under the name of *anomalous scaling*, or *(inertial range) intermittency*.

The estimation had been made on the second order longitudinal structure function D_{LL} (see section 2.2.2). More generally, we can consider the longitudinal velocity increments

$$\delta v_L(\mathbf{x}, \mathbf{r}) = [\mathbf{U}(\mathbf{x} + \mathbf{r}) - \mathbf{U}(\mathbf{x})] \cdot \frac{\mathbf{r}}{r} \tag{3.4}$$

as the projection of the increment onto the distance vector $\mathbf{r}$, and use them to define the *structure function of order p*:

$$S_p(r) = \langle \delta v_L(\mathbf{x}, \mathbf{r})^p \rangle \tag{3.5}$$

The K41 theory predicts that the structure function of order p scales with an exponent $p/3$ over the inertial range. This relation has been tested experimentally for a long time. It turns out that it is *not exactly true*. In fact, structure functions follow a power-low in the inertial range:

$$S_p(r) \sim r^{\zeta_p} \tag{3.6}$$

but the values of ζ_p, the so-called exponents of the structure function, do not match exactly the K41 prediction. For example, the values found for ζ_2 are approximately 0.7-0.73, instead of $\frac{2}{3} = 0.66$; and we also have $zeta_6 \approx 1.8$ instead than 2.

The fact that such deviations from the Kolmogorov lows are present, even if not conspicuous, make plausible that a correction to the K41 theory of inertial range. Intermittency theory developed in the last years, essentially through the development of phenomenological descriptions which accept the idea of the energy cascade proposed by Richardson, but try to incorporate a form of intermittency with the help of new models that consider the *fractal dimension* of eddies, in order to obtain an analytic form for the function ζ_p. We don't concern ourselves here with this models. In the next section we complete the picture of intermittency by looking at those features that are of interest for our discussion; for a complete descriptions of these recent trends in intermittency, we refer to [7], [13] , [5], [6].

3.3 Localness and the presence of vortex filaments

From a physical point of view, the problem of the K41 theory is the assumption of a dissipation which is uniform throughout the turbulence. As we pointed out, the most important quantity in the Richardson cascade model is the energy dissipation rate ε. Experiments show that, in a turbulent field, it is possible to find patches of intense small eddies, with consequently a high dissipation, and other patches involving little dissipation. Each patch is made of eddies with different scales, down the cascade. As the eddies get smaller,

the fraction of volume in which they are active decreases. As a consequence, the rate of energy transfer per unit mass must *increase* as the length-scales get smaller, or as the wave-number get higher. This considerations affects the derivation of the Kolmogorov lows, with the consequent arising of intermittency.

Thus, the main problem in the K41 theory is that it doesn't take into account the *localness* of the dissipation rate ε. But where exactly does this localness arise? Physically, we have already pointed out that a central role in the generation of smaller scales is played by the vortex stretching, which essentially increases the magnitude of vorticity and reduce the cross-section of vortices, also generating three-dimensional structures. Looking back to the K41 theory, it must be noted that Kolmogorov's work *ignored any structure* which can be present in the flow.

As long as these *coherent structures* are confined in the energy-containing range, their presence does not affect the inertial-range universality theory. Traditional visualization of flows, where the velocity of the field is recorded by a probe, does not show the presence of any small-scale structure. However, in the last thirty years discrepancies from the theoretical predictions have been found, and they have led to the suggestion that smaller scales have fractal properties. However, all the fractal and multi-fractal models proposed so far have a probabilistic nature; no physical assumption about the geometry of the small scales is made. Nevertheless, there is growing evidence of the presence of *structures of non-trivial geometry* at the level of small scales, in the inertial range and probably down to the Kolmogorov range. Above all, numerical experiments show that turbulence generates a tangle of intense elongated structures, known as **vortex filaments**. Such simulations indicate that vortex filaments are regions of *high vorticity* and *low dissipation*; this property can be used to visualize the structures in a direct experiment. Their presence and nature is still a matter of research. Vortex filaments are modelled essentially as *elongated tubes* with an approximately circular cross-section. The vortices are long; a length is hard to define, and depending on the definition, it can reach the order of integral scale [5]. The cross section diameter is of the order of the Kolmogorov scale ($R \approx 5\eta$ according to Jimenez). The definition of such structures makes sense, because they act as essentially independent of the weaker fluctuations that surround them. The vorticity is stronger in the center of the filament, and goes down with the radius; a model of distribution of the axial vorticity in the radial direction

can be given by a Gaussian profile

$$\omega = \omega_{MAX} exp(\frac{-r^2}{R^2}).$$

These filaments are observed to be instable. "When a vortex tube opens up, the strength of vorticity decreases; the longest filaments can thus transform into large, long-lived eddies" ([7], pag.185).

Also the matter of the formation of vortex filaments is still an open problem. Some authors point out that they seem to develop in regions in which large structures create a thin layer with both stretching and shearing. Jimenez propose that they are formed when stretched vortex sheets, in which vorticity becomes much stronger than in the neighborhood, decouple from the background and roll from themselves. Three dimensionality is gained by a sort of axial strain. Longer filaments can arise from the fusion of short pieces, due to a sort of axial homogenisation process. It has also been proposed that some of them can be generated near solid boundaries, where vorticity can be generated.

Clearly, more remains to be understood about the behavior of these kind coherent structures into a turbulent field, and about their statistical properties and influence on the spectra of turbulence. We will try to gain some information about their presence and distribution among the scales, from the point of view of a new quantity that will be defined in the next chapter.

3.4 Intermittency indices

Today there is a little doubt that intermittency influences the dynamics of turbulence. However, in the general case of a inhomogeneous flow, a operative measure of intermittency itself is hard to give. According to the physical considerations of the previous section, a signature of intermittency can be found in the vortex stretching and filaments. A measure of vortex stretching is given by the skewness of the velocity derivatives, as pointed out by Frisch ([7]). The problem is that the measure of the velocity differences, which allow to evaluate the derivatives, requires very accurate experiments to get reliable results.

Thus, the most used index of intermittency is the study of statistics of the velocity field, and the comparison to the ideal Gaussian process. One can evaluate the probability density function and compare it to the normal function. Or alternatively, one can evaluate the moments of the process. This

is the approach followed in our work. The results we present on intermittency comes from the study of the third and fourth standardized moments, the skewness S and the kurtosis K of the velocity field. Thus our study of intermittency deals with the non-Gaussian features of the flow. Actually, recalling the original definition of intermittency, the intuitive meaning can be understood as follows. We said that an intermittent signal displays activity during only a fraction of time. This means that the small turbulent structures *are not* distributed everywhere, in a "homogeneous" way, in the flow domain. This inhomogeneity and localness of the small eddies generates the intermittent signal $\mathbf{U}_{\mathbf{x}_0}(t)$ with isolated peaks; and it is evident that such a signal cannot be Gaussian. In conclusion, an estimation of intermittency is usually obtained by observing these two parameters: the skewness S, and the kurtosis K compared by the Gaussian value: $K - 3$.

Chapter 4

Definition of a small scale localization criterion

4.1 Computational simulation problems

Turbulence itself is a non-linear problem. Phenomena like turbulent combustion or turbulent reacting flows are very important in modern science and technology, from propulsion system to energy generation. In astrophysics, one usually has to deal with supersonic winds and jets, where velocities are about 400 km/s; in some cases, for example outflows from collapsed objects like black holes, jets can reach the speed of light. These extreme conditions, the presence of chemical reactions, for example, with heat release and change in the fluid density, add more non-linearity. The consequence is that one has to face serious modelling problems.

4.1.1 Numerical methods

The study of turbulence is known to be a difficult problem; an analytic approach requires more and more complex models, and also the assumption of hypothesis that simplify the model, with consequent loss of physical meaning. Instead, the hope is that the increasing power of computers can allow to calculate the properties of interest through computational simulations. After almost half a century, a wide range of numerical methods has been developed. A complete description of the numerical tools is beyond the aim of this discussion; we refer the interested reader to (POPE). Let us just say that there is a range of models that differ in level of description, computational cost and accuracy; and no all these methods can be applied to every situation.

In the following, we remind the guidelines for two of the most used methods: the *direct numerical simulation (DNS)*, and the *large-eddy simulation (LES)*

The Direct Numerical Simulation is conceptually the simplest possible approach, as it consists in solving the Navier-Stokes equations, with appropriate initial and boundary conditions. As a result, we obtain a *realization* of turbulent field, in which *all* the scales are resolved. This method is the most accurate, and it gives the best description of turbulence. However, its computational cost is extremely high. To give a rough idea of its requirements, let's say that the simulation box size must be large enough to represent the energy-containing motions; the grid spacing Δx must be small enough to describe the small scales. Thus, if N^3 is the number of grid nodes, it is clear that il must increase with the Reynolds number. This dependence can be found to be

$$N^3 \sim R_\lambda^{\frac{9}{2}}$$

Furthermore, the flow must evolve for a time long enough to reach the state of fully-developed turbulence (experience shows about four times the dissipation time scale $\tau = \mathsf{k}/\varepsilon$). Consideration about the convergence of the method (the CFL condition) force the time-step Δt to remain small. As a consequence, it can be shown that the number M of time steps usually required grows with the Reynolds number as

$$M \sim R_\lambda^{\frac{3}{2}}$$

(see POPE for the derivation of these relations). Thus we obtain that the number of operation grows approximately as $N^3 M \sim R_\lambda^6$. This means that, at the state of the art, accurate simulations for $R_\lambda \sim 10^3$ would take years to be completed! The increasing power of modern computers is expanding the range of Reynolds number for which DNS can be performed; but in general this approach is limited to flows of moderate Reynolds number.

In Large Eddy Simulations only the large scale motions are directly represented. These are the scales in which the effects of boundary conditions is present, thus they depend on the experiment, they are not universal. The effect of the smaller scales is modelled. The main conceptual steps are the followings. The velocity field is decomposed into the sum of a *filtered component* $\bar{\mathbf{U}}(\mathbf{x}, t)$, and a *residual or sub-gride scale component* $\mathbf{u}'(\mathbf{x}, t)$:

$$\mathbf{U}(\mathbf{x}, t) = \bar{\mathbf{U}}(\mathbf{x}, t) + \mathbf{u}'(\mathbf{x}, t)$$

Note that this filtering is conceptually different from the Reynolds decomposition: actually here $\bar{\mathbf{U}}(\mathbf{x}, t)$ is a random field, and in general the filtered residual is not zero, $\bar{\mathbf{u}}'(\mathbf{x}, t) \neq 0$.

The equation for the evolution of the filtered field is obtained from conservation equations. Here again, the momentum equation contains the presence of the residual velocity field, in the form of a *residual stress tensor*. This problem of closure is resolved with the help of a *model*; the most used is the eddy-viscosity model (see section 1.4.1). Then, the resulting evolution equations for $\bar{\mathbf{U}}(\mathbf{x}, t)$ are solved numerically. This provides a reliable approximation of the energy-containing range motions, while the effect of small scale is contained and described in the eddy-viscosity model. While the DNS is not applicable to high-Reynolds number flows, for its computational effort is expended on the dissipative scales, the LES approach avoid this computational cost, at the price of a less accurate description of small scales.

4.2 A new small scale localization criterion

The direct numerical simulation (DNS) of the Navier-Stokes system and of the other conservation equations can give complete information about the turbulent flow. Actually, DNS *should* resolve all the scales involved in the turbulent process, with no need of other model. Unfortunately, this approach can't be followed in most real cases. This is due to the actual state of technology, as the computer power does not allows a complete resolution of all scales involved in a real phenomenon of a certain complexity (like the ones previously described). Turbulent flows in nature involve very high Reynolds numbers. For example, in the case of astrophysical flows, we can have to handle Reynolds numbers that reach $10^{10} - 10^{13}$. Consequently, an enormous range of scales is produced. Direct numerical simulations of such flows can reproduce the largest scale behavior, but fails in the description of the development of turbulent motions and smaller scales. Thus in general, only the large scales can be simulated, and the LES approach is considered appropriate; with a consequent loss of information. Such information could be gained with the help of sub gride scales models. Thus a general purpose is to develop a method that allows the detection of small turbulence scales, such that the sub gride scale model can be introduced selectively. The aim of this section is to describe the definition of one of these tools.

4.2.1 Definition

The idea is to define and measure a quantity involved in the arising process of small scales. The definition of the function is

$$f(\mathbf{U}) = \frac{|\boldsymbol{\omega} \cdot \nabla \mathbf{U}|}{|\boldsymbol{\omega}|^2} \tag{4.1}$$

where $\mathbf{U}$ is the velocity field, and $\boldsymbol{\omega} = curl(\mathbf{U})$ is the vorticity vector.

The numerator of the function $|\boldsymbol{\omega} \cdot \nabla \mathbf{U}|$ is the *stretching-twisting term* that arises in the vorticity equation (see section 1.2). As we have shown, this term governs the *vortex stretching* and *twisting* phenomena, and it is responsible for the transmission of energy from larger to smaller scales. Note that this term is deeply related to *three-dimensionality* of the structures, as it is zero in two-dimensional flows. As $\nabla \mathbf{U}$ is a order-two tensor, $\boldsymbol{\omega} \cdot \nabla \mathbf{U}$ is a vector quantity; we take the magnitude of this quantity, in order to define a scalar parameter.

The denominator $|\boldsymbol{\omega}|^2$, the magnitude of vorticity, is also referred to as *enstrophy*, and it is a normalizing term.

With this definition, f depends on the total field $\mathbf{U} = \langle \mathbf{U} \rangle + \mathbf{u}$. As we want to avoid the dependence on laminar flow features, we can subtract the contributions of the mean velocity and vorticity flows. The new definition is

$$f(\mathbf{U}) = \frac{|(\boldsymbol{\omega} - \langle \boldsymbol{\omega} \rangle) \cdot \nabla (\mathbf{U} - \langle \mathbf{U} \rangle)|}{|(\boldsymbol{\omega} - \langle \boldsymbol{\omega} \rangle)|^2} \tag{4.2}$$

where, as usual, $\langle \cdot \rangle$ brackets represent average quantities. This definition makes sense only if we can prove a (statistical) link between this quantity and the presence of small scales in a homogeneous isotropic turbulence set of data. In other words, it is necessary to establish a relationship between the presence/absence of small scales and ranges of values which can/cannot be measured for f. If that happens, f can be considered a local indicator of the presence of small scales. This is what we would like to show in the next sections.

4.2.2 Values of f and localization criterion

First, the values of f have been measured on a fully resolved homogeneous isotropic incompressible turbulence, at a given time. The values obtained

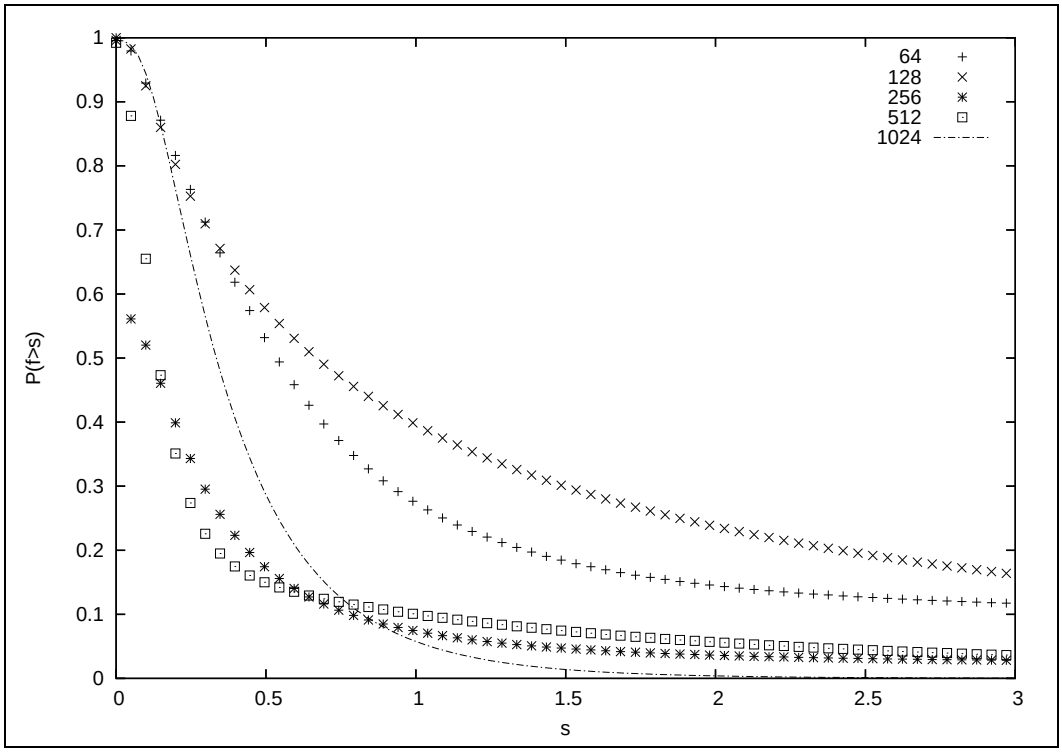

Figure 4.1: Comparison between the control functions of different LES fields. The *unresolved* fields are obtained on 64^3, 128^3, 256^3 and 512^3 cubes

are taken as representatives of a field in which also the dissipative scales have been resolved (see [4]). These data come from a DNS performed at CINECA on a 1024^3 grid. The Reynolds number Re_λ is about 280. These features make this set of data one of the most accurate simulation of high Reynolds number homogeneous isotropic turbulence obtained since now; thus we consider it our reference field.

Then, f is calculated over some under-resolved isotropic turbulence fields. Thus, the results are compared to obtain typical values for f.

Thus, the function f has been computed over the reference field. The range of values assumed by f is large; in some point can reach some hundreds. In order to obtain a criterion, a *threshold* x_t has been defined; thus the indicator parameter is related to *the probability that f assumes values grater than* x_t. We have plotted the results in fig.4.1.

It shows the cumulative distribution function (cdf) $F(s) = P(f \leq s)$ but

in the form

$$1 - F(s) = P(f > s).$$

In the following we will refer to this plot as the *control function* plot. This allows a more intuitive interpretation, as we will see. It has been found that the probability that $f > s_t \approx 2$ is very low, almost zero. Thus the value $f(\mathbf{u}) = 2$ can be considered as *the maximum value that f can reach* when the turbulence is simulated with a fine grain. On the contrary, when f is measured on unresolved turbulent fields, we have a non-zero probability associated to values *greater than 2*.

The small scale localization criterion can thus follow from these considerations. If in a simulation of a fully developed turbulent flow f assumes values grater than 2, then the flow must be considered *under-resolved*. In this case the activation of a LES method with a sub-grid scale term should be performed. Thus, we can consider the regions in which the values of f are higher than 2 as under-resolved regions, and select them for the application of the sub-gride scale model. This is a consequence of the definition of the function as

$$f(\mathbf{u}(\mathbf{x}))$$

so that it carries local information about the field.

Chapter 5

Test of the function over filtered fields

A criterion for the localization of small scales in turbulent flows has been proposed. It is based on the definition of a particular function which measures, in such a way the presence of vorticity and stretching and twisting of vortices. We now would like to further analyze the properties of this function. Actually, the numerator represents the vortex-stretching term, while the denominator is a measure of vorticity. The behavior of both terms have been studied in meany ways and using different approaches (see [5], [6]), above all in homogeneous isotropic turbulence. It can be interesting to study how they act together under the new point of view of this function f, trying to give a more physical interpretation of this quantity. In particular, we would like to understand and weight the influence the the different length scales, and the different coherent structures present in the flow have on f. In order to reach this aim, we want to obtain new fields from the original one using apposite filters; and then to apply the function f on these fields in order to figure out the contributions that the different structures must have on f. But first, some considerations about the reference field need to be pointed out.

5.1 A new reference field

As we already said, our analysis was carried out on a 1024^3 DNS field, obtained at $Re_\lambda = 280$. This field has been obtained by *forcing the turbulence*. Energy is injected at an average rate by keeping constant the energy of the two first wave-number shells. That is, the field is obtained by forcing the

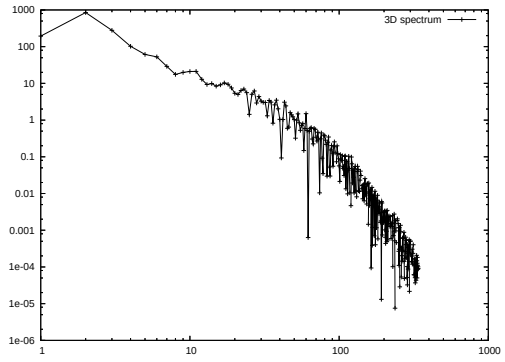

Figure 5.1: 3D energy spectrum of original field

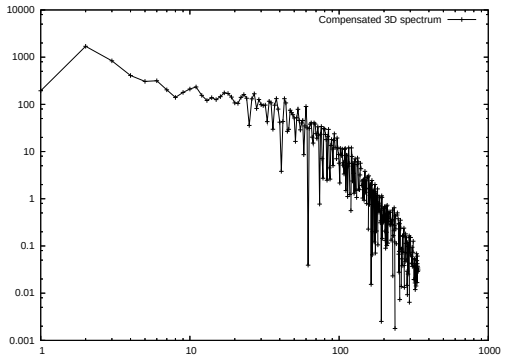

Figure 5.2: Compensated energy spectrum

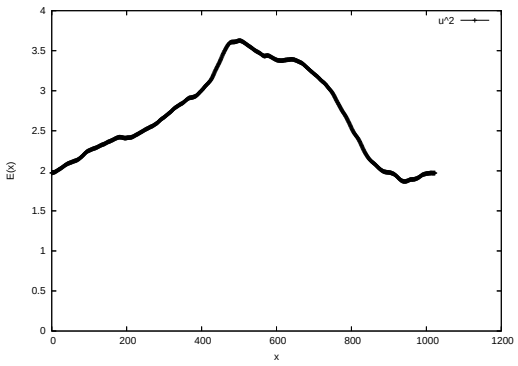

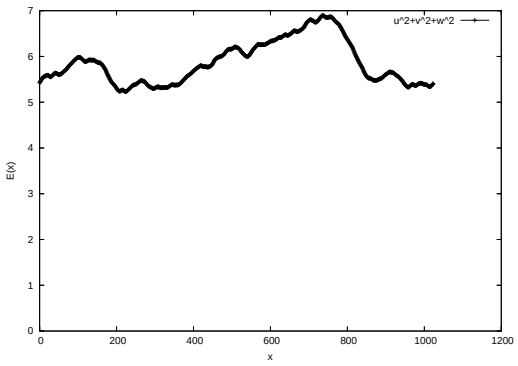

Figure 5.3: Energy inhomogeneity

contribution of structures whose wave-number magnitude is 1 and 2; thus, forcing the evolution behavior of the largest scales ([4]). This procedure is often used in the simulation of turbulent flows. Nevertheless, one thing about this method must be kept in mind: as a consequence, the large-scale statistics do not result isotropic, as they are expected to be. This happens to be exactly the case under consideration.

In fig.5.1 we show the energy spectrum of the original, unfiltered field. It extends until $k \sim 340$. Although the field is a 1024^3 simulation, higher wave-numbers are affected by aliasing error, thus that part of wave-length range ($k > 340$) does not contain reliable information. Looking at the central part of this spectrum, we can make the first considerations on our field. Actually, we note that the inertial range, subject to $-\frac{5}{3}$ low, seems to extend from $k \sim 5-10$ to $k \sim 30$. Actually in this range we can assume the compensated

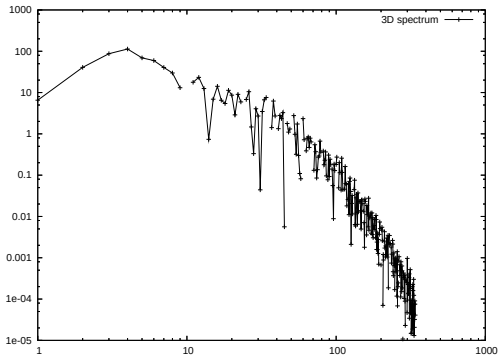

Figure 5.4: 3D energy spectrum, after removing the two initial shells

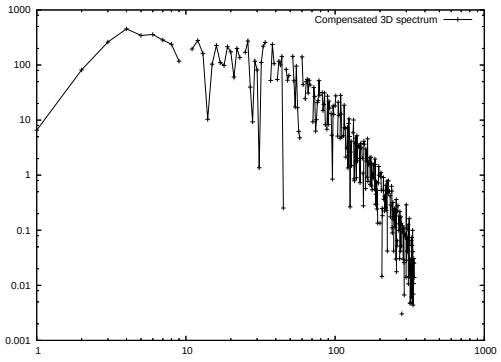

Figure 5.5: Compensated energy spectrum

spectrum to be *constant* (see section 2.5). It must be said that our definition of inertial range could be extended to $k \sim 70$, as we will see.

We now come back to the problem of large-scale inhomogeneity. We have got evidence of such a bias in the database. This comes from a check up of the energy homogeneity in the field. The total energy $u^2 + v^2 + w^2$ as a function of the space coordinate x results to be affected by inhomogeneity of 20%, as shown in figure 5.1. This inhomogeneity grows by considering the single contribute u^2. This could suggest that a sort of large-scale vorticity might be present. Although this inhomogeneity does not influences the smaller scale statistics, we try to mitigate this non-physical condition, as it could affect our analysis.

Thus, a new reference field was obtained, by filtering the contribution of those structures whose wave-number have a magnitude smaller than 2. This choice was made in order to balance the effect of the forcing of the field, which was carried out on the two smallest shells. The 3D spectrum of the modified field is shown in figures 5.4. The effect of the large scale forcing is now lighter, the energy contribution of the largest structure is more balanced in comparison to the rest of the structures. Thus, in the following, this new field will be used as a reference for filters and further results.

5.2 Filtering the elongated structures

From now on, our considerations will be made above all from the wave-number point of view. Actually, the filters have been thought to affect the

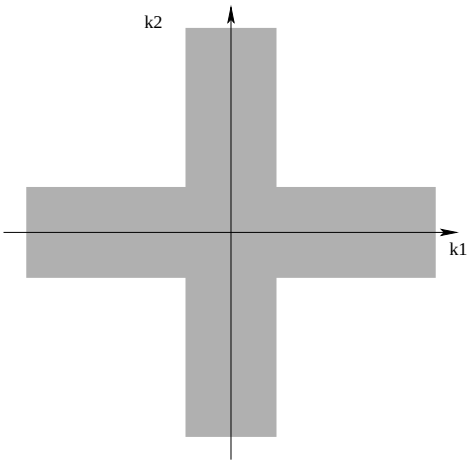

Figure 5.6: Action of CROCE used as a high-pass filter: the wave-numbers under a certain threshold are cut

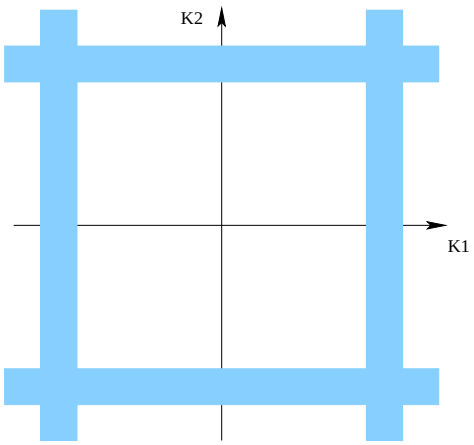

Figure 5.7: CROCE can be used to remove the contributions of a variable band

contribution of certain structures; and this is made more easily if we work in the Fourier domain instead of the physical domain, having the energy spectrum as a reference.

The first filter we use is referred to as CROCE. CROCE is thought to remove the structures with *at least one small* wave-number. We have already seen that the study of structures of non trivial geometry, like vortex filaments, in one of the trends in the intermittency analysis. In this sense, when we define a local function of the velocity field, and we test its statistical behavior, we have to take into account the presence of such structures, and possibly try to figure out their influence on the quantity under consideration. The physical meaning of this filter is to avoid the presence of *elongated structures* from the field, and see the consequence of this action on the statistical behavior of f. The principal results are discussed in the following; a collection of all results is presented in fig. 5.18 to 5.26.

5.2.1 Low wave-numbers

The first filter allows to remove the contribution of those structures that are characterized by a *large axial dimension*. This means that, from the Fourier point of view, we want to remove the structures whose wave-number has *at least one small component*. In this sense, CROCE can be seen as a sort of high-pass filter, which affects all wave-numbers, in each direction,

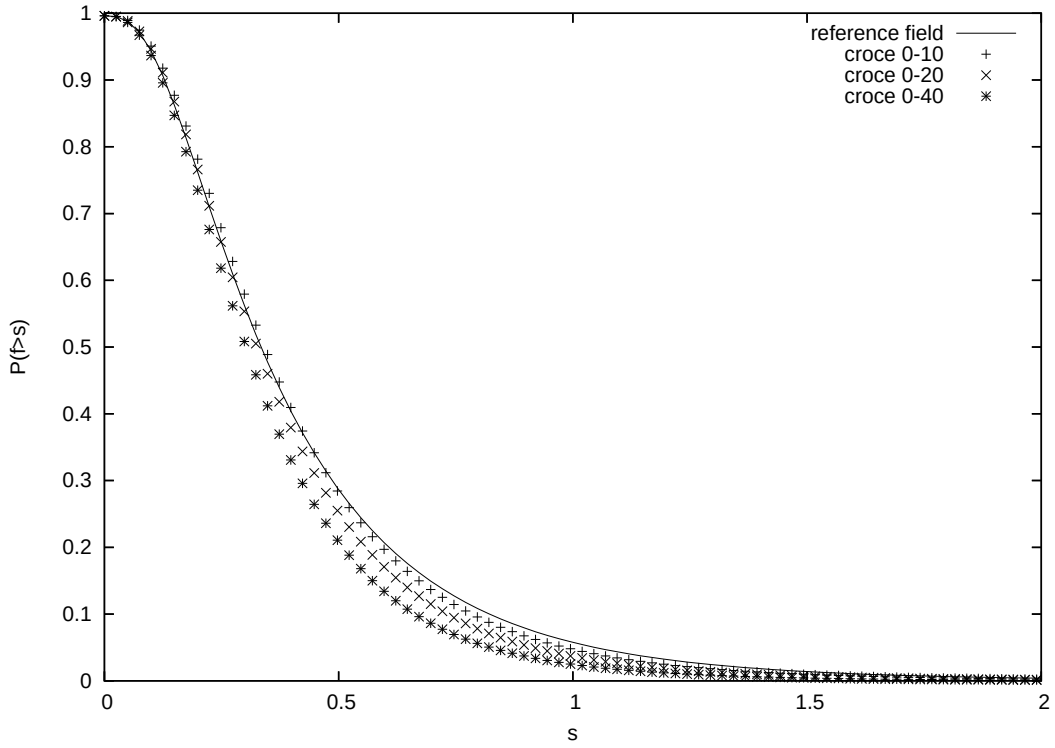

Figure 5.8: Control function $1 - F(x)$, high-pass filters

under a certain threshold. Given a the threshold k_{MAX}, the filter removes the contribution of the modes with

$$k_1 < k_{MAX} \text{ or } k_2 < k_{MAX} \text{ or } k_3 < k_{MAX}.$$

For a detailed definition of the filter function, see the appendix. An idea of the filter action on wave-numbers is sketched in fig.5.6. For sake of simplicity, the plane represent a two-dimensional wave-number space; the colored areas are those affected by the filtering operation. We have one control parameter to act on, in this case, which is the width of the range that we want to cut, k_{MAX}. The analyzed filtered ranges are 0-10, 0-20, 0-40, compared on fig.5.8. That means that the first one completely affects the energy-containing range, while the other two reach the inertial range, as defined as the $\frac{5}{3}$-law behavior range.

These plots have a coherent behavior. Actually, the control function of

the 0-10 filter show a slight difference with the reference one, at the values of the former are under the line of the latter. This trend is confirmed by the other two filters, and the difference grows as the threshold increases. This indicates that the high-pass filters have the (statistical) effect of *decreasing* the values of the function $f(x)$ on the domain. The wider is the cut range, the stronger is the effect on f, that is the more f decreases. Alternatively, this fact can be seen from the plot of the pdf of f.

5.2.2 Higher wave-numbers

The next step is to move from the energy-containing range to the inertial and dissipative ranges. Then we used CROCE to cut the contribution of a variable band

$$k_{MIN} < k_1 < k_{MAX} \text{ or } k_{MIN} < k_2 < k_{MAX} \text{ or } k_{MIN} < k_3 < k_{MAX}.$$

(see fig.5.7) thus selectively affecting the structures with a certain axial dimension. Now we have two control parameters, the amplitude and the position of the band. Firstly, we consider a fixed amplitude and we move the band through the inertial range.

The first range to be cut is 10-40, in order to compare with the 0-40 filter. The result is plotted in fig.5.9, which shows the comparison with the high-pass filters.

The figure clearly shows that the trend of the previous plots is *not* respected. Instead, filtering 10-40 wave-numbers produce a small *increasing* of the control function, which can be seen as a (statistical) increase of the values of f.

This fact is more difficult to interprete. We suspect that this is due to the large scale vorticity which affects the field, as said before.

Let us move into the inertial range, by filtering higher wave-numbers. We now consider the inertial range in a an *extended way*, which includes the $-\frac{5}{3}$ range plus all the scales which are not yet dissipative ($Re_k = \frac{\lambda_k u_k}{\nu} > 10$).

Partial filtering in the inertial range are carried out by removing the intervals 40-70, 70-100, 100-130. The resulting control functions are compared in fig.5.10.

Here all the filters induce the same effect: a slight *increasing* of the values of $f(x)$. Notice that when we act in this range, the effects on f seem to

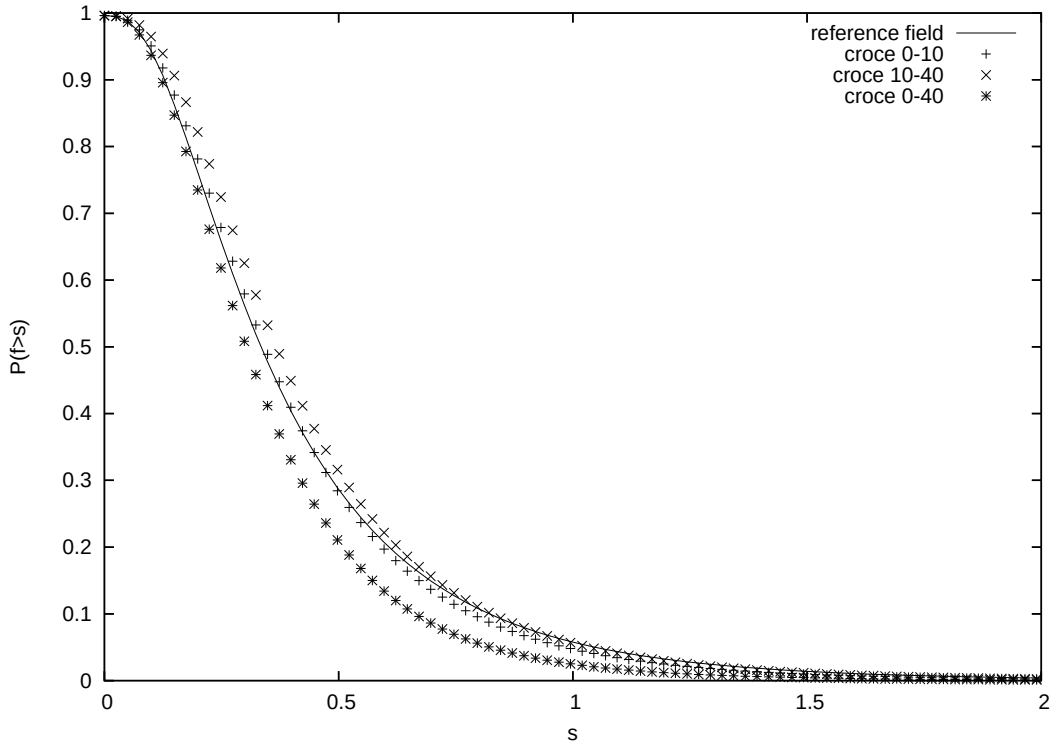

Figure 5.9: Opposite behaviors for 0-40 and 10-40 control functions

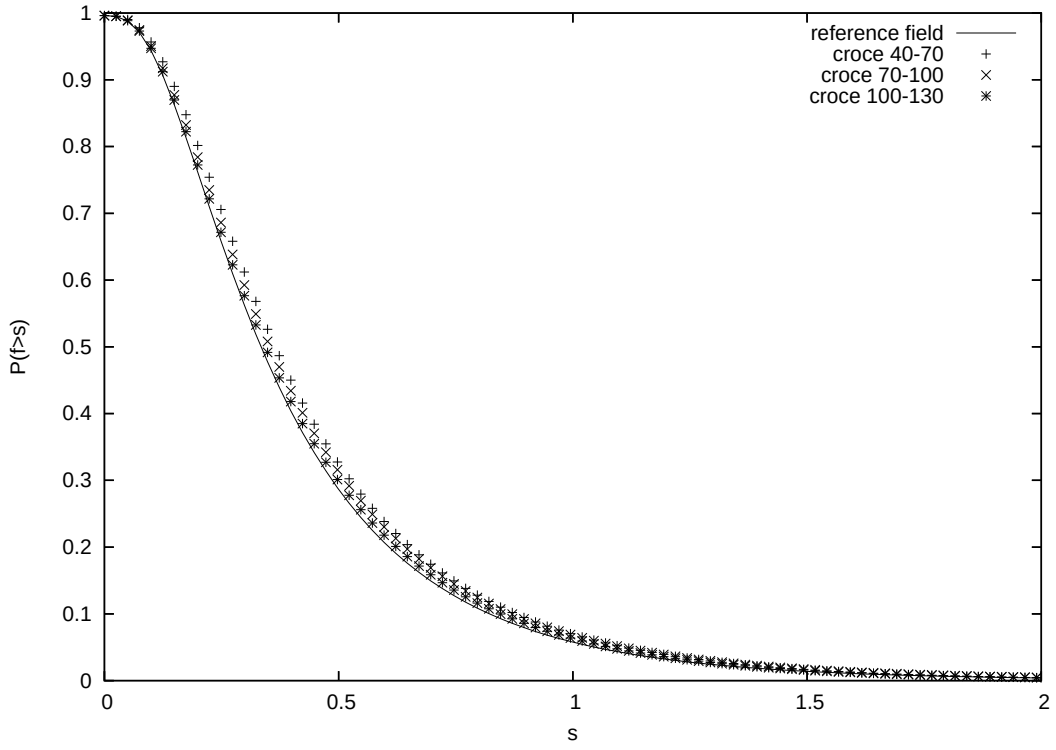

Figure 5.10: Control function, comparison of filters between 40 and 130

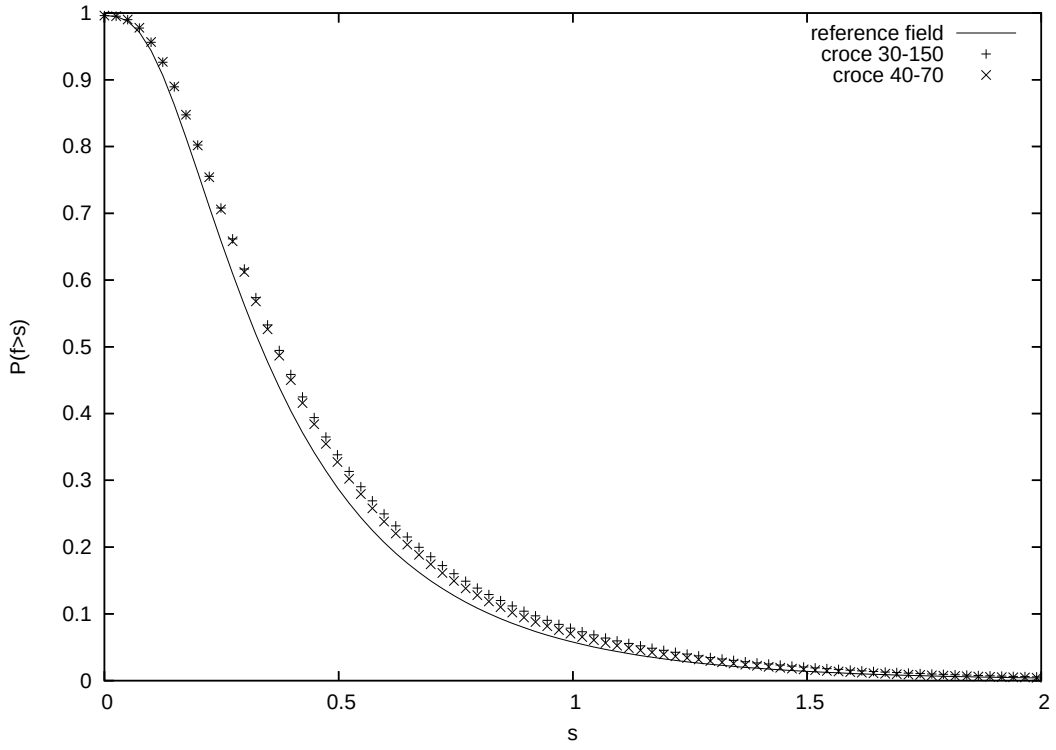

Figure 5.11: Control function obtained by filtering all the inertial range

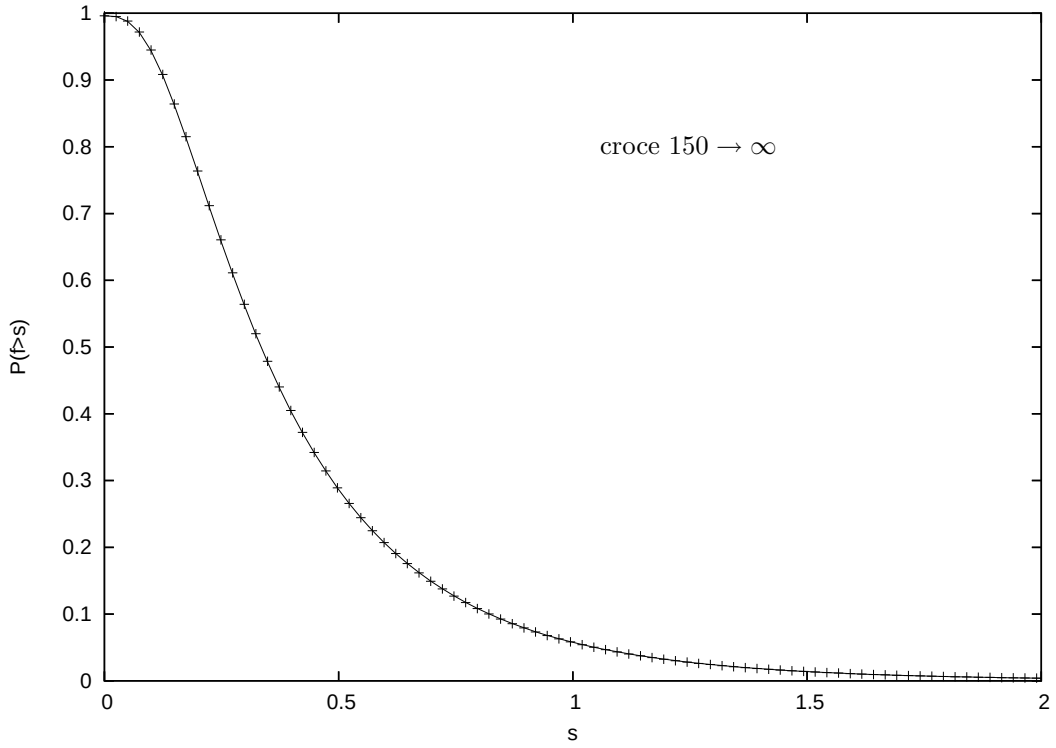

Figure 5.12: Control function, filtering the dissipative range

be slighter. The most effective (i.e. the one which produces the strongest increasing) seems to be the 40-70 one; but the difference are not so large.

Even when we try to act on the other control parameter, the amplitude of the band, the situation does not change much. Filtering values of k between 30 and 150 means that we affect the whole inertial range; and generates a further increasing of the function $f(x)$ (see fig. 5.11), but the results are still comparable with the 40-70 filter.

Finally, we investigate the contribution of such elongated structures whose axial dimension is in the Kolmogorov range. This is the opposite of the first case; actually here CROCE can be seen as a sort of low-pass filter. Involving this structures has a lighter effect. In figure 5.12 there is the plot of the control function of $f(x)$ when CROCE is used as a low-pass filter with threshold 150. The increasing of $f(x)$ is slight, although we have removed the contribution of more or less 200 wave-numbers.

5.3 Further consideration on elongated structures

In our attempt to understand the influence of elongate structures on the function f, we have to deal with structures like vortex filaments, described in the previous sections. In a simplified model, the can be seen as long and thin vortices, having the axial dimension *much greater than the radial dimension*. It is soon realized that a filter which exactly select those structures in a turbulent field is very hard to build. This is due to the intrinsically non-trivial geometrical nature of this kind of coherent structures.

Nevertheless, results in this direction have been obtained using the CROCE filter to remove the structures with a long axial dimension. This filter can be made more selective by asking to remove the structures that have *one small and two large* wave-numbers. So now we have more degrees of freedom: one can decide what is the range of small wave-numbers, $(KMIN, KMAX)$; and also a threshold, above which a wave-number is considered large: $KTOP$. We remove the structures that show

$$k_{MIN} < k_i < k_{MAX} \text{ and } k_{TOP} < k_j, k_h$$

for at least one choice of $i, j, h \in \{1, 2, 3\}$ (obviously different each other). Several attempts have been made using this kind of filter, which we refer to as FILAMENTO filter. According to recent papers ([5]), the radial dimension of filaments in turbulence can nearly reach the Kolmogorov scale: $r \sim 5\eta$. Thus the first choice for the value of the threshold is $k = 130$, a value that seems to be at the bottom of the inertial range. Simulations have been carried out, varying the range $(KMIN, KMAX)$: 0-40, 40-70, since to cover the range 30-130. *No significative change* in the behavior of the function $f(x)$ has been discovered, see figures 5.13.

The action of this filter results to be weak. It must be noted that it affects only a *particular kind* of elongates structures: those which have one small and two large components in the cartesian frame of reference for the wave-number vector $\mathbf{k}$. This means that, due to the geometrical complexity of the velocity field pattern, their contribution can be quite small in comparison to all the other structures in the field.

More substantial results are obtained by moving the KTOP threshold down to 50. This value has been chosen also as the KTOP value, so that the

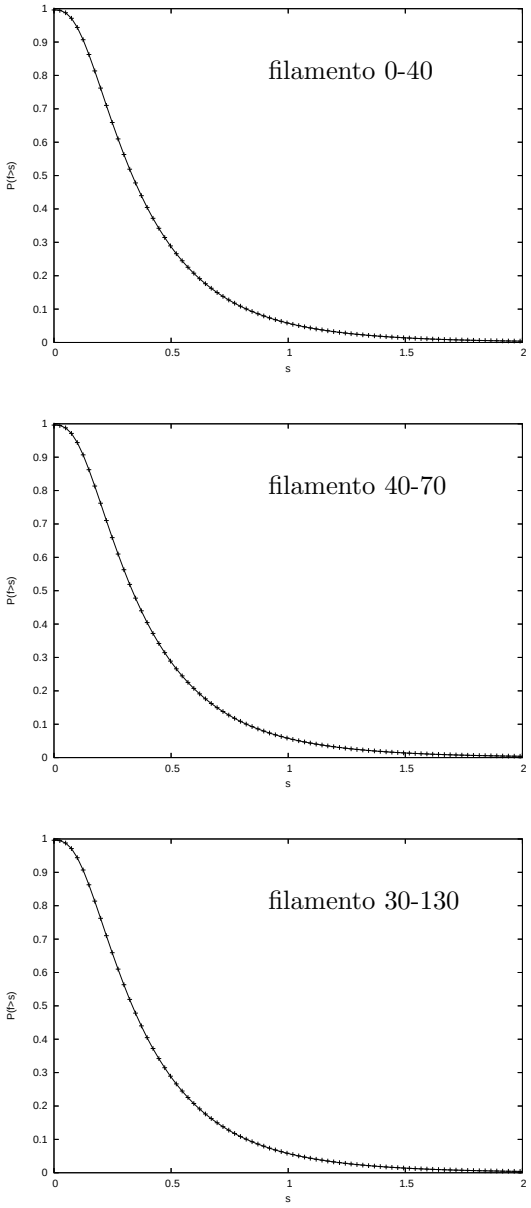

Figure 5.13: FILAMENTO filter has a weak effect

small wave-number is defined between 0 and 50, and the other two must be greater than 50. Result is shown in figure 5.27 .

5.4 Filtering the shells

As we have done with the elongated structures, we also would like to weight the influence of another kind of coherent structures: those which have a more regular shape, that is more or less the same dimension in the three spatial directions. From the point of view of the wave-number space, we are dealing with eddies that are characterized by a strong contribution of modes whose wave-vectors have different directions, but more or less *the same magnitude*. Thus, the filter used in this analysis allows to remove the contributions of those wave-vectors which that lye on *shells of given radius*.

This filter has name SFERA. This is the same kind of filter we have used to obtain the reference field from the original field. But now we want to extend its use in order to remove different bands of wave-vector magnitudes k. Thus, given a certain band $[k_{MIN}, k_{MAX}]$, the filter removes the contribution of those modes with

$$k = \sqrt{k_1^2 + k_3^2 + k_3^2} \in [k_{MIN}, k_{MAX}].$$

The results are shown in fig. 5.29 to 5.36.

5.4.1 Low wave-numbers

Following the study we have done with the filter of elongated structures, we fist start with the energy-containing range. As k_{MIN} is set to zero, we have the high-pass filter. The results are shown in figure 5.14. Already from these first results, we note that the behavior of f under this filter is different from what we obtained with the CROCE filter. Actually, when the filtering range is limited to $0 - 10$ and even $0 - 20$, we obtain a very slight influence of the statistics of f. The graphs seem to show a different behavior for the two filtering ranges: for the range $0 - 10$, the values of f (statistically) increase; when we extend the range to $0 - 20$ the effect is the opposite. But the differences between the control functions are so small that we can assume that this filters have a negligible effect on the field. Instead, when the threshold reaches higher values, like 40, we see that the values of f (statistically) decrease. This is coherent with the results obtained with the previous filters.

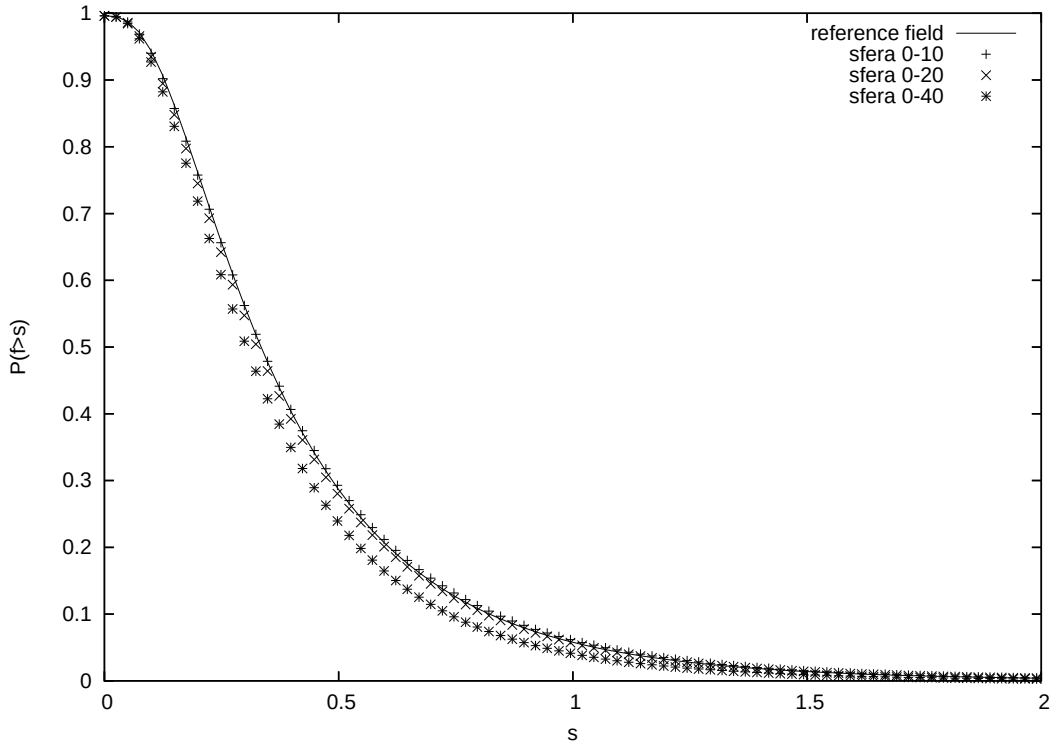

Figure 5.14: Control function $1 - F(x)$, high-pass filters

5.4.2 Higher wave-numbers

We now move to che inertial range, again using a band-filter:

$$k_{MIN} < k < k_{MAX}.$$

In order to compare with the previous results, we divide the (extended) inertial range in sub-ranges: $10-40$,$40-70$,$70-100$. We extend the analysis until $100-130$, as borderline region between the inertial and Kolmogorov ranges. The results are presented in fig. 5.15.

Here, we note that when we filter in the subregion of low (inertial range) wave-number, the trend of the $0-40$ filter is confirmed. Removing those structures causes a decrease of the function f. Instead, if we move to smaller-scale sub regions of the inertial range, we obtain an increase of the values of f. Also, the control functions obtained from the filters $40-70$, $70-100$, $100-130$ have approximately the same shape; this seem to indicate that the presence of spherical coherent structures is in such a way uniformly distributed in the range $40-130$.

Finally, we can think of filtering very large ranges. In order to compare with the CROCE results, we filter the range 30-150, and than all the dissipative range $k > 150$. In the first case (fig.5.16), the results of the sub-filters are confirmed, and the influence is much deeper when compared, for example, to the 40-70 filter. This fact did not happened with the CROCE filter. About the Kolmogorov range, both in CROCE and in SFERA results show that few coherent structures seem to be present, as expected (fig. 5.26 and 5.36).

5.5 Conclusions

5.5.1 Results

A test of the function

$$f(\mathbf{u}) = \frac{|\boldsymbol{\omega} \cdot \nabla \mathbf{u}|}{|\boldsymbol{\omega}|^2} \tag{5.1}$$

over different fields has been carried out, in order to understand the influence of the structures of various length-scales on that function. At the same time, information about the interactions of the scales in homogeneous isotropic turbulence have been deduced from the behavior of the function f.

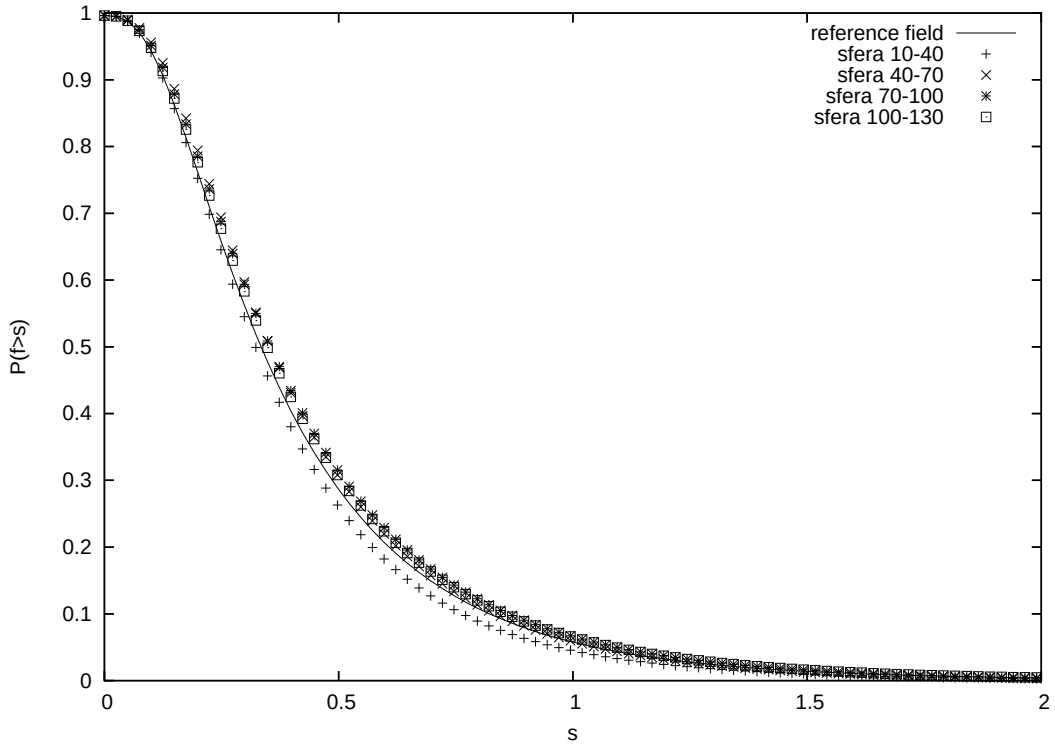

Figure 5.15: Control function, comparison of filters between 10 and 130

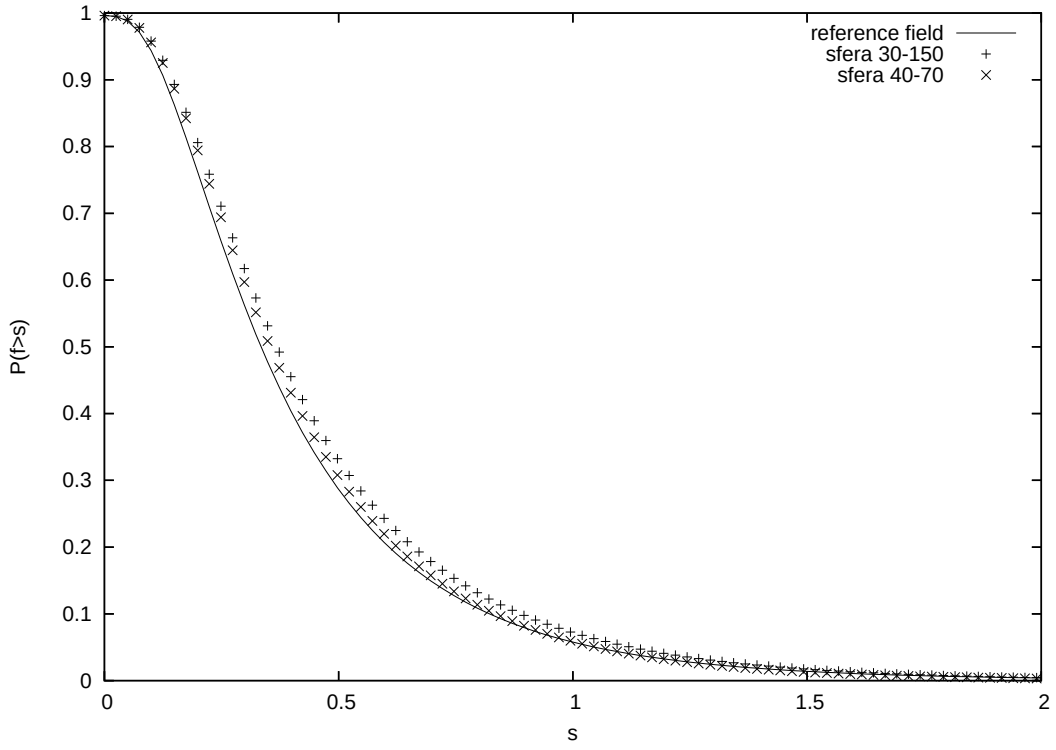

Figure 5.16: Control function obtained by filtering the range 30-150

This analysis has been done by means of three filters, in order to point out the contribution of the elongated and spherical coherent structures. A complete list of the evaluated statistics is presented in table 5.1.

In all cases, the graphs and the statistics presented show that there is high probability that the ratio stretching-twisting term over enstrophy is bounded by a value less than 1:

$$\frac{|\boldsymbol{\omega} \cdot \nabla \mathbf{u}|}{|\boldsymbol{\omega}|^2} < C, \quad C < 1 \tag{5.2}$$

The mean value is much lower than unity, of the order of 10^{-2}, but the variance is high compared to it, thus discouraging the assumption $|\boldsymbol{\omega} \cdot \nabla \mathbf{u}| \approx E(f) \cdot |\boldsymbol{\omega}|^2$; but we could assume that $|\boldsymbol{\omega} \cdot \nabla \mathbf{u}| \approx |\boldsymbol{\omega}|^2$ keeping in mind that the the right hand side is a bound for the left hand side (with high probability).

When we act in the energy-containing range, where k is low, by removing the large-scale structures, the function goes under a general *decrease*. The mean value of f goes down; and the wider is the range we affect with the filter, the lower becomes the mean value. This suggests that the large-scale structures contribute more to the stretching-twisting term (the numerator of f) than to the vorticity of the flow (the denominator).

This behavior is common to the CROCE and SFERA filters, although the croce filter is almost not effective since the filtered interval becomes high (0-40). This seems to suggest that the elongated structures with axial dimension comparable to the large scales have a stronger effect on the values of f.

The transition to the inertial range gives different results for the two filters. When we move the band up for the SFERA filter, the values of f start to increase in a "smooth" way. Let's consider the 10-40 filter values: they are higher than the 0-40 ones, but still lower than the reference unfiltered values. Moving to 40-70, 70-100 and 100-130, the trend is respected and the function grows up more and more. The same transition (from lower to higher values than the reference) comes out for the CROCE filtered fields, and thus when we act on the elongated structures, but in a "sharp" way. The 0-40 filter generates a decrease of f. Once we leave the lowest values, moving to 10-40, the values of f immediately becomes larger than the reference. Thus, dealing with elongated structures, we can see a very different (we can say opposite) behavior of the energy-containing and inertial range: the structures

in the latter contribute to vorticity more than to vortex stretching. When we move the filtered band towards the Kolmogorov range, the effect becomes more evident. This trend is a clue of the strong difference in behavior between the energy-containing range, not universal and influenced by boundary conditions, and the inertial and Kolmogorov ranges, whose dynamics are universal. The limit values for this process are obtained by removing the whole inertial range. We can also note that, in this range, the effect obtained acting on the elongated structures is comparable to the effect obtained acting on the spherical structures.

Finally, the very small scales have little effect on the function values. This is expected because this range is dominated by diffusion and energy dissipation, so very few structures can survive. This fact shows that the function f is not a good tool to investigate the Kolmogorov range, as the influence of the dynamics of the diffusive scales on f is very week.

5.5.2 Spectral considerations on $f(x)$

In order to help a deeper understanding these phenomena, we carried out a spectral analysis of the function f. We plotted the 1D spectra of $f(x)$: if $F_1(k_1)$ is the 1D transform of $f(\mathbf{x})$, we plot the 1D energy spectrum

$$S(k) = |F_1(k_1)|^2 \tag{5.3}$$

computed on the reference field, and we compared to the spectra computed after the action of the filters. The graphs are presented for each filtering, in figures 5.18 to 5.36.

The 1D spectra give a first useful, although uncomplete, description of the spectral contributions to the function f. Note that, for example, a phenomenological point of view would give no result in this sense. Actually, both the stretching-twisting and the enstrophy term represent spatial derivatives of velocity, both behaving as $\sim ku$. Thus, in the inertial range where $u \sim k^{-\frac{5}{3}}$ their average contribution is qualitatively the same; and no information can be deduced from the ratio of such quantities. Thus, the spectral behavior of f is determined by two factors. First of all, the large scale range of the spectra have a strong influence on the flow dynamics. From a physical point of view, the large eddies correlate points of the domain which can be much far apart; they represent the top of the energy cascade, their generate the

smaller structures. The quantities involved in this process are vorticity and the generation of stretching of this large, non universal, range; and their separate behavior generates the shape of the spectrum of f.

Second, the spectra give an *average* description of the dynamics. As we have seen, real turbulence presents eddies, coherent structures, filaments and vortices. For example, according to Jimenez ([5], [6]) the vortex filaments are *not* regions of high values of stretching; actually he measured the axial stretching in the filaments and he found out that it is comparable to the background value of stretching. Thus, looking back to our simulations from this point of view, it is the vorticity of the structures that generates the differences in the pdf of f obtained filtering the large-scale or the inertial ranges. In conclusion, the distribution of vorticity ad stretching on structures of different size is still matter of research; our function f is influenced by the *local* concentration of these quantities through the flow, it can be interesting to carry out a spectral analysis of this quantity. Furthermore, when we modify a turbulent flow acting on such structures the spectrum of f goes under important changes.

The consequence of the filtering process is strongly evident in the high-pass filters. The contribution of the low wavelengths is reduced; furthermore, note that the action of filters is spread outside the filtering range. For example, let us consider the CROCE filtered fields, and observe the spectrum of the (0-10)-filtered field (fig. 5.18). It remains parallel to the original one, and lower than it, until $k \sim 20$, more or less twice the filter threshold. The trend is the same in the other two cases. (0-20)-filter affect the contribution of wave-numbers until 40 (fig. 5.19), and (0-40)-filters until 80 (fig. 5.20).

On the other hand, there seems to be a sort of *energy concentration* on the wave-number *not* affected by the filter: actually the spectra of the filtered fields grow *over* the reference one on the non-filtered ranges. This effect is present in all simulations, and becomes more evident when we filter a wider range.

The plot of spectra of the remaining fields show a different behavior, which is evident above all in the CROCE filtered fields. The spectral values of the filtered wave-numbers is reduced, of course, and the energy concentration effect is shown to be present on smaller wave-numbers, which now increase their spectral values; but an opposite effect on the smaller scales is evident. The tail of the filtered spectra decrease much faster than the unfiltered ones. Thus, removing the contribution of inertial range scales seems to have evident

consequences also on the spectral distribution of f on the dissipative scales. In this sense, the most significant plots are the 30-150 one (fig. 5.25 and 5.5.3), where an evident change in energy distribution took place. The plots generated by the filtering of the structures of the Kolmogorov range, confirm that this range has a very week effect on the stretching-twisting normalized term.

If we have a look to the spectrum obtained from the FILAMENTO filter with $KTOP = 50$ in fig. 5.27, we see that the filtering has increased the contribution of most wave-numbers, until ~ 200, and only in the last part of the spectrum the values decrease. This seems to suggest that in the large and inertial range, the filter has affected the field in such a way that the vorticity has decreased with respect to the stretching-twisting term; while in the very small scales, the change has been the opposite.

5.5.3 Further considerations

We have studied the influence that different coherent structures have on the statistical properties of the function

$$f(\mathbf{u}) = \frac{|\boldsymbol{\omega} \cdot \nabla \mathbf{u}|}{|\boldsymbol{\omega}|^2}. \tag{5.4}$$

The physical consideration which can be deduced by the observation of f completely agree with the knowledge which comes from laboratory experiments about the distribution of vortex stretching and vorticity over the different scales. This makes the function f a powerful instrument. Usually, all information about the dynamics and interaction of scales in a turbulent flow is derived from a spectral analysis, which can give a description of the energy distribution over the scales. But the study of spectra requires a global analysis, carried out over the whole domain. The attempt to define a local quantity which could be usefully related to the dynamics of the structures of different scale has beeb made here, and we proved the consistency of this approach with experimental results known in literature.

Many features of such quantity f have been studied. Evidences of the fact that the elongated structures have a strong influence on f have been given, above all for large-scale structures. The elongated structures correlate points of the fields which are far apart; thus, although $f(\mathbf{x})$ is a local quantity,

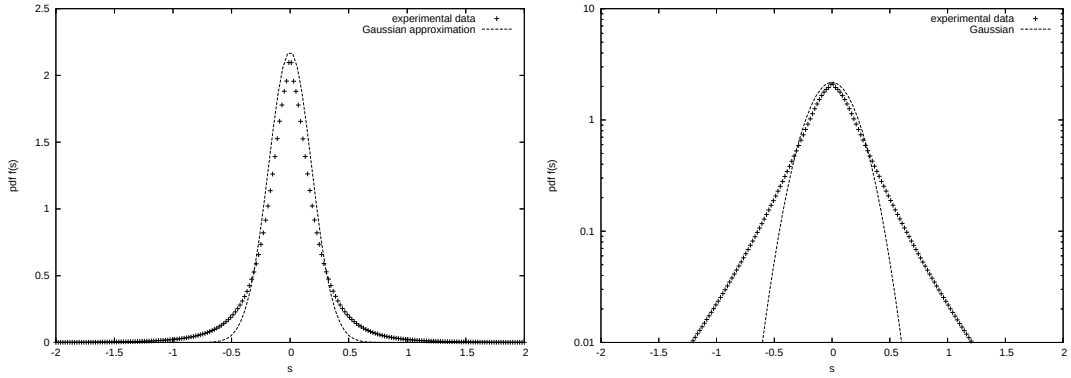

Figure 5.17: Pdf of $\frac{\boldsymbol{\omega}\cdot\nabla u}{|\boldsymbol{\omega}|^2}$ and comparison with gaussian model; , linear (left) and logarithmic (right) plots

it carries information about non-local behavior and thus can be a useful instrument of analysis.

Nevertheless, possible trends can be identified for a future work on this function. For example, while f is strongly sensitive to the dynamics of the energy-containing and inertial range, it is a week instrument to analyze the Kolmogorov range. A research in this direction could create a more complete instrument of analysis, able to investigate the whole range of scale interaction.

Another possible aim is the research of an explicit model for the pdf of f. This model is still missing, although a preliminary attempt has been made, studying the statistic properties of the vector

$$\frac{\boldsymbol{\omega}\cdot\nabla\mathbf{u}}{|\boldsymbol{\omega}|^2} \tag{5.5}$$

whose magnitude is exactly our function f.

In figure 5.17, we show the pdf of the first component of this vector:

$$\frac{\boldsymbol{\omega}\cdot\nabla u}{|\boldsymbol{\omega}|^2}.$$

The other two components show the same behavior, as the field is statistically homogeneous and isotropic. This pdf is bell-shaped; symmetry with respect to the vertical axis is expected for isotropy: the skewness is approximately 10^{-2}. These features can lead us to test a possible model for this quantity: i.e. it can be interesting to know if this function could be approximated with a *gaussian* function. The approximation is not far from the experimental data,

but it does not agree completely; indeed, the actual kurtosis is approximately 55, very far from the gaussian value of 3. So the tails of the experimental pdf are thicker than the tails of the gaussian. This behavior is evident in the logarithmic plot of the pdf. A complete medelling of this quantity and of f is a possible trend for future study.

	$E(f)$ $(\cdot 10^{-1})$	$Var(f)$ $(\cdot 10^{-1})$	σ	S	K
REFERENCE	4.22	1.06	0.32	2.31	12.47
croce 0-10	4.16	0.89	0.29	2.18	11.97
croce 0-20	3.93	0.76	0.27	2.21	12.64
croce 0-40	3.6	0.62	0.24	2.22	13.32
croce 10-40	4.44	0.92	0.3	1.98	9.88
croce 40-70	4.55	1.14	0.33	2.06	10.11
croce 70-100	4.45	1.16	0.34	2.2	11.22
croce 100-130	4.33	1.12	0.33	2.29	12.12
croce 30-150	4.65	1.22	0.35	2.11	10.24
croce >150	4.22	1.06	0.32	2.31	12.52
sfera 0-10	4.25	1.11	0.33	2.31	12.38
sfera 0-20	4.14	1.07	0.32	2.34	12.75
sfera 0-40	3.8	0.87	0.29	2.46	14.42
sfera 10-40	4	0.9	0.3	2.35	13.5
sfera 40-70	4.36	1.01	0.31	2.09	10.66
sfera 70-100	4.43	1.12	0.33	2.14	10.83
sfera 100-130	4.39	1.14	0.33	2.24	11.63
sfera 30-150	4.59	1.15	0.34	2.05	9.86
sfera >150	4.28	1.1	0.33	2.31	12.37

Table 5.1: Table of the moments of f for the reference and filtered fields: expected value, variance, standard deviation, skewness, kurtosis

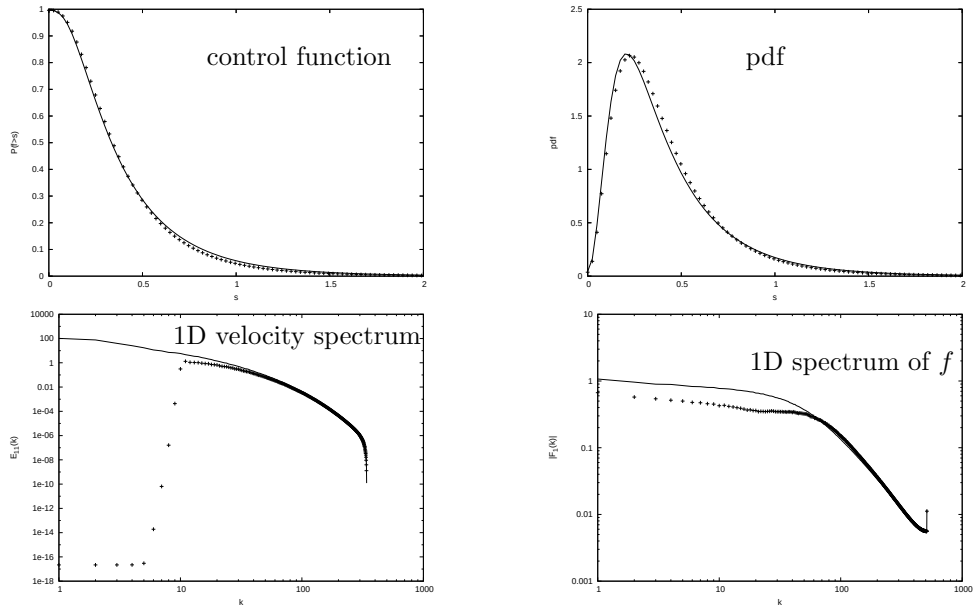

Figure 5.18: CROCE 0-10 filter plots (+), in comparison to reference field

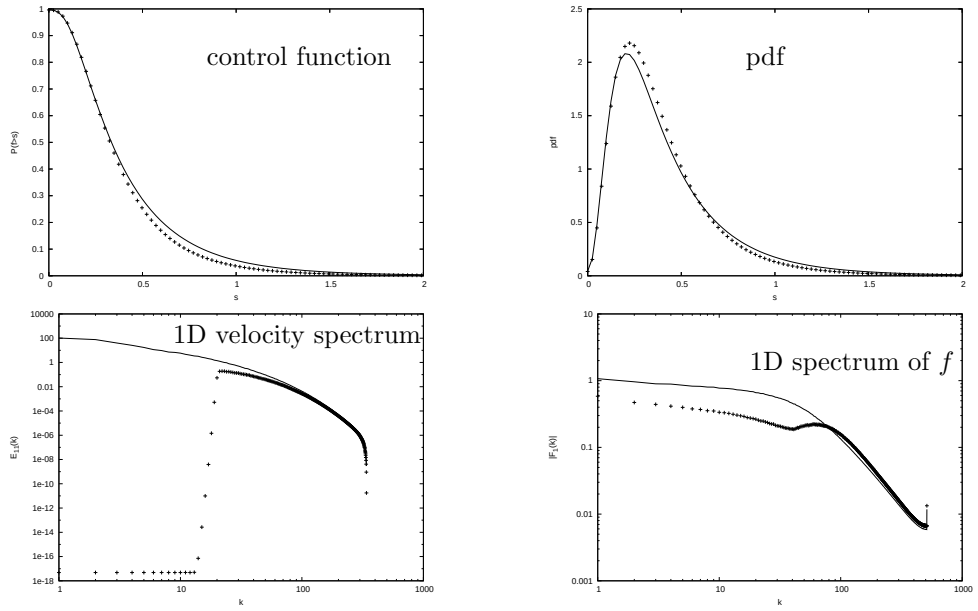

Figure 5.19: CROCE 0-20 filter plots (+), in comparison to reference field

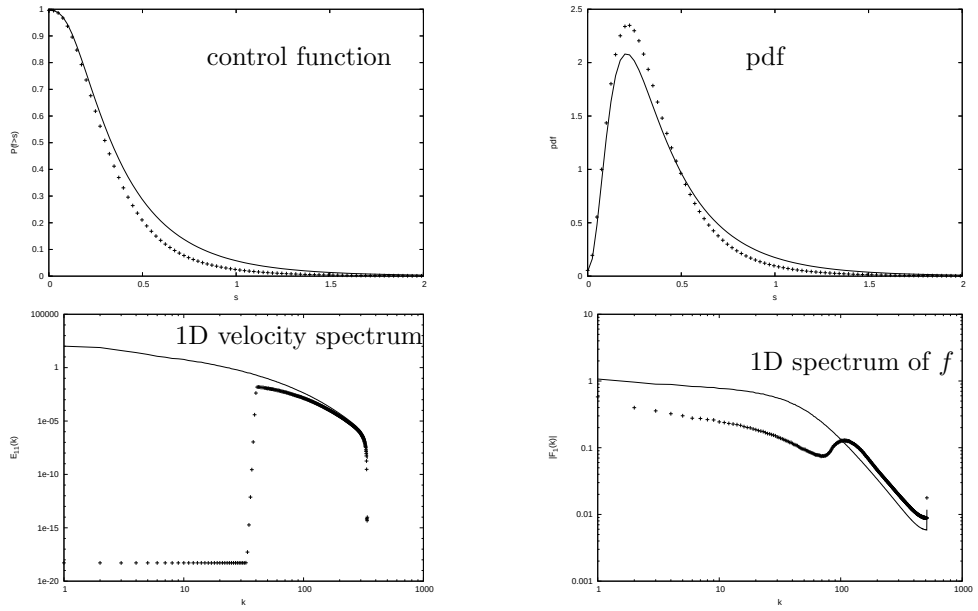

Figure 5.20: CROCE 0-40 filter plots (+), in comparison to reference field

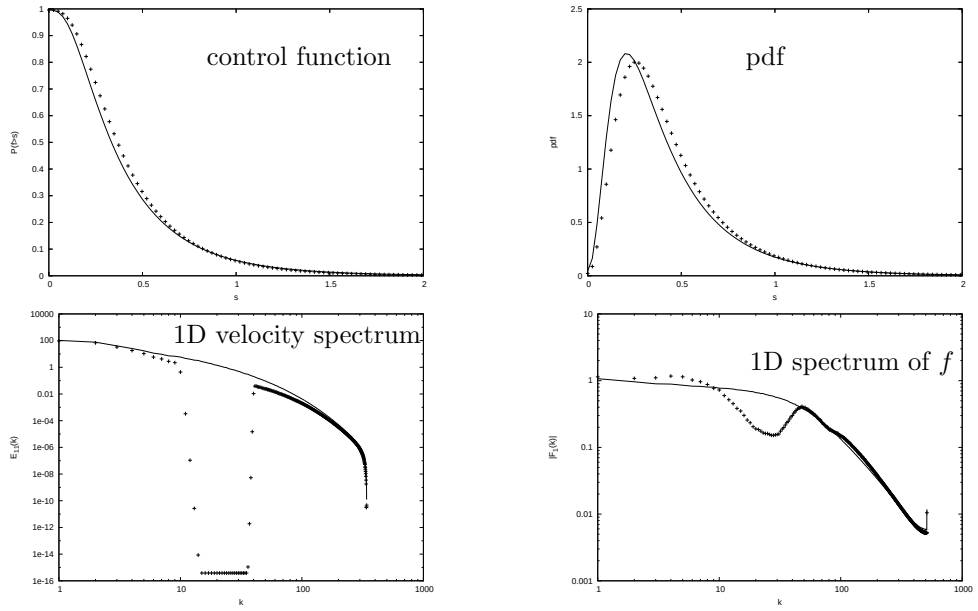

Figure 5.21: CROCE 10-40 filter plots (+), in comparison to reference field

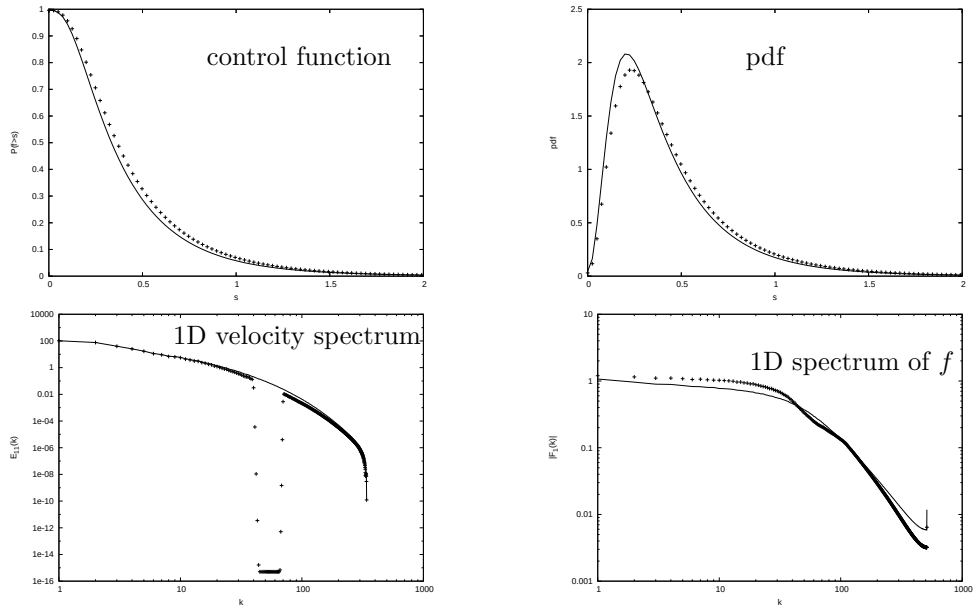

Figure 5.22: CROCE 40-70 filter plots (+), in comparison to reference field

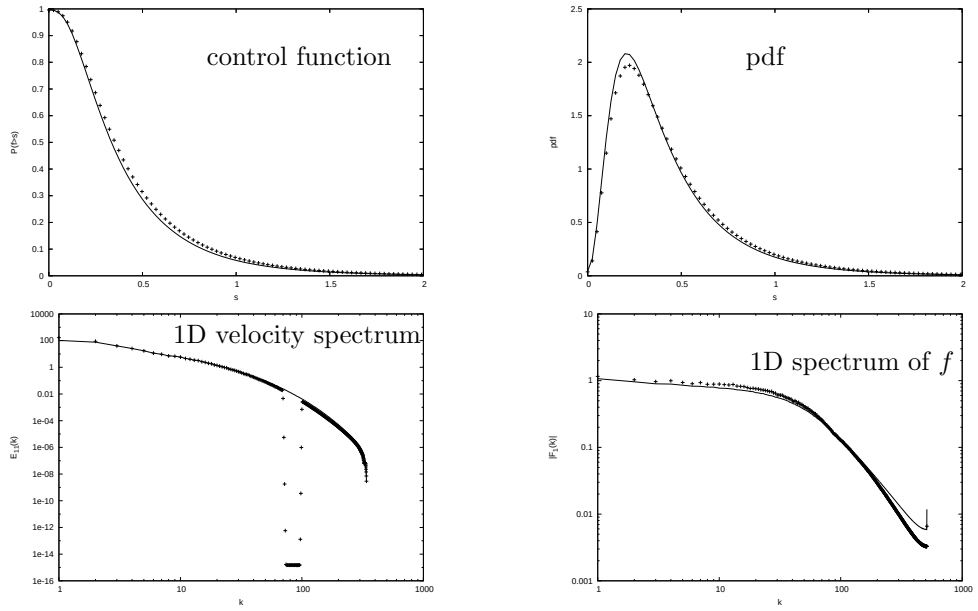

Figure 5.23: CROCE 70-100 filter plots (+), in comparison to reference field

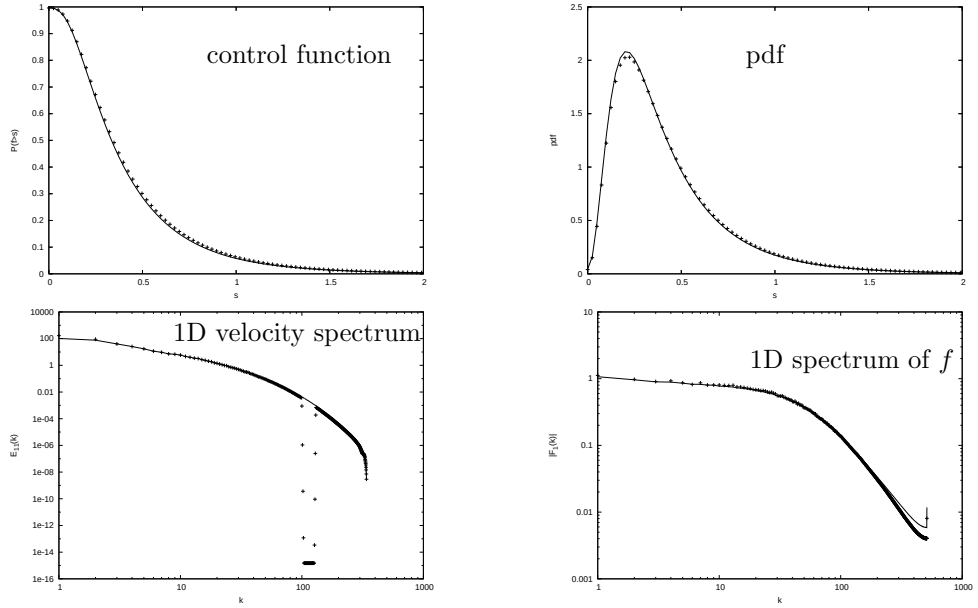

Figure 5.24: CROCE 100-130 filter plots (+), in comparison to reference field)

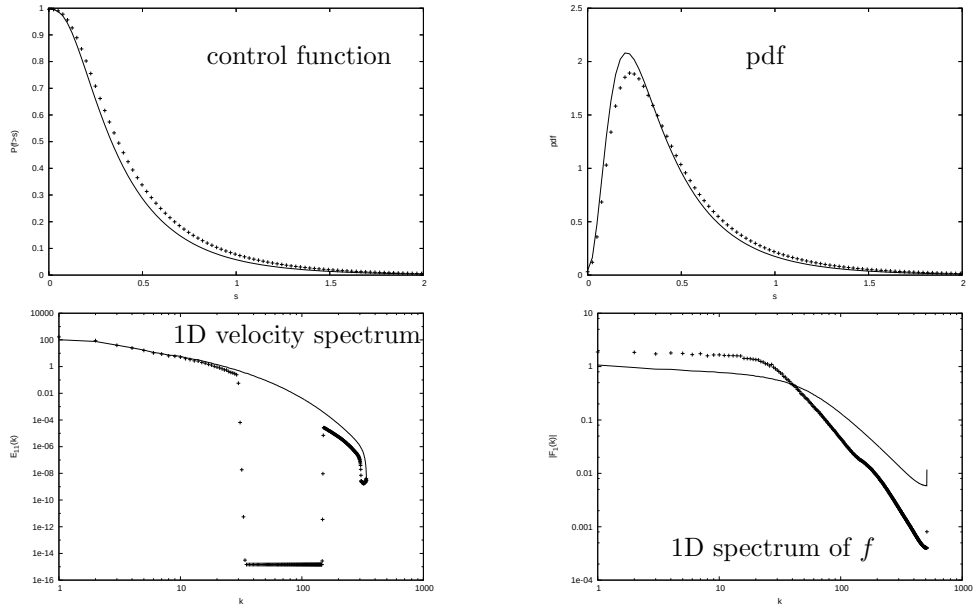

Figure 5.25: CROCE 30-150 filter plots (+), in comparison to reference field)

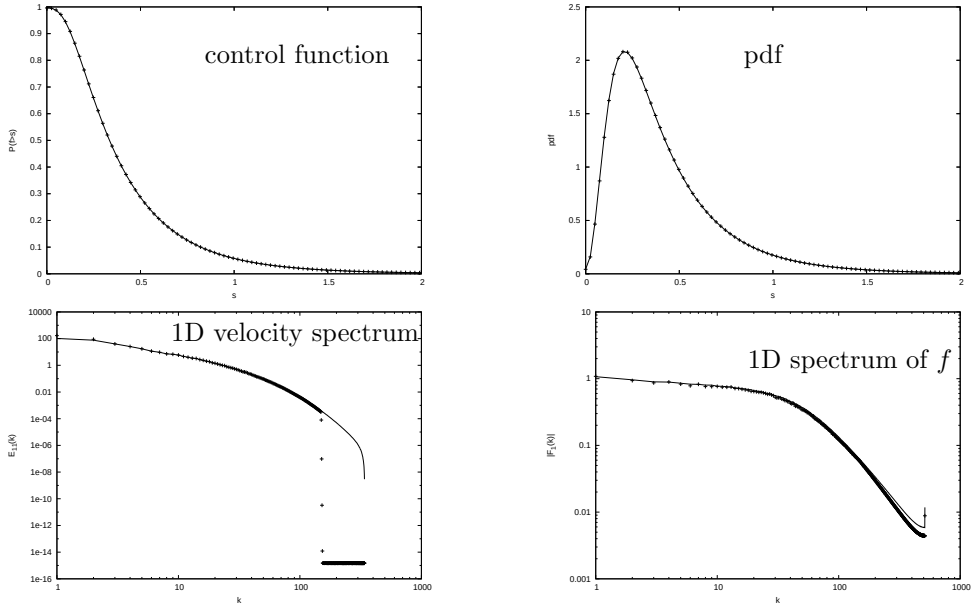

Figure 5.26: CROCE 150-500 filter plots (+), in comparison to reference field

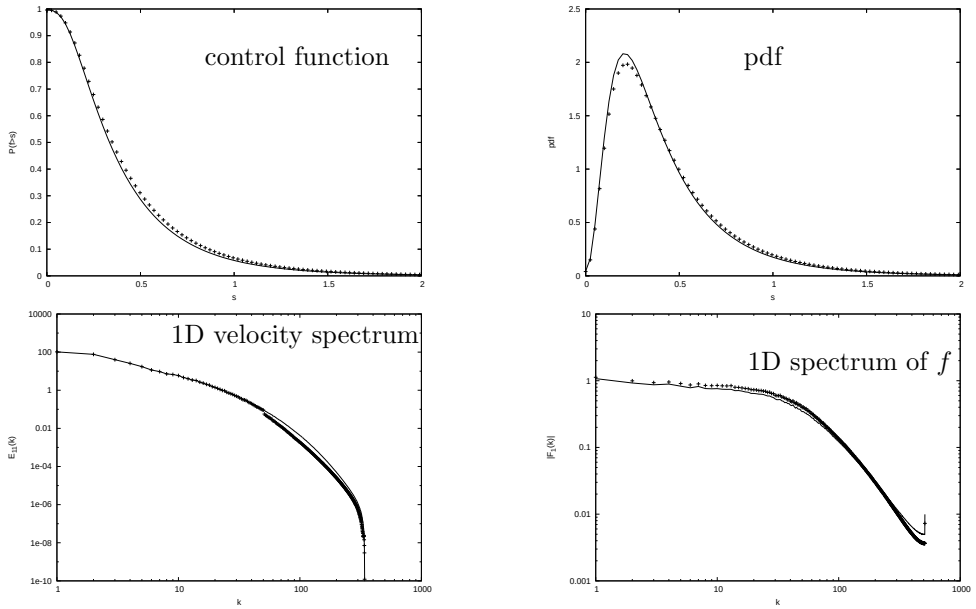

Figure 5.27: FILAMENTO 0-50, KTOP=50 filter plots (+), in comparison to reference field

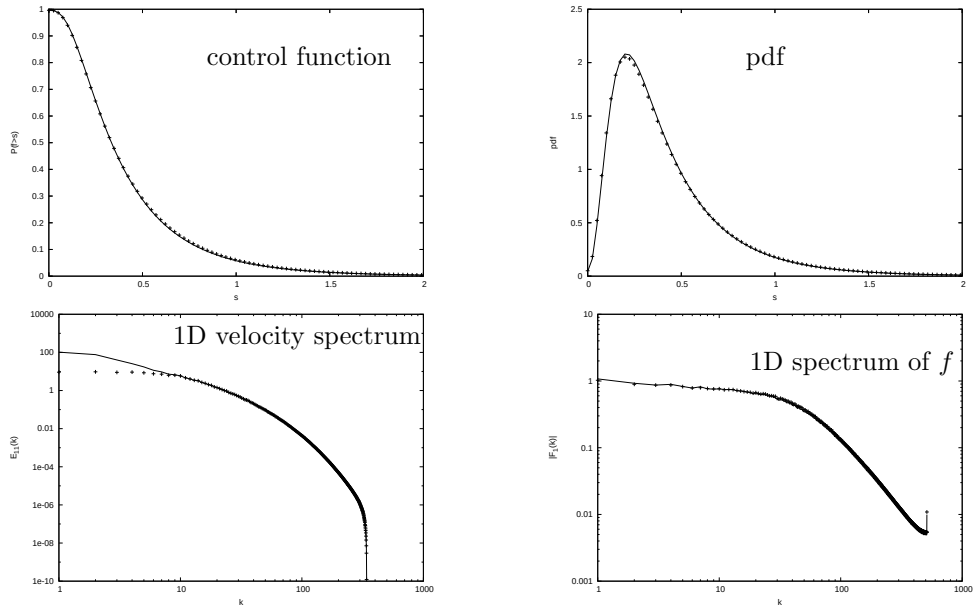

Figure 5.28: SFERA 0-10 filter plots (+), in comparison to reference field

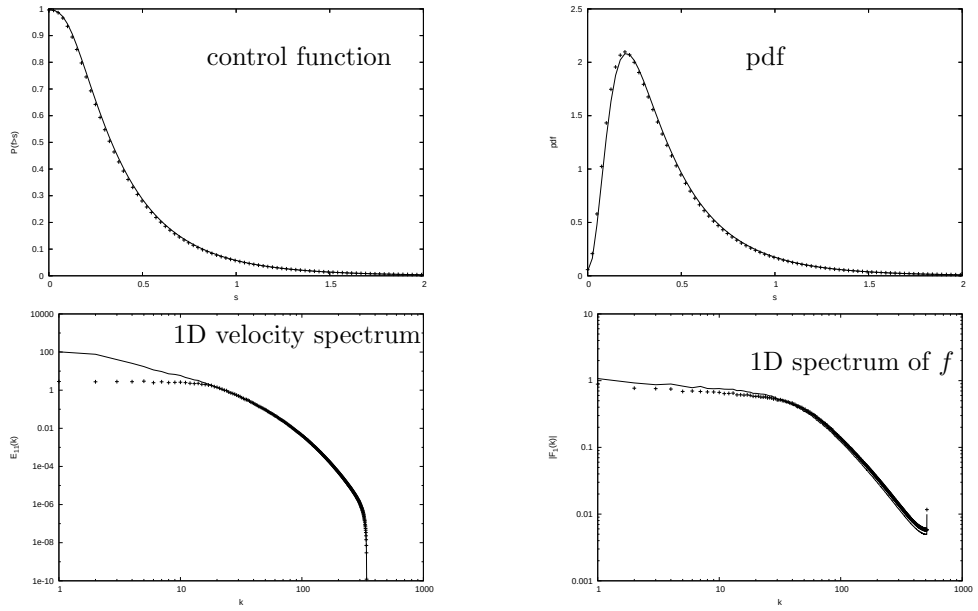

Figure 5.29: SFERA 0-20 filter plots (+), in comparison to reference field

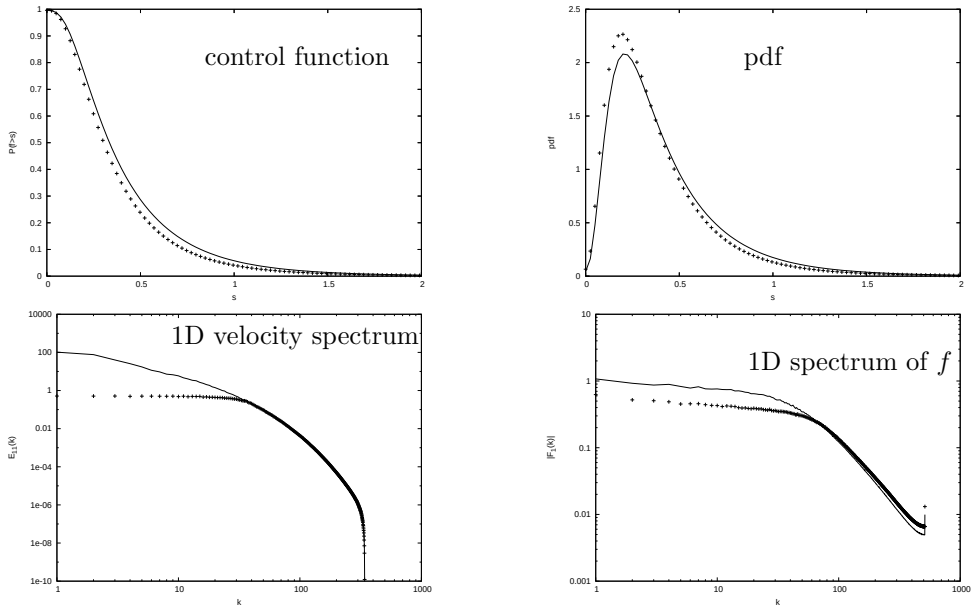

Figure 5.30: SFERA 0-40 filter plots (+), in comparison to reference field

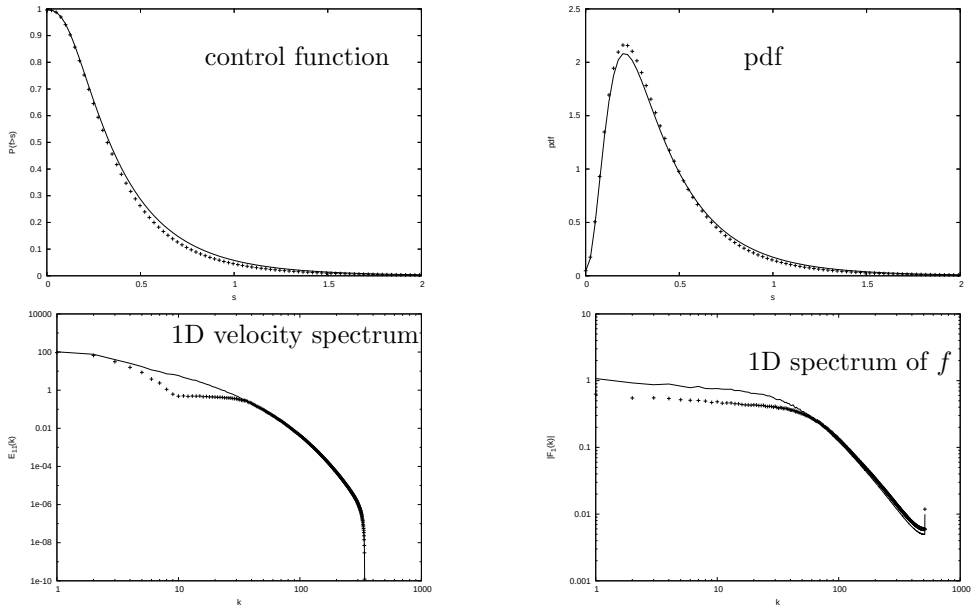

Figure 5.31: SFERA 10-40 filter plots (+), in comparison to reference field

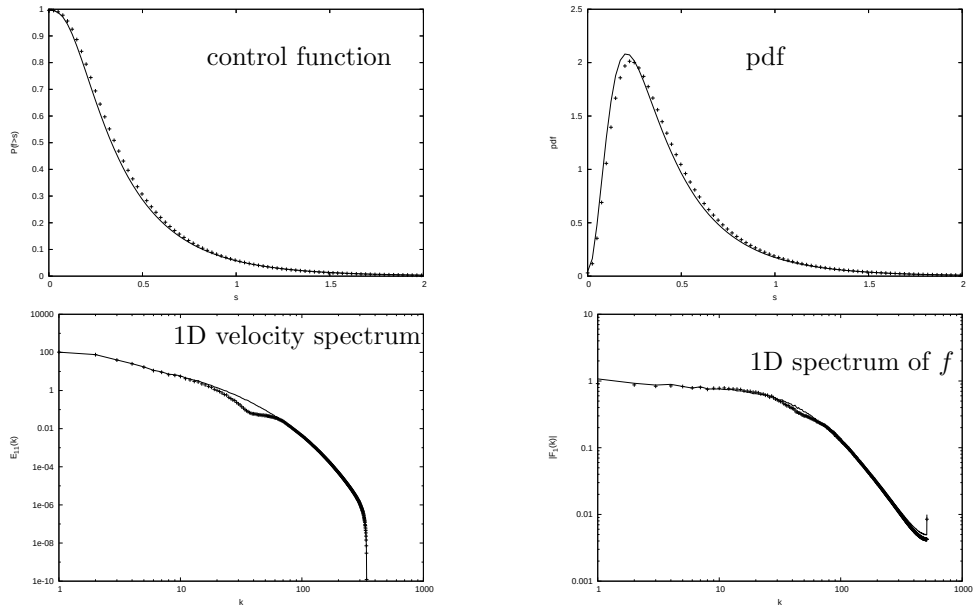

Figure 5.32: SFERA 40-70 filter plots (+), in comparison to reference field

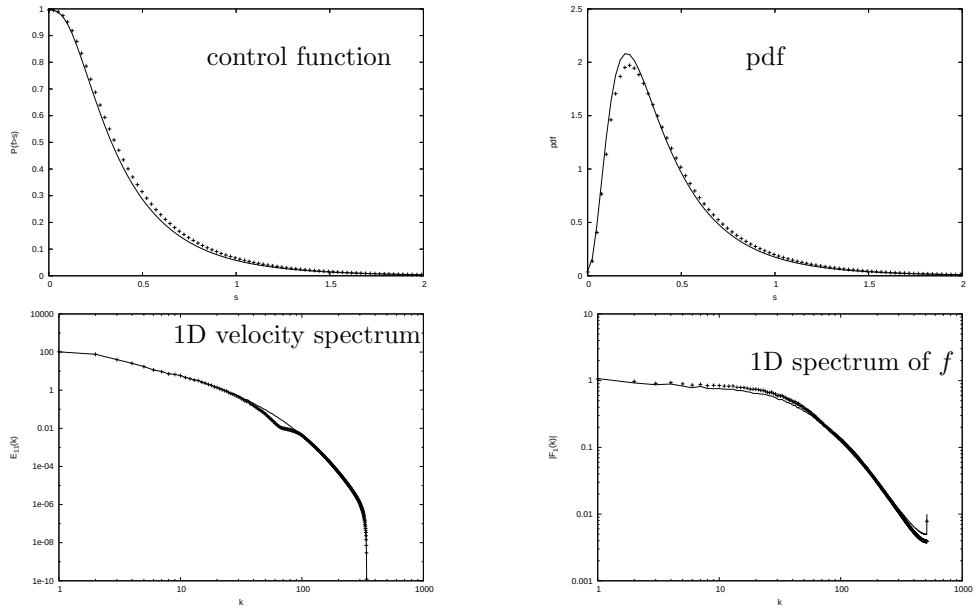

Figure 5.33: SFERA 70-100 filter plots (+), in comparison to reference field

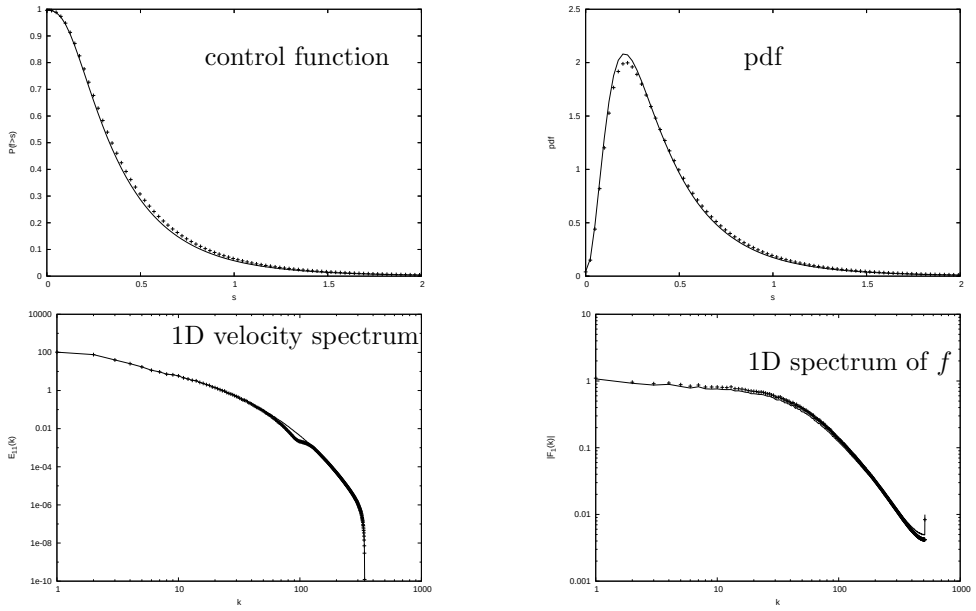

Figure 5.34: SFERA 100-130 filter plots (+), in comparison to reference field

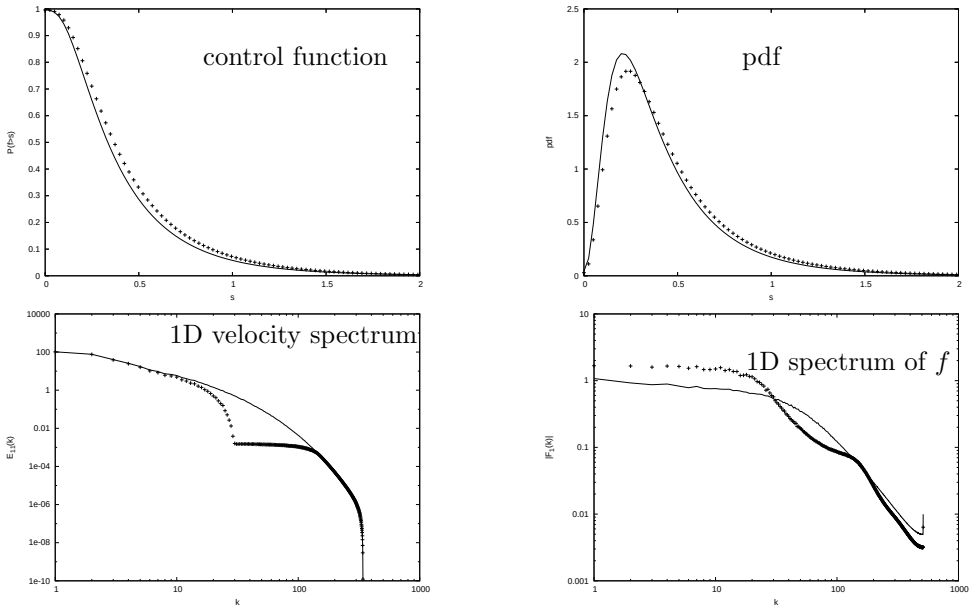

Figure 5.35: SFERA 30-150 filter plots (+), in comparison to reference field

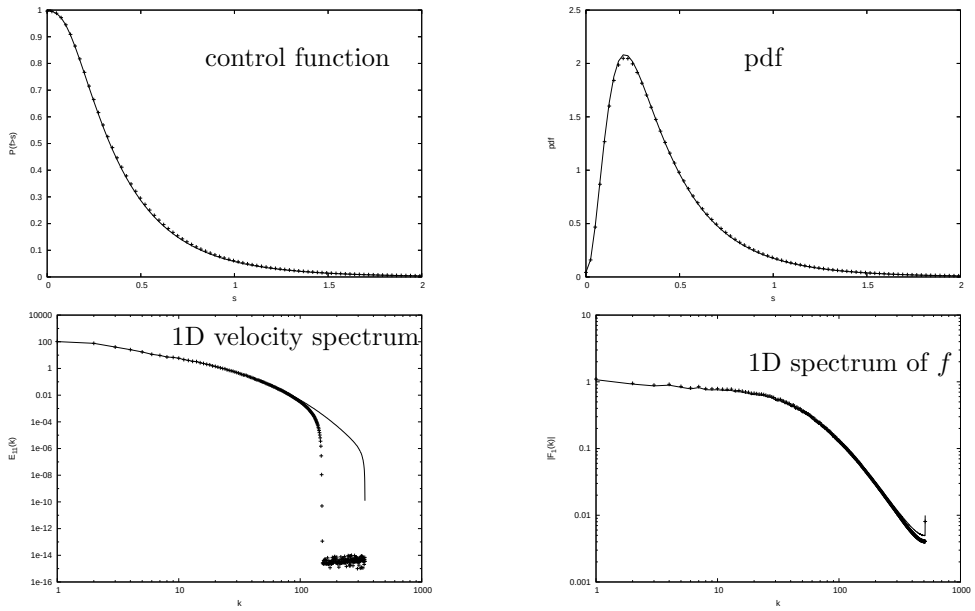

Figure 5.36: SFERA 150-500 filter plots (+), in comparison to reference field

Chapter 6

The shearless mixing layer

It is easily seen that the frame of reference of homogeneous isotropic turbulence allows a set of simplifications and hypothesis such that a very powerful theory can be developed. Nevertheless, it requires a set of assumptions that are hardly satisfied in real turbulent flows. In order to understand the behavior of turbulent flows in general, it is necessary to deal with anisotropy and non-homogeneity. The simplest way to reach this aim is to consider the interaction between two turbulent flows in the so-called *shearless mixing layer*. Consider a (ideal) box containing two homogeneous isotropic turbulence flows with different features (kinetic energy, length scales, statistics) but uniform mean velocity, which are decaying. At the beginning, the two turbulence flows are separated by a rigid wall. When the wall is removed, the flows begin to interact, in a region (mixing layer) which extends with time. The absence of mean shear avoids the arise of turbulence production; the spread of the mixing layer is thus governed by fluctuations. For its importance in applications, from chemical reactions to different flows interactions in engines, the mixing layer has been recently studied following different approaches. In particular it can be important to verify and understand the presence of intermittency in the mixing process, subject which is still now matter of discussion. In the following we present the "classic" results, describing how physical experiments can be performed by mixing grid turbulences. Later on some results coming from numerical simulations of mixing layers are shown. Using such results, we would like to show how the mixing layer features change, as we change the features of the two interacting flows.

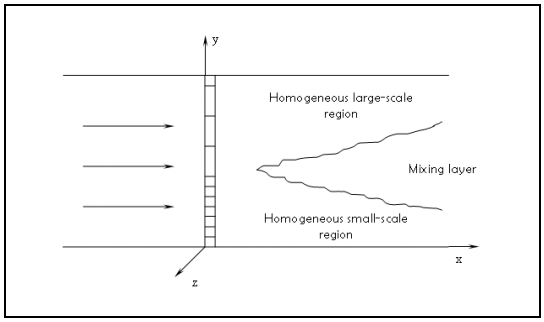

Figure 6.1: Mixing layer generated by two grid turbulences

6.1 Intermittency and asymptotic states

Since the 80s, several experiments on shearless mixing layer have been performed. We now focus on the laboratory experimental study of Veeravalli & Warhaft (1989), which is the best account on shearless mixing layer dynamics in literature. A sketch of this experiment is presented in fig.6.1

The flow is obtained in a decaying grid turbulence, where the mean velocity is constant, but two distinct scales of turbulence are generated by varying the mesh size. Thus, beyond the grid, two different scales of turbulence are created. Each flow presents a homogeneous region, far from the center of the canal, which becomes thinner and thinner as the flow evolves; and a mixing layer is formed, where the two turbulences penetrate and diffuse one into another. This situation has been obtained in a vertically oriented wind tunnel in two different ways: using parallel bar grids and perforated plates. The obtained length-scale ratios $\frac{l_2}{l_1}$ are 2.42 and 4.32 for the grids, and 2.23 for the perforated plate. The shearless mixing layer is very difficult to describe experimentally, for an accurate description of problems and solutions we refer to the original paper [2].

It is worthy to note that this system evolves because of the interaction of the two turbulences, without the generation of turbulence due to shear. This situation is different from the mixing layer formed by instability of parallel streams with different velocities, which is another classical experiment; there, turbulence is a consequence of the presence of the mixing region. To keep this in mind, we can refer to our shearless mixing layer as a *turbulence mixing layer*, instead of the *turbulent* mixing layer.

The experiments set up by Veeravalli & Warhaft (in the following V&W)

give information about how the length-scale ratio influences the evolution of the system. In particular, it shows a situation in which the dynamics of the system are controlled by *two scales*. This is the case of the parallel bar grid with $\frac{l_2}{l_1} = 2.42$ and the perforated plate ($\frac{l_2}{l_1} = 2.23$). In this cases, the variances of the three components (i.e. the three contributions to the total turbulent kinetic energy) show a sort of asymmetry in the spatial profile (plotted as a function of the grid direction y), which is due to the presence and strong interaction of two different scales.

On the other hand, the case of the grid with $\frac{l_2}{l_1} = 4.32$ appears to show energetics controlled by a *single scale* as the large scale essentially dominates the mixing layer. Under these conditions, the variance profile (as a function of y) is well fitted by an error function, while in the previous cases evident differences from such a fit appeared in the high-turbulence side.

Another fundamental aspect of the V&W paper is that, for the fist time, they observed the presence of intermittency in the mixing layer. Actually, previous experiments about the mixing layer had been performed by Gilbert [**?**]. But the phenomenon observed by Gilbert was essentially Gaussian, without intermittency. Despite of this fact, the 1989 experiment of V&W presents non-Gaussian velocity statistics and a mixing layer which is strongly intermittent. Evidences of this fact are to be found in the profiles of the third and forth moments, skewness and kurtosis.

The skewness is null out of the mixing layer, as expected, but becomes different from 0 where the turbulences interact. In particular, negative values are observed for the skewness of the first and second component (S_u and S_v), while S_w is positive in the mixing layer. The negative values of S_v is due to the fact that in the low turbulence side of the mixing region the deviations from the homogeneous behavior is due to the influence of the large scale side, and so they are more likely to be negative. Instead, the values of S_u are due to the Reynolds stresses $\langle uv \rangle$, which appear in the evolution equation of $\langle u^3 \rangle$ (see V& W). Furthermore, the distance from zero value of the skewness (in particular of S_v) is shown to *increase* as the energy ratio (which depends on the mesh size ratio) between the two turbulences increases. Thus the strongest non-Gaussian behavior is obtained for the grid with $\frac{l_2}{l_1} = 4.32$ where a peak of -2.5 is found.

Also the values of kurtosis K_u, K_v, K_w are different from the Gaussian value of 3, reached in the region external to the mixing layer. This leads to important physical considerations. Considering for example K_u, it has

peak values of ~ 4. If we assume that the evolution of the mixing layer is dominated uniquely by a diffusive phenomenon, (*turbulent diffusion*), this would lead to a Gaussian behavior and $K_u \sim 3$. This was the behavior observed by Gilbert. On the other hand, if we assume that the process consists only of turbulent penetration (of the two scales into one another), this model would lead to peak values of $K_u \sim 6$ (see V& W). Hence, the intermediate value for the observed peak is a proof of the presence of both mechanisms in the mixing layer, whose evolution is thus dominated by *both penetration and turbulent diffusion*. Again, the excess factor $(K-3)$ increases as the energy ratio increases.

To summarize, what comes out from the V&W experiment, and from the previous knowledge, is the existence of two asymptotic states. The first is obtained when the length-scale ratio $\frac{l_2}{l_1}$ approaches unity, $\frac{l_2}{l_1} \to 1$: the flow is essentially dominated by a single scale, although the variances at the two sides of the mixing layer are different. This fact had been pointed out for example by Gilbert (1980), who observed a Gaussian non-intermittent behavior. The other asymptotic state is reached when the length-scale ratio is large enough. Here, the energetics of flow are dominated by large-scale side, because the energy contribution of the other side is too week to effect the evolution of the system. Here the error function fit is again good for the variance profile. But unlike the previous case, this state shows the presence of a strong intermittency in the mixing layer, with highly non-Gaussian statistics. Finally, it exists an intermediate range of this ratio over which *two scales* are dominant. It is the case of $\frac{l_2}{l_1} \sim 2$, for example, as shown in V&W. Here, the variance does *not* follow an error function profile, and highly intermittent statistics are found out. Furthermore, the higher is the energy ratio between the two flows, the stronger is the non-Gaussian behavior in the mixing layer.

The description given until now to the mixing layer experiment has been shown to be uncomplete when, in 1996, Briggs, Ferziger, Koseff and Monismith (see [1]) obtained results not consistent with the existence of the Gaussian asymptotic state. They used direct numerical simulations of a shear-free mixing layer to reproduce situations analogue to the parallel bar grid and perforated plate of V&W; in this case the evolution if the flow is obtained in time, instead of in space as in the physical experiment. As an initial condition, only an energy gradient of about 7.5 was created, leaving inalterate the length-scale which is the same for both the turbulences. What we see

after after a temporal evolution ($t = 1.72$) is that the length-scale ratio is still close to one (0.93), closer than the value proposed by Gilbert, but *intermittent features* appear. Actually, the statistics of the flow are not Gaussian; in particular the vertical skewness S_v reaches negative values until about 1, and the kurtosis K_v shows a peak of more than 4. These data, in contrast with Gilbert experiment, are comparable to the ones obtained in the case of the perforated plate experiment by V& W.

These results clearly showed that the evolution of the system towards a Gaussian asymptotic state cannot be predicted as a function of the length-scale ratio only. In 2005, Tordella and Iovieno proposed an interpretation of this fact (see [3]): the presence of a Gaussian asymptotic state must be studied as a function of both the *length-scale ratio* $\frac{l_2}{l_1} = \mathcal{L}$ and the *kinetic energy ratio* $\frac{\mathsf{k}_2}{\mathsf{k}_1} = \mathcal{E}$. For example, coming back to the experiment of Briggs, we see that the energy ratio was about 7.5, much higher than the one in Gilbert's experiment (1.48), but comparable to the energy ratio of the perforated plate experiment (6.26); from this new point of view, the behavior of these experiments is thus coherent. A more systematic study of the influence of the two parameters (energy and length-scale ratio) on the evolution of the mixing layer is presented in the following sections.

6.2 Results on intermittency

6.2.1 Features of the experiment

The following results are obtained from numerical simulations of a mixing layer, carried out using both DNS and LES approaches. The integration of the Navier-Stokes system is carried out by means of the technique developed by Iovieno, Cavazzoni and Tordella in 2001 (for details see [11]).The numerical domain consists of two cubes, $L = 2\pi$, with 128^3 points each. As initial condition, the two velocity fields are matched using a hyperbolic tangent function, whose width is 1/40 of the total resulting $4\pi(2\pi)^3$ parallelepiped:

$$\mathbf{u}(\mathbf{x}) = \mathbf{u}_1(\mathbf{x})p(x) + (1 - p(x))\mathbf{u}_2(\mathbf{x}) \tag{6.1}$$

$$p(x) = \frac{1}{2}[1 + \tanh(12\pi\frac{x}{L})\tanh(12\pi\frac{x - L/2}{L})\tanh(12\pi\frac{x - L}{L})]$$

where now x is the inhomogeneity direction. Time integration adopts a four-stage fourth-order explicit Runge-Kutta scheme.

As a definition of integral scale, the longitudinal integral scale has been adopted

$$l(t) = \frac{1}{3}\sum_{i=1}^{3}\frac{\int_0^\infty R_{ii}(r,t)\,dr}{R_{ii}(0,t)}. \tag{6.2}$$

This definition has two good features. First it can be directly measured quite easily. Second, it is a quantity normalized by the kinetic energy: thus the integral scale *does not depend on the level of kinetic energy*, just on the way it is distributed over the wave-numbers. For example, let's consider two turbulence fields obtained by multiplying the same velocity field by two different constants. The energy spectrum will result scaled by constants, so the energy levels will be different; but the constants will disappear in the ratio (6.2) and the flows will have the same integral scale. So, it is the *shape* of the spectrum which determines the integral scale. In particular, the distribution of low wave-numbers modes has a strong effect on the resulting integral scale, being the non-universal part of the spectrum.

In order to modify the shape of the spectrum, and thus the integral scale, two methods were used. A low-pass filter effect was obtained by letting the initial homogeneous isotropic field evolve in time. Actually, a decayed field has a lower energy and a higher integral scale than the initial field. Thus, one can generate *opposite* energy and integral scale gradients.

As high-pass filters, CROCE and SFERA filters, introduced in chapter 5, are used. Both of them have been tested, in order to study a possible influence of the filtering method on the final statistics; no effect due to a particular choice of one filter was detected.

Another important consideration must be made, as the kinetic energy and the integral scale of the flows are time-depending. An estimate of the evolution for these quantities can be obtained by recalling two facts. First, the integral scale can be estimated using the equation

$$l(t) = \frac{\mathsf{k}(t)^{3/2}}{\varepsilon} f(Re) \tag{6.3}$$

where ε is the dissipation rate $\varepsilon = -\frac{d\mathsf{k}}{dt}$, and $f(Re)$ is an order-one function which should be estimated experimentally. In the hypothesis of statistical equilibrium, one could use the simplified relation $l = \frac{\mathsf{k}^{3/2}}{\varepsilon}$; but many authors have shown that this hypothesis is not fully satisfied if the Taylor Reynolds

number Re_λ is less than 70 (see Batchelor, Dimotakis). Thus, we refer to the more general relation.

Second, in the homogeneous parts of the flows, the evolution of the kinetic energy is well known in literature (see for example [12]):

$$\mathsf{k}(t) = A(t + t_0)^{-n} \tag{6.4}$$

where the constants t_0 and n are to be determined experimentally. Times are normalized by the eddy turnover time $\tau = l/\mathsf{k}^{1/2}$. Using (6.4) we can rewrite (6.3) in the form

$$l(t) = \frac{1}{n} f(Re_\lambda)\sqrt{A}(t - t_0)^{1-n/2} \tag{6.5}$$

which shows the explicit evolution of the integral scale as a function of time. Considering the integral scale and energy ratios, they must evolve as

$$\frac{\mathcal{L}(t)}{\mathcal{L}(0)} = (1 + \frac{t}{t_{01}})^{1-n_1/2}(1 + \frac{t}{t_{02}})^{-1+n_2/2} \tag{6.6}$$

$$\frac{\mathcal{E}(t)}{\mathcal{E}(0)} = (1 + \frac{t}{t_{01}})^{-n_1}(1 + \frac{t}{t_{02}})^{n_2} \tag{6.7}$$

In the experiments carried out, all values of the constants t_{01}, t_{02} and n_1, n_2 are very close to each other (see [3] pag.4). This means that the ratios in (6.6) and (6.7) can be assumed time-independent, giving almost constant conditions for the evolution of the mixing layer.

6.2.2 Results

The two control parameters which take part in a mixing layer simulation are the integral scale ratio $\mathcal{L}$ and the energy ratio $\mathcal{E}$. In order to investigate the presence of the asymptotic state, the numerical experiments reproduce the state with $\mathcal{L} = 1$, letting the energy ratio grow. In Tordella & Iovieno [3], $\mathcal{E}$ is let vary from 1 to 58. According to these simulations, *the asymptotic hypothesis is not confirmed*. Actually, all simulations of the mixing layer appear to be intermittent. As an example, we present the plot of the skewness and the kurtosis of the velocity component in the inhomogeneity direction (y according to fig.6.1) through the mixing layer. The spatial coordinate is centered in the position of the center of the layer, i.e. the position where the average kinetic energy $\frac{\mathsf{k}_1+\mathsf{k}_2}{2}$ is measured; and it is normalized by the length of the layer, as defined in [3] (pag.7). The plots 6.2 show data coming from

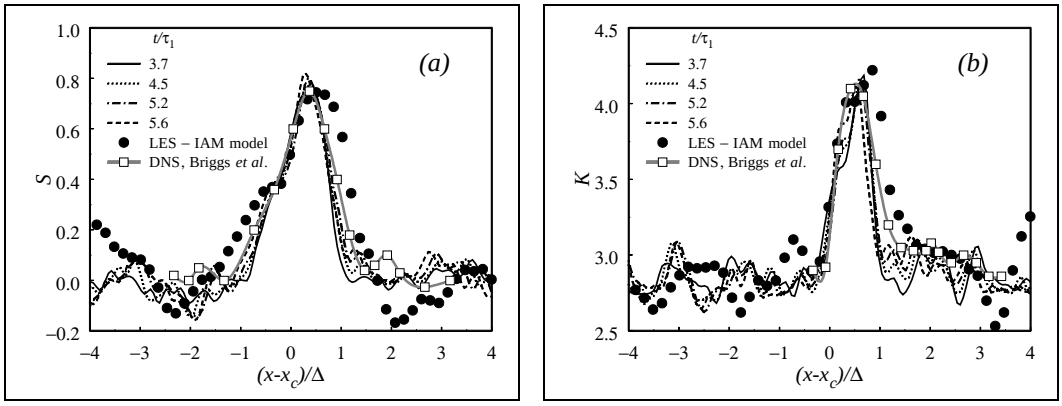

Figure 6.2: Skewness (a) and kurtosis (b) of the velocity component in the inhomogeneity direction x. Comparison with values of Briggs *et al.* and LES method implemented by Tordella & Iovieno

different values of (normalized) times: Furthermore, data coming from LES simulations and from Briggs experiment are presented for comparison. Both skewness and kurtosis are far from the Gaussian values, proving the presence of intermittent features in the turbulence mixing layer dynamics.

To gain a deeper understanding of such phenomenon, a further study has been carried out. Such analysis focuses the evolution in time of the non-Gaussian features; precisely, we have captured the maxima of the kurtosis (for each time step) in the mixing layer, and showed their trend in time.

Moreover, we complete the picture on the dependence of such features on the energy ratio, by letting $\mathcal{E}$ grow until values of the order of 10^3. We present the results obtained about the kurtosis, but a similar analysis can be carried out for the third moment.

At low time, the evolution is quite expected. In particular, the initial condition is associated to a Gaussian value of three. This value is soon abandoned, the curve kurtosis-time steeply grows at the beginning. Observe that values larger than 3 are reached in a short time. Nevertheless, the increasing of this curve is stronger if the energy ratio is higher. For example, consider for example the normalized time $t/\tau = 2$. The kurtosis values (more precisely, the values of the maximum kurtosis reached in the mixing layer) for simulations with high energy ratio as $\mathcal{E} = 100$ have reached $K \approx 9$, while $K \approx 10.5$ for $\mathcal{E} = 1000$; instead, at the same time, the maximum kurtosis for

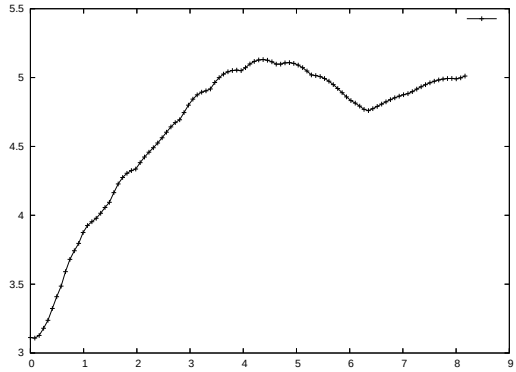

Figure 6.3: Time evolution of kurtosis maximum, $\mathcal{E} = 12$

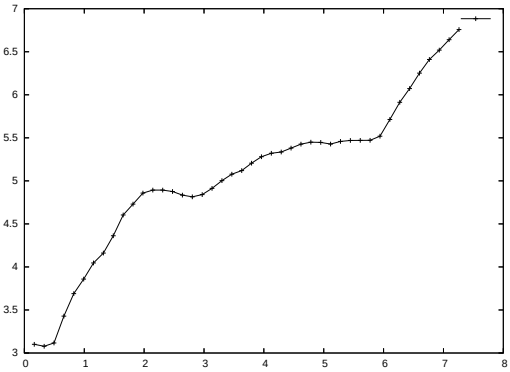

Figure 6.6: Time evolution of kurtosis maximum, $\mathcal{E} = 20$

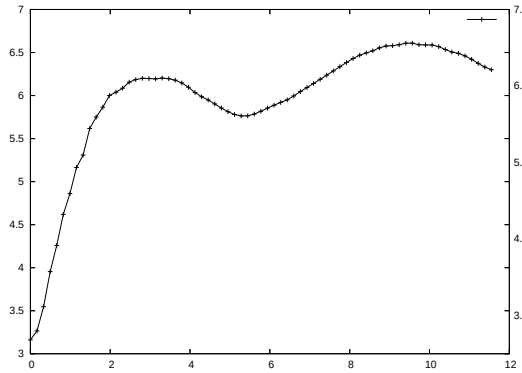

Figure 6.4: Time evolution of kurtosis maximum, $\mathcal{E} = 140$

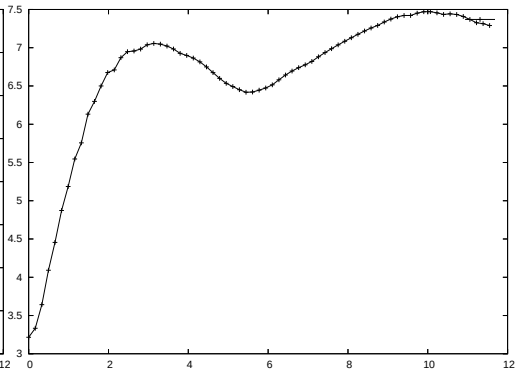

Figure 6.7: Time evolution of kurtosis maximum, $\mathcal{E} = 60$

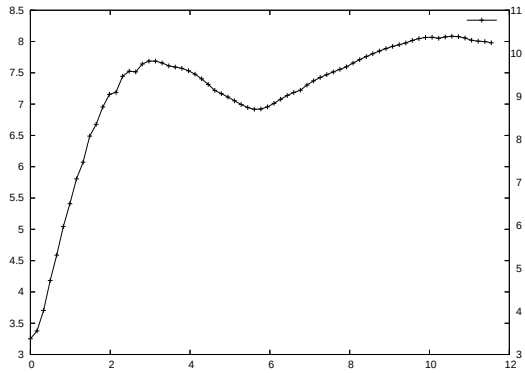

Figure 6.5: Time evolution of kurtosis maximum, $\mathcal{E} = 80$

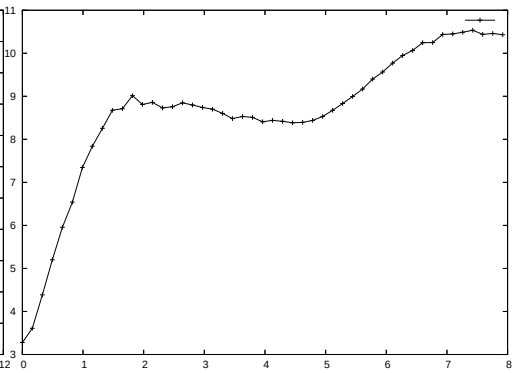

Figure 6.8: Time evolution of kurtosis maximum, $\mathcal{E} = 100$

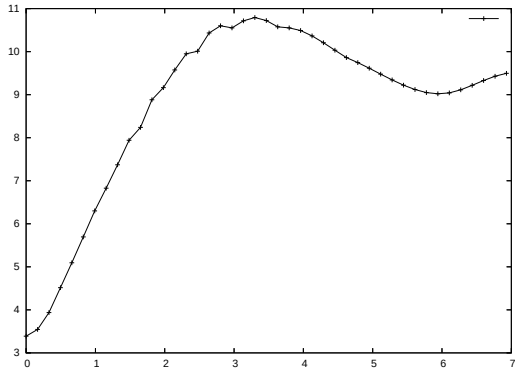

Figure 6.9: Time evolution of kurtosis maximum, $\mathcal{E} = 300$

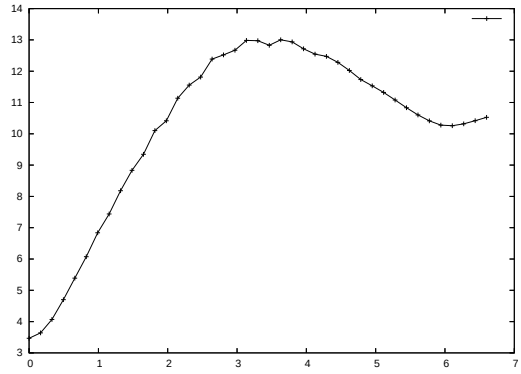

Figure 6.11: Time evolution of kurtosis maximum, $\mathcal{E} = 10000$

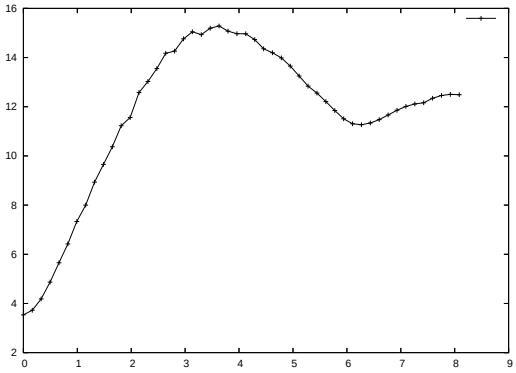

Figure 6.10: Time evolution of kurtosis maximum, $\mathcal{E} = 10000$

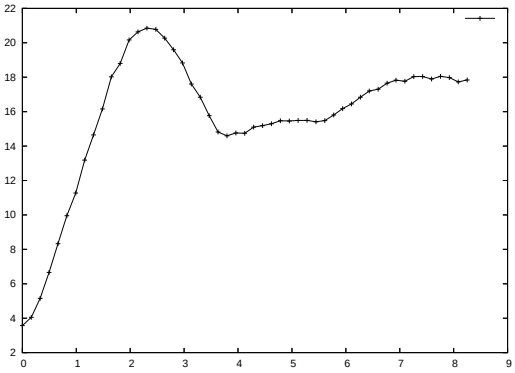

Figure 6.12: Time evolution of kurtosis maximum, $\mathcal{E} \to \infty$

the $\mathcal{E} = 12$ appears to be less than 4.5.

Second, as already mentioned, we show evidence that *the kurtosis reaches a maximum value* during the decaying of the mixing layer. After a steep growth, actually the kurtosis reaches a sort of peak, after which there is a region in which it begins decreasing. Note that such maximum is reached in approximately 3-4 normalized time units t/τ for every value of energy ratio. The only simulation which differs in behavior is the $\mathcal{E} = 20$ one. A possible explanation is the difficulty in the identification of the maximum of K in presence of two peaks in the kurtosis profile; here we show the plot of this simulation for sake of completeness, but further analysis should be carried out.

We can also note that the range of decreasing is wider for higher values of $\mathcal{E}$. For example, when $\mathcal{E} = 80$, K goes down from 7.5 to 6.5 giving a $\Delta K \approx 1$; while $\Delta K \approx 4$ in $\mathcal{E} = 10000$, where K passes from 15 to 11.

High values of kurtosis indicate that intermittency is strongly present in the dynamics of the mixing layer. In particular, when the kurtosis grows up to $K \approx 10$, $K \approx 15$, the intermittency is active and the turbulent penetration dominates the evolution of the mixing layer. The turbulent diffusion seems to balance the turbulent penetration only after an initial period: this seems to be indicated by a decreasing of the intermittent features, once 4-5 t/τ has passed.

Finally, as the system further evolves, our analysis becomes less reliable: the turbulence, not forced, is going to slowly disappear. It is still matter of discussion if the kurtosis presents other fluctuations, before disappearing. Some simulations seem to suggest that the kurtosis starts again to increase. Such a growth seems to reach a new maximum value ($t \sim 10\tau$). Note that this new maximum is higher than the first peak value for the mixing layers with $\mathcal{E} < 100$; while in high energy ratio simulations the kurtosis seems to fluctuate around values lower than the first peak. This trend needs more simulations and analysis to be confirmed; hopefully, laboratory experiments could help to prove and understand this behavior for high values of τ.

The intermittent features have been studied asymptotically, as a function of the energy ratio. To each value of $\mathcal{E}$, one value of kurtosis has been associated. We have seen that the kurtosis reaches two peaks in the studied time interval; moreover, for some simulations the first maximum is higher than the second, but not for all. Thus, we preferred to study the behavior of an *average* kurtosis, instead of the maximum. This average kurtosis has

been calculated considering a time window and averaging the values of the maxima on this time interval. The window is shorter than the total time range (usually $t/\tau \in [0, 12]$), in order to avoid the influence of the initial evolution (the system is influenced by initial conditions) and the final decayed field. A sort of limit case has been simulated letting $\mathsf{k}_2 \to 0$: the high energy field is diffusing and penetrating in a zero velocity field. The results are presented in picture 6.13. A continuous growth is evident, much steeper for lower values of $\mathcal{E}$. We also show a fit obtained using a power law function

$$K(\mathcal{E}) - 3 \approx a(\mathcal{E} - 1)^b$$

with $a \approx 2.4$, $b \approx 0.18$. A better fit is obtained with a logarithmic function

$$K(\mathcal{E}) - 3 \approx a \log(b\mathcal{E})$$

where $a \approx 3$, $b \approx 4.3$ The fit is good for low values of $\mathcal{E}$.

6.3 Conclusions

The shearless turbulence mixing layer has been investigated using numerical simulations. In particular, a post-processing analysis has been carried out on the kurtosis of the velocity component in the direction of inhomogeneity, dealing with simulated interacting fields with the same integral scale but different kinetic energy. The results clearly shows that the intermittency of the mixing layer is an increasing function of the energy ratio of the two turbulences. This fact confirms the observations in Tordella-Iovieno. It shows that, even if the length-scales of the interacting turbulences are comparable ($\mathcal{L} \approx 1$), an intermittent behavior appears when the energy ratio moves away from 1; and if we let $\mathcal{E}$ grow, the intermittency becomes stronger and stronger. So, if we want to predict the behavior of a mixing layer, the parameter $\mathcal{E}$must be taken into account, as it influences the non-Gaussian processes such intermittent transport and penetration of a one turbulence into the other. Possible models for this dependence on $\mathcal{E}$have been presented, based on logarithmic and order 4 functions.

We also showed that the evolution of the kurtosis, which is an index of intermittency, in time presents a nonlinear growth, with the presence of one maximum and successive fluctuations. This growth is steeper when the energy ratio is high.

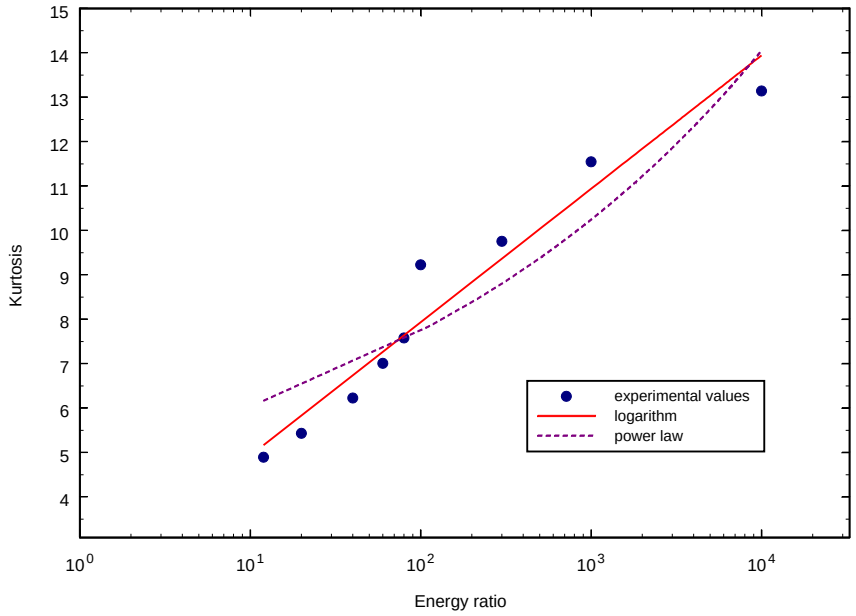

Figure 6.13: Kurtosis as function of energy ratio. Least square fits with logarithmic and power law function

This results help to draw a more precise picture of the evolution of a shearless mixing layer. Nevertheless, this picture must be regarded as the first step towards the understanding of mixing layers. The introduction of shear, and the consequent generation of turbulence, is necessary in order to develop a model for real mixing experiments taking place in science and engineering. Once we have established the importance of the control parameter $\mathcal{L}$ and $\mathcal{E}$, further research should be carried out in that direction.

Bibliography

[1] D.A. Briggs, J.H. Ferziger, J.R. Koseff, S.G. Monismith, *Entrainment in a shear-free turbulent mixing layer*, J. Fluid Mech. (1996), vol.310, pp.215-241

[2] S.Veeravalli, Z. Warhaft, *The shearless turbulence mixing layer*, J. Fluid Mech. (1989), vol.207, pp.191-229

[3] D. Tordella, M. Iovieno, *Numerical experiments on the intermediate asynptotics of shear-free turbulent transport and diffusion*, J. Fluid Mech. (2005), vol.000, pp.1-13

[4] L. Biferale, G. Boffetta, A.Celani, A. Lanotte, F. Toschi, *Particle trapping in three-dimensional fully developed turbulence*, Physics of fluids 17, 021701 (2005)

[5] J. Jimenez, *Small scale intermittency in turbulence*, Eur. J. Mech., B/Fluids, 17, n.4, 405-419, 1998

[6] J, Jimenez, A.A. Wray, *On the characteristics of vortex filaments in isotropic turbulence*, J. Fluid Mech. (1998), vol.373, pp.255-285

[7] U. Frisch, *Turbulence - The legacy of A.N. Kolmogorov*, Cambridge University Press, 1995

[8] H. Tennekes, J.L Lumley, *A first course in turbulence*, MIT Press, 1972

[9] A.S. Monin, A.M. Yaglom, *Statistical Fluid Mechanics*, vol.1, MIT Press, Cambridge 1979

[10] D. Tordella, M. Iovieno, S. Massaglia, *Small scale localization in turbulent flows.* A priori *test applied to a possible Large Eddy Simulation of compressible turbulent flows*, Comput. Phys. Commun. (2007), doi: 10.1016/j.cpc.2006.12.004

[11] M. Iovieno, C. Cavazzoni, D. Tordella, *A new technique for a parallel dealiased pseudospectral Navier-Stokes code*, Comput. Phys. Commun. 141, 365-374

[12] G.K. Batchelor, *The theory of homogeneous turbulence*, Cambridge University Press, 1953

[13] A. Celani, A. Mazzino, A. Pumir, *Turbulence and Stocastic processes*, Lect. Notes Phys. 636, 173-186 (2003)

[14] S.B. Pope, *Turbulent flows*, Cambridge University Press, 2000

Appendix A

Postprocessing details

A.1 Filters

Essentially, three filters have been used to modify the velocity fields. All these filters act in the wave-number domain, in order to allow considerations about the spectra and the energetics of a field.

The SFERA high-pass filter is based on the use of the function

$$g_s(\mathbf{k}; A, k_0|) = \frac{1}{1 - e^{-A(|\mathbf{k}|-k_0)}} \tag{A.1}$$

which is a sort of smooth step function. The parameter $\mathbf{k}_0$ controls the width of the band, while A determines the steepness of the step. This is a spherical filter that cuts the contribution of any wave-number whose magnitude is larger than a certain threshold. A bandpass filtering has been obtained using the same kind of function:

$$\begin{aligned} \tilde{g}_s(\mathbf{k}; A, k_{min}, k_{max}) &= [1 - g_s(\mathbf{k}; A, k_{min})] + g_s(\mathbf{k}; A, k_{max}) \\ &= [1 - \frac{1}{1 - e^{-A(|\mathbf{k}|-k_{min})}}] + \frac{1}{1 - e^{-A(|\mathbf{k}|-k_{max})}} \end{aligned} \tag{A.2}$$

The CROCE high-pass filter is thought to suppress any wave-number that has at least one component lower than a certain threshold. Thus it is defined as

$$g_c(\mathbf{k}; A, k_0) = \prod_{i=1}^{3} \Phi(k_i; A, k_0) \tag{A.3}$$

$$\Phi(k_i; A, k_0) = \frac{1}{1 - e^{-A(k_i-k_0)}}$$

Again, we can filter the band $[k_{min}, k_{max}]$ on each component of $\mathbf{k}$ by defining

$$\tilde{\Phi}(k_i; A, k_{min}, k_{max}) = [1 - \Phi(k_i; A, k_{min})] + \Phi(k_i; A, k_{max})$$

Finally, the filter FILAMENTO evaluates the components k_1, k_2, k_3 separately. If one of them, say k_j, falls in the filter range $[k_{min}, k_{max}]$ and the other two are greater than a certain threshold (KTOP), then the filter function is

$$g_f(\mathbf{k}; A, k|) = \tilde{\Phi}(k_j; A, k_{min}, k_{max}) \tag{A.4}$$

A.2 Program instructions

The data of the 1024^3 velocity field are stored in 64 files, each of them representing a "slice" of domain of $N \times N \times NX$, where $N = 2\pi$ and $NX = 2\pi/64$; the total dimension is about 13 gigabytes. We must say that one main difficulty in our work was to handle this huge mole of data, as we needed to carry out global operation on the whole domain (for example, Fourier transforms) but the calculator can process just portions (the slices) of domain. Thus, each program has been thought to use one slice per time, with particular care for operations which require more than one spatial point (like derivatives and transforms).

First, the velocity field $\mathbf{v}(\mathbf{x})$ is transformed in order to obtain the Fourier coefficients $\mathbf{v}(\mathbf{k})$. The transform is implemented by use of the routine **nag**, which operates a 1D transform. As the data are contained in 64 files instead then one, and each file consist of a part of domain of dimension $N \times N \times NX$ (N in the y and z directions, and NX in the x direction), the transform is operated in two steps. First, we transform file by file in the two directions y and z. Then we create a new set of domain slices with dimension N in x and y directions and NX in z direction, and perform the last 1D transform in the x direction.

Once we have the data set in the wave-number domain, we perform the filtering. The programs which filter the field are based on the same subroutine **F**:

```
IF(KMIN.LE.0)THEN
G=0.E0
ELSE
ETA1=EXP(-A*(K-KMIN))
```

```
G=1.0E0-1/(1.0E0+ETA1)
END IF

ETA2=EXP(-A*(K-KMAX))
F=G+1/(1.0E0+ETA2)
```

Then the filter **sfera** acts on the magnitude of vector **k**:

```
DO 50 L1=0,N-1
  CALL N_ONDA(L1,K1,N)
DO 50 L2=0,N-1
  CALL N_ONDA(L2,K2,N)
DO 50 L3=0,NX-1
  L3vero=L3+IFETTA*NX
  CALL N_ONDA(L3vero,K3,N)

   KK=(K1**2+K2**2+K3**2)**0.5E0
   COEFF=F(KK,A,KMIN,KMAX)

  DO 60 J=1,3
  U(L1,L2,L3,J)=U(L1,L2,L3,J)*COEFF
60    continue
50    continue
```

while **croce** acts on the components of the coefficient vector:

```
DO 50 L1=0,N-1
  CALL N_ONDA(L1,K1,N)
  COEFF1 = F(K1,A,KMIN,KMAX)
DO 50 L2=0,N-1
  CALL N_ONDA(L2,K2,N)
  COEFF2 = F(K2,A,KMIN,KMAX)
DO 50 L3=0,NX-1
  L3vero=L3+IFETTA*NX
  CALL N_ONDA(L3vero,K3,N)
  COEFF3 = F(K3,A,KMIN,KMAX)

  COEFF=COEFF1*COEFF2*COEFF3
  DO 60 J=1,3
```

```
      U(L1,L2,L3,J)=U(L1,L2,L3,J)*COEFF
 60    continue
 50    continue
```

and **filamento** operates through an *if* structure:

```
 IF((K1.GE.KMIN).AND.(K1.LE.KMAX).AND.(K2.GT.KTOP)
>.AND.(K3.GT.KTOP))THEN
   COEFF=F(K1,A,KMIN,KMAX)

 ELSE IF((K2.GE.KMIN).AND.(K2.LE.KMAX).AND.(K1.GT.KTOP)
>.AND.(K3.GT.KTOP))THEN
 COEFF=F(K2,A,KMIN,KMAX)

 ELSE IF((K3.GE.KMIN).AND.(K3.LE.KMAX).AND.(K2.GT.KTOP)
>.AND.(K1.GT.KTOP))THEN
 COEFF=F(K3,A,KMIN,KMAX)

 ELSE
  COEFF=1.0
 END IF
```

Then we come back to the space domain with the same **nag** routine, and evaluate the values of the function $f(\mathbf{u}) = \frac{|\boldsymbol{\omega}\cdot\nabla\mathbf{u}|}{|\boldsymbol{\omega}|^2}$. The routine **stretch** calculate the values of f. The core of the program is the following. Calculation of the vorticity:

```
 do i=1,NX
 do j=1,N-2
 do k=1,N-2
   Inew=I-1

   omega(Inew,j,k,1) = (w(i,j+1,k)-w(i,j-1,k))/(2*dx) -
& (v(i,j,k+1)-v(i,j,k-1))/(2*dx)
   omega(Inew,j,k,2) = (u(i,j,k+1)-u(i,j,k-1))/(2*dx) -
& (w(i+1,j,k)-w(i-1,j,k))/(2*dx)
   omega(Inew,j,k,3) = (v(i+1,j,k)-v(i-1,j,k))/(2*dx) -
& (u(i,j+1,k)-u(i,j-1,k))/(2*dx)
```

```
      end do
      end do
      end do
```

Computation of the gradients (subroutine *grad0*):

```
c.....1)  du1/dx1
        write(*,*)'Inizio grad0 - calcolo grad(1)'
        do K=0,N-1
        do J=0,N-1
        do I=1,NX
        Inew=I-1
        gu(Inew,J,K,1)= (u(i+1,j,k)-u(i-1,j,k))/(2*dx)
        end do
        end do
        end do

c.....2) du1/dx2
        write(*,*)'Inizio grad0 - calcolo grad(2)'
        do K=0,N-1
        do I=1,NX
        do J=1,N-2
        Inew=I-1
        gu(Inew,J,K,2)= (u(i,j+1,k)-u(i,j-1,k))/(2*dx)
        end do
        end do
        end do
        gu(Inew,0,K,2)= (u(i,1,k)-u(i,0,k))/dx
        gu(Inew,N-1,K,2)= (u(i,N-1,k)-u(i,N-2,k))/dx

c.....3) du1/dx3
        write(*,*)'Inizio grad0 - calcolo grad(3)'
        do J=0,N-1
        do I=1,NX
        do K=1,N-2
        Inew=I-1
        gu(Inew,J,K,3)= (u(i,j,k+1)-u(i,j,k-1))/(2*dx)
        end do
```

```
        end do
        end do
        gu(Inew,J,0,3)= (u(i,J,1)-u(i,J,0))/dx
        gu(Inew,J,N-1,3)= (u(i,J,N-1)-u(i,J,N-2))/dx
```

Computation of the numerator:

```
c.................. Gradiente UI
      call grad0(UI,gutot,dx)
C.................. Prodotto scalare wj*d_j(u1)
      do 10 L3=0,N-1
      do 10 L2=0,N-1
      do 10 L1=0,NX-1

      str_tot(L1,L2,L3,1)=0.0
       do k=1,3
       str_tot(L1,L2,L3,1)=str_tot(L1,L2,L3,1) +
     &                     wtot(L1,L2,L3,k)*gutot(L1,L2,L3,k)
       end do
10    CONTINUE

c.................. Gradiente VI
       call grad0(VI,gutot,dx)
c.... ............. Prodotto scalare wj*d_j(u2)
      do 20 L3=0,N-1
      do 20 L2=0,N-1
      do 20 L1=0,NX-1

      str_tot(L1,L2,L3,2)=0.0
      do k=1,3
        str_tot(L1,L2,L3,2)=str_tot(L1,L2,L3,2) +
     &                     wtot(L1,L2,L3,k)*gutot(L1,L2,L3,k)
      end do
20    CONTINUE

c.................. Gradiente WI
        call grad0(WI,gutot,dx)
```

```
c..................... Prodotto scalare wj*d_j(u3)
      do 30 L3=0,N-1
      do 30 L2=0,N-1
      do 30 L1=0,NX-1

      str_tot(L1,L2,L3,3)=0.0
      do k=1,3
        str_tot(L1,L2,L3,3)=str_tot(L1,L2,L3,3) +
     &                      wtot(L1,L2,L3,k)*gutot(L1,L2,L3,k)
      end do
```

Computation of f:

```
      EPS=Wmedio*(0.02)

      DO 40 I=0,NX-1
      DO 40 J=0,N-1
      DO 40 K=0,N-1

      STR_MOD=0
      DO LL=1,3
      STR_MOD=STR_MOD+ str_tot(I,J,K,LL)**2
      END DO
      STR_MOD=STR_MOD**0.5E0

      WMODULO=0
      DO LL=1,3
      WMODULO=WMODULO+ Wtot(I,J,K,LL)**2
      END DO

      DO LL=1,3
      FVETT(I,J,K,LL)=STR_TOT(I,J,K,LL)/(WMODULO+eps)
      END DO
      F(I,J,K)=STR_MOD/(WMODULO+eps)
```

This program also makes a check on the average value of vorticity $\boldsymbol{\omega}^2$. This value is added in the denominator ($EPS = |\boldsymbol{\omega}|^2 * (0.02)$), because the vorticity could become very small in some points. Finally, the routine

momenti obtains the statistics of the function f. We calculate the moments up to the fourth; and the cumulative distribution function and the probability density function. This is carried out by considering the N^3 values as N^3 realizations of f, and averaging over the whole domain.

```
c... Calcolo media
      DO 10 I=0,NX-1
      DO 10 J=0,N-1
      DO 10 K=0,N-1
         MEDIA=MEDIA+F(I,J,K)
10    CONTINUE
      MED(INOME)=media/(N*N*NX)
900   CONTINUE

      MEDIA=0
      DO II=0,63
      MEDIA=MEDIA+MED(II)
      END DO
      MEDIA=MEDIA/64

c... Calcolo momenti centrati
      DO 20 I=0,NX-1
      DO 20 J=0,N-1
      DO 20 K=0,N-1
        VAR=VAR+(F(I,J,K)-MEDIA)**2
        MOM3C=MOM3C+(F(I,J,K)-MEDIA)**3
        MOM4C=MOM4C+(F(I,J,K)-MEDIA)**4

c... Calcolo cdf
      DO 100 II=0,M
        IF(F(I,J,K).LE.X(II)) THEN
         CONTA(II)=CONTA(II)+1
        END IF
100   CONTINUE
20    CONTINUE

      VAR_T=VAR_T+VAR/(N*N*NX)
      MOM3C_T=MOM3C_T+MOM3C/(N*N*NX)
      MOM4C_T=MOM4C_T+MOM4C/(N*N*NX)
```

```
800   CONTINUE

      VAR=VAR_T/64
      DEV_STD=SQRT(VAR)
      MOM3C=MOM3C_T/64
      SKE=MOM3C/(DEV_STD**3)
      MOM4C=MOM4C_T/64
      KURT=MOM4C/(DEV_STD**4)

      DO II=0,M
       CDF(II)=FLOAT(CONTA(II))
       CDF(II)=CDF(II)/(N**3)
      END DO

c... Calcolo pdf
      DO II=1,M-1
       PDF(II)=(CDF(II+1)-CDF(II-1))/(2*DX)
      END DO
       PDF(0)=(CDF(1)-CDF(0))/DX
       PDF(M)=(CDF(M)-CDF(M-1))/DX
```